THE APPLICATION OF ON-LINE ESTIMATION TO A DOUBLE EFFECT EVAPORATOR

A thesis submitted for the degree of

Doctor of Philosophy

by

Stephen Gerald Payne

Department of Chemical Engineering

University of Aston in Birmingham

August 1974

SUMMARY

For the implementation of on-line process control, it is often necessary to determine the true state of the plant, in real time, from insufficient and noisy measurements. Further information may be available in the form of a mathematical model: the measurements and model predictions can be combined to give a 'best' estimate of the process state. One such technique is the minimum variance recursive estimator or Kalman filter.

This research is primarily an on-line application of the Kalman filter to the estimation of the temperatures, flows and overall heat transfer coefficients of a double effect evaporator. Two dynamic models are derived - a comprehensive eighteen order system and a fourth order reduced model.

Two major software packages are developed - ASP, for interactive digital simulation and BASELINE for interactive data logging. Both packages are not confined to the double effect evaporator system as they are specifically designed for any programmer with a knowledge of BASIC.

From on-line steady state experiments, accurate heat transfer coefficient correlations are derived which provide supporting equations for dynamic simulation. The results of comprehensive model simulation prove that the system response cannot be determined without a knowledge of the vapour phase dynamics. The response of the reduced model simulation closely follows the plant response to an identical disturbance and so this model is adopted for Kalman filter experiments.

The Kalman filter algorithm is implemented on-line in real time and further off-line experiments are carried out to determine the influence of the process noise statistics on the estimation of states and parameters (the overall heat transfer coefficients). Best estimation is achieved both by separating the elements of the process noise covariance matrix that correspond to the measured variables and the parameters, and also by utilising the heat transfer coefficient correlations as parameter prediction equations.

PREVIOUS PUBLICATIONS OF THE WORK

"Interactive Digital Simulation on a Small Computer"

B. Gay and S. G. Payne, The Computer Journal, 16,2,118-121, 1973.

"Development and Use of a High Level Language Compiler for Interactive Data acquisition and Processing"

S. G. Payne and B. Gay, Paper presented at the 1st Annual Research Meeting, The Institution of Chemical Engineers, Imperial College, London, April 1974.

Copies of the above papers are to be found in the wallet inside the back cover of the thesis.

ACKNOWLEDGEMENTS

The author wishes to express his gratitude to the following:-

Professor G. V. Jeffreys, Head of the Department of Chemical Engineering, University of Aston in Birmingham, for the use of departmental research facilities.

Dr. B. Gay, for his supervision and guidance.

Messrs. M. Lea and D. Bleby, departmental electronics technicians for maintaining the computer-plant system and constructing the hardware interface.

Miss Joy Harris for her accurate and patient typing.

CONTENTS

CHAPTER 1

INTRODUCTION

The fundamental goal of estimation is to obtain the 'best' estimate of an unknown quantity by combining and interpreting imperfect information about that quantity. The term 'best' implies the existence of a cost function which is minimised by proper use of the information. In a chemical engineering context, the quantity may be a state variable or parameter required for process control which is either unmeasurable or subject to measurement errors. In addition to measurements, the state of the process can be predicted by some form of mathematical model. The results of such predictions are also subject to errors due to inherent simplifying assumptions and an inability to describe mathematically the random disturbances which are evident in all processes. In a situation where little information is reliable, optimal control may still be feasible provided that 'best' estimates of the current state of the system are available.

Thus the problem of optimal control in the presence of poor measurements and predictions centres around state estimation. Linear estimation with a least squares cost was applied by Gauss (1) as early as 1809 to determine the orbital elements of celestial bodies from uncertain measurements. More recently, Wiener (2) and Kalman (3) have extended the theory to estimate states described by a set of linear differential equations. The optimal, sequential, discrete-time estimation technique of Kalman, the so-called Kalman filter, has received much attention from researchers in the aerospace industry (4).

Extensions for non-linear systems have been proposed but in most applications there remains no guarantee that estimates are 'best'.

There are few reported applications of this technique to the estimation of states and parameters of chemical process systems. Coggan and Noton (5) demonstrated the extension of the techniques to industrial processes with simulated measurements and like many other reported applications, the simulations are performed by machines of far greater power than a process control minicomputer. In a real process application, it is necessary to execute the filter algorithm and integrate the model equations in real time so that states and parameters can be used in an optimal control scheme. There are few reported applications of real time, on-line Kalman filtering in chemical engineering.

This thesis is concerned with estimation of states and parameters of a double effect evaporator by the extended Kalman filter algorithm. The research is composed of the following four tasks:

(1) A survey of Kalman filtering techniques and their applications with special reference to the computational features of the algorithm. The thermal dynamics of heat exchangers is also briefly reviewed.

(2) Construction of the hardware and software links between the computer and evaporator.

(3) On-line and off-line simulation of steady-state and dynamic models of the evaporator. Dynamic modelling is restricted to the heat transfer mechanisms of the evaporator.

(4) On-line and off-line filtering experiments to prove the feasibility of implementing the algorithm in real time and to investigate the influence of filter statistics upon accuracy of estimation.

Thesis Outline by Chapter

Chapter 2 is devoted to a review of the linear and non-linear Kalman filter algorithms. Particular attention is paid to reported improvements in computational efficiency in terms of execution time and numerical errors involved in approximations. Finally, a brief review of heat exchanger dynamics, relevant to the double effect evaporator, is presented.

The double effect evaporator, its operation and instrumentation and the link to the computer system are described in Chapter 3. Detailed plant description is provided in Appendix 1, and the construction of the computer/data logger interface is given in Appendix 2.

Chapter 4 describes the computer programs available for the computer-plant system. This includes the standard manufacturers software and packages developed as part of the research for interactive on-line operations - BASELINE (Appendix 3) and interactive digital simulation - ASP (Appendix 4). Once constructed, the packages are available to any programmer with a knowledge of BASIC.

In Chapter 5, the steady state and dynamic models of the double effect evaporator are derived. From an eighteen order system (Appendix 5), a fourth order reduced dynamic model is derived by assuming the system vapour pressure is controlled. This simplified model is suitable for implementation in the real-time Kalman filter algorithm.

Chapter 6 describes the on-line implementation of steady state and dynamic models. The on-line experimental method and computer programs (Appendix 6) are presented for calibrations, steady state runs, dynamic logging and Kalman filtering. Off-line simulation of the comprehensive and reduced models of Chapter 5 is also discussed.

In Chapter 7, the results of the experiments described in Chapter 6 are analysed and discussed. Relevant tables and figures are to be found in Appendix 7. The principal study of Kalman filtering is extended from on-line implementation to an off-line investigation into the influence of the process noise statistics upon filter convergence. The results of filtering with two alternative parameter prediction strategies, over a wide range of plant operations, are compared.

Chapter 8 presents a concluding summary of results and recommendations for further study.

CHAPTER 2

LITERATURE REVIEW

2.1 Introduction

In the application of control to chemical engineering plant, some form of mathematical description of the physical process is required. A process operator is aware of simple relationships between operating conditions and measurements and adjusts controls accordingly. For sophisticated process control and optimisation, a detailed mathematical model, describing steady-state and dynamic responses, must be formulated. In many cases, the physical information available for developing an accurate model is limited and many variables may not be accessible for measurement. In other instances, the physical form of the model and perhaps some of the parameters are known from theoretical analysis or previous tests. However, in all cases, the model cannot be described accurately without the estimation of unknown parameters from experimental results. The installation of an on-line computer provides high-speed access to measurements and sufficient computing power to apply modern theory in the identification of the model. A great number of methods can be utilised in the solution of these process identification and parameter estimation problems, each depending upon the modelling method and the availability of experimental data.

The purpose of this review is to survey the methods available for on-line process identification (taken to include the special case of parameter estimation) with special reference to the technique of Kalman filtering. The computational difficulties of implementing this technique in real time are considered together

with reported applications, including those to chemical engineering. Finally, the mathematical modelling of heat transfer equipment is briefly reviewed.

2.2 Process Identification

Process identification is defined by Åström (6) as,

"the determination, on the basis of input controls and output measurements, of a mathematical model equivalent to the process under consideration."

Identification techniques vary according to the structure of model, the criterion chosen to determine equivalence, the calculation technique and the quantity and quality of the experimental data. The following broad classes of problems necessitate identification techniques:-

1. The determination of parameters in algebraic models from experimental measurements.

2. The off-line determination of states and parameters in dynamic models from plant output data.

3. The on-line modelling of noisy dynamic processes, where a plant output signal is used to generate an instantaneous estimate of state and parameters in a process model.

Although this review is concerned principally with the third class of problem, a number of general reviews of identification techniques in all three classes are reported by Nieman et al (7), Seinfeld (8) and Cuenod and Sage (9).

Techniques for the solution of the third type of problem are classified as sequential or non-sequential. In the sequential approach, state variables and

parameter estimates are generated at each sampling (measurement) instant. In non-sequential methods, the estimation is based on a series of samples over a known period of time. Further, in non-sequential methods, the structure of the model may be known, from a physical description of the process, or completely unknown (the 'black-box' approach). These include the methods of quasilinearisation by Bellman (10), correlation analysis by Briggs et al (11), and the numerical inversion of the Laplace transform applied by Price (12).

A sequential solution to the estimation problem is also referred to as a filter since current state estimates as well as parameter estimates are generated as the output measurements become available, hence continuously filtering the system. Thus the filtering problem is concerned with estimating the current state of a dynamic system based on all past and present measurements. The weighting of previous measurements in the filter calculations is referred to as the filter memory.

Historically, filtering theory has passed through three consecutive periods. The first period started with the Wiener-Kolmogorov theory of steady state filtering for stationary stochastic processes (2) where solutions are obtained in the frequency domain. The work of the second period is based on the linear, discrete time filtering problems for non stationary processes using the concept of state variables. This work is referred to as Kalman filtering after the original classical paper by Kalman (3). Finally, in the third period, the work is directed towards Kalman filtering for non-linear systems, e.g. Jazwinski (13), and distributed parameter systems by Seinfeld (14).

2.3 Mathematical Representation of the Process

The structure of the model selected to represent the process has a great influence upon the identification technique and hence the required on-line computation time. In the technique of Kalman filtering the distinction between linear and non-linear models is of great significance. The systems under consideration are restricted to non-distributed parameter models.

2.3.1. Linear system

A linear dynamic stochastic system can be described by the vector set of first order differential equations,

$$\dot{x}(t) = A(t)\,x(t) + B(t)\,u(t) \qquad 2.3.1$$

$$y(t) = M(t)\,x(t) + v(t) \qquad 2.3.2$$

where x is an n x 1 state vector, y is an m x 1 measurement vector, u is a p x 1 vector of system disturbances, v is a m x 1 vector of random measurement disturbances, A(t) is the n x n plant matrix, B(t) is the n x p driving matrix and M(t) is the p x n measurement matrix.

A special case of the general linear system is the linear stationary model,

$$\dot{x}(t) = A\,x(t) + B\,u(t) \qquad 2.3.3$$

$$y(t) = M\,x(t) + v(t) \qquad 2.3.4$$

By integration equation 2.3.1 can be converted into a discrete state equation giving

$$x(k+1) = \Phi(k+1,k)x(k) + \Gamma(k+1,k)\,u(k) \qquad 2.3.5$$

$$y(k) = M(k)\,x(k) + v(k) \qquad 2.3.6$$

where $\Phi(k+1,k)$ and $\Gamma(k+1,k)$ are the state transition matrices for the

interval t_k to t_{k+1}; $\Phi(k,k) = 1$ and $\Phi(k+1,k) = 1$ at steady state.

For a linear system the transition matrices are given by

$$\Phi(k+1,k) = \exp(A \cdot \Delta t) \qquad 2.3.7$$

$$\Gamma(k+1,k) = \int_{t_k}^{t_{k+1}} \exp(A \cdot (t + \Delta t - \tau)) \cdot d\tau \qquad 2.3.8$$

where $\Delta t = t_{k+1} - t_k$

2.3.2 Non-linear system

A non-linear stochastic system can be represented by

$$\dot{x}(t) = f(x(t), u(t), p(t)) + w(t) \qquad 2.3.9$$

$$y(t) = h(x(t), u(t)) + v(t) \qquad 2.3.10$$

where $p(t)$ is a vector of unknown parameters, $u(t)$ are the system inputs and controls, $w(t)$ are the system random disturbances and f and h are non-linear functions.

Åström (6) differentiates between non-linearity in the state variables and non-linearity in the parameters. These two aspects of linearity have no relation since a system normally referred to as linear may be non-linear in the parameters. By expanding the state vector to include the parameter vector,

$$\dot{x}(t) = f(x(t), u(t)) + w(t) \qquad 2.3.11$$

the estimation of states and parameters becomes one kind of calculation.

The discrete non-linear system is given by,

$$x(k+1) = f'(x(k), u(k)) + w(k) \qquad 2.3.12$$

$$y(k) = h'(x(k), u(k)) + v(k) \qquad 2.3.13$$

where f' and h' are non-linear transition functions.

As a first approximation, a randomly varying parameter can be represented by

$$\dot{x}_p(t) = 0 \qquad 2.3.14$$

or in discrete form

$$x_p(k+1) = x_p(k) \qquad 2.3.15$$

where the corresponding diagonal element of the augmented transition matrix is unity.

Coggan and Noton (5) and Noton (15) define a parameter as a continuous variable with random increments added at each sampling time. During the sampling interval, the effect of the added increment is to cause the variable to decay towards the mean,

$$x'_p(t) = \frac{(\bar{x}_p - x_p(t))}{T_p} \qquad 2.3.16$$

and the corresponding transition equation is

$$x_p(k+1) = \alpha_p x_p(k) + (1 - \alpha_p)\bar{x}_p + (1 - \alpha_p^2)^{\frac{1}{2}} \sigma_p \quad w(k) \qquad 2.3.17$$

where $w(k)$ is an uncorrelated random process having zero mean and unit covariance, α_p is the autocorrelation coefficient for x_p over the sampling interval s, T_p is a filter time constant and

$$\alpha_p = \exp(-s/T_p), \qquad 2.3.18$$

σ_p^2 is the variance and $\bar{x}_p$ the mean of $x_p(k)$. The rate of decay to the mean value is a function of α_p . When $\alpha_p = 1$, the $x_p(k)$ are correlated, equation 2.3.17 becomes identical to equation 2.3.14. When $\alpha_p = 0$, the $x_p(k)$ are uncorrelated, $x_p(k+1)$ is a random variable oscillating about the mean $\bar{x}_p$.

2.4 The Kalman Filter

2.4.1 Linear Systems

A number of approaches to the linear filtering problem have been proposed in the literature. Different criteria, usually minimum-variance or least-squares have been used to derive a discrete or continuous recursive filter algorithm. In the work of Kalman (3) and Kalman and Bucy (16) the estimate of state is treated as a conditional expection viewed as an orthogonal projection in Hilbert space. The same problem is solved by Bayes theorem by Ho and Lee (17) and Cox (18), who uses a dynamic programming formulation. Bellman et al (19) use variational methods to derive a two-point boundary-value problem which is solved by invariant imbedding. A theorem of least-squares due to Gauss is used by Goldman and Sargent (20), and Aoki (21), utilises the concept of maximum-likelihood.

For a linear stationary system, where the process and measurement noise is Gaussian, the maximum-likelihood, minimum-variance and least-squares estimates are the same. Even for non-linear, non-Gaussian noise the least-squares estimate minimises the covariance of the estimate (3). A number of different derivations of the linear Kalman filter are provided by Sorensen (22).

Consider the linear discrete stochastic system described by

$$x(k+1) = \Phi(k+1,k)\,x(k) + \Gamma(k+1,k)\,w(k) \qquad 2.4.1$$

$$y(k) = M(k)\,x(k) + v(k) \qquad 2.4.2$$

The respective covariances of w(k) and v(k) are given by

$$Q(k) = E\{w(k)\, w(k)^T\} \qquad 2.4.3$$

$$R(k) = E\{v(k)\, v(k)^T\} \qquad 2.4.4$$

The filter algorithm may be written as a set of prediction and estimation equations as follows :-

Prediction :

$$x(k+1|k) = \Phi(k+1,k)\, x(k|k) \qquad 2.4.5$$

$$P(k+1|k) = \Phi(k+1,k)\, P(k|k)\, \Phi^T(k+1,k) + \Gamma(k+1,k)\, Q(k+1)\, \Gamma^T(k+1,k) \qquad 2.4.6$$

Estimation :

$$K(k+1) = P(k+1|k)\, M^T(k+1)\left[M(k+1)\, P(k+1|k+1)\, M^T(k+1) + R(k+1)\right]^{-1} \qquad 2.4.7$$

$$x(k+1|k+1) = x(k+1|k) + K(k+1)\left[y(k+1) - M(k+1)\, x(k+1|k)\right] \qquad 2.4.8$$

$$P(k+1|k+1) = \left[I - K(k+1)\, M(k+1)\right] P(k+1|k) \qquad 2.4.9$$

$$P(k+1|k+1) = \left[I - K(k+1)M(k+1)\right] P(k+1|k)\left[I - K(k+1)M(k+1)\right]^T + K(k+1)\, R(k+1)\, K^T(k+1) \qquad 2.4.10$$

where $x(j|i)$ denotes the estimate of the state x at time j, given observations through time i. $P(j|i)$ denotes the covariance of the error in this estimate. The term $\left[y(k+1) - M(k+1)x(k+1|k)\right]$ of equation 2.4.8 represents the difference between the measurement and the predicted measurement. The estimate of the state vector $x(k+1|k+1)$ is the sum of predicted state $x(k+1|k)$ and the weighted measurement error. The weighting matrix $K(k+1)$ is called the filter gain matrix. The initial state estimate and the initial covariance, $x(o|o)$ and $P(o|o)$, determine the basic speed of response of the filter. The magnitude of the initial state error will cause an initial error in the covariance matrices which

results in an initial error in the filter gain $K(k+1)$. This initial error affects the time required for the filter to reach its steady state (convergence). Similarly, if $P(o|o)$ is large the filter gain will be large initially. This also increases the time to reach steady state, since the filter will initially rely upon current noisy measurements.

Aoki (21) shows that the alternative equation for correcting the error covariance matrix (equation 2.4.10) is preferable to equation 2.4.9 since the right hand side of 2.4.10 is the sum of two symmetric positive definite matrices while 2.4.9 is at best the difference of two positive definite matrices. Consequently, 2.4.10 is better conditioned for numerical computation and will retain the positive definiteness and symmetry of $P(k+1|k+1)$.

In the original derivation of the algorithm (3) a number of valuable features of the linear estimator are described. Namely, that the estimate is uniformly assymptotically stable and that the convergence of the variances of the estimates, as each successive measurement is processed, is insensitive to round off errors provided the system is observable and controllable. Coggan and Noton (5) interpret the concepts of observability and controllability as follows:

(1) A system is observable, if with perfect measurements and no random disturbances, all the state variables can be determined after a finite number of measurements.

(2) A system is controllable if all the states are excited by the random disturbances $w(k)$.

The recursive algorithm has great appeal in on-line applications because

the filter utilises all the available data, including all current observations and prior data without storing previous measurements. It is clearly optimal to base an estimate on all the available information. However, the algorithm depends upon a knowledge of the dynamics, measurement function and statistical properties of the system, Q(k) and R(k). If the dynamics are imprecisely known, the filter may diverge from the true state due to model inaccuracies (23). Jazwinski (24) has suggested that divergence can be minimised by limiting the memory of the filter, thus placing less weight on the earlier measurements. One such filter developed by Tarn and Zaborsky (25), exponentially increases the measurement noise covariance matrix of old observations. The resulting modification to the filter algorithm is at equation 2.4.6 which becomes

$$P(k+1|k) = \frac{1}{c}\,\Phi(k+1,k)\,P(k|k)\,\Phi^{T}(k+1,k) + \Gamma(k+1,k)\,Q(k+1)\,\Gamma^{T}(k+1,k) \qquad 2.4.10$$

where $c \leqslant 1$ and is chosen a priori by the designer and has the effect of escalating exponentially with time the covariance matrix of each past observation, i.e. making past observations have less effect upon current estimates. Goldman and Sargent (20) successfully utilise a number of limited memory filters including the oscillating memory filter of Jazwinski, in which the memory is cleared at regular intervals and the filter is restarted. Improvement of the filter in uncertain environments is reviewed by Leonedes and Pearson (26) who conclude that the optimal technique depends upon each particular problem, its accuracy requirements and available computer storage. Errors in the mathematical model have been studied analytically by Huddle and Wismer (27) and Griffin and Sage (28) to enable the reduction of high order systems.

The linear estimator requires a knowledge of the process and measurement noise covariance matrices Q(k) and R(k). In most on-line systems they are

unknown and must be approximated. Mehra (29 and 30) proposes an on-line method for their estimation which assumes the system is time invariant and completely controllable and observable. A similar approach based on an autogressive moving-average model is developed by Krause and Graupe (31).

2.4.2 Non-linear Systems

Non-linear filtering theory has developed from the classical linear Kalman filter in two ways. The first, is basically an extension of the linear theory in which a Taylor series expansion, neglecting second and higher order terms, is used to linearise the state and/or measurement functions. Conditions of optimality of the estimate and its error covariance are no longer guaranteed and divergence and bias affect the numerical stability of the filter algorithm. The second approach is based on the exact equations satisfied by the conditional expectation, minimum variance, or conditional probability density function. It can be shown that the optimal filter cannot be obtained by a finite dimensional system. Finite dimensional approximations have been employed to derive suboptimal filters, each derivation based upon the definition of optimality and the approximation. Amongst the many reported derivations of suboptimal filters, those of Jazwinski (32) and Kushner (33) are representative.

Consider the non-linear stochastic system described by

$$x(k+1) = f'(x(k), u(k)) + w(k) \qquad 2.4.11$$

$$y(k) = h'(x(k), u(k)) + v(k) \qquad 2.4.12$$

where $w(k)$ and $v(k)$ are white Gaussian noise processes with covariances

given by

$$E\ \{w(k)\ w^T(k)\} = Q(k) \qquad 2.4.13$$

$$E\ \{v(k)\ v^T(k)\} = R(k) \qquad 2.4.14$$

If the system equations are linearised about the current estimate of state by means of a truncated Taylor series expansion, the state transition matrix becomes,

$$\bar{\Phi}(k+1,k) = \Delta t\ \frac{\partial f'(x(k),\ u(k))}{\partial x(k)}\ \Big|_{x(k|k)} + I \qquad 2.4.15$$

and the measurement matrix is linearised about the predicted state,

$$\bar{M}(k+1) = \Delta t\ \frac{\partial h'(x(k),\ u(k))}{\partial x(k)}\ \Big|_{x(k+1|k)} + I \qquad 2.4.16$$

where the bar is taken to represent linearisation about the current estimate.

The linearised filter equations are as follows:

Prediction :

$$x(k+1|k) = x(k|k) + \int_{t_k}^{t_{k+1}} f'(x(k|k),\ u(k))\ dt \qquad 2.4.17$$

$$P(k+1|k) = \bar{\Phi}(k+1,k)\ P(k|k)\ \bar{\Phi}^T(k+1,k) + Q(k+1) \qquad 2.4.18$$

Estimation :

$$K(k+1) = P(k+1|k)\ \bar{M}^T(k+1)\left[\bar{M}(k+1)\ P(k+1|k)\ \bar{M}^T(k+1) + R(k+1)\right]^{-1} \qquad 2.4.19$$

$$x(k+1|k+1) = x(k+1|k) + K(k+1)\left[y(k+1) - \bar{M}(k+1)\ x(k+1|k)\right] \qquad 2.4.20$$

$$P(k+1|k+1) = \left[I - K(k+1)\ \bar{M}(k+1)\right]\ P(k+1|k)\left[I - K(k+1)\bar{M}(k+1)\right]^T + K(k+1)\ R(k+1)K^T(k+1) \qquad 2.4.21$$

where $K(k+1)$ is the filter gain. This algorithm is the first-order or extended Kalman filter. Unlike the linear filter, there is no theoretical proof of

convergence and stability but it is possible to determine by inspection whether or not the state variables are excited by the random disturbances (controllability). Observability is not always obvious, and Aoki (21) suggests that it can be determined during computation. The algorithm has been extended to account for non-Gaussian noise and disturbances by Friedland and Bernstein (34).

Convergence can be improved by the inclusion of second-order terms in the Taylor series expansion of equations 2.4.15 and 2.4.16, but only at the expense of computation time. The justification of added complexity and computational requirements in these so called second-order filters depends upon the degree of non-linearity of the system. Reported filtering of simulated systems, such as Athans (35) and Schwartz and Stear (36) are in disagreement as to the value of such improvements. The simulated systems are, however, formulated solely for the purpose of testing the usefulness of extensions to the filter equations. Athans (35) states that unpublished results indicate that second-order filters diverge more than first order filters. This could be true if the Taylor series expansion of equation 2.4.15 is divergent.

Denham and Pines (37) have proved that the effect of measurement function non-linearity can be reduced by iterating about the prediction stage of the algorithm. The estimate obtained at equation 2.4.20 is used to recalculate $\bar{M}(k+1)$ for equations 2.4.19 and 2.4.20 until the estimate convergences. Errors due to the linearisation of the state equations can be iterated similarly. An estimate obtained at equation 2.4.20 is used to recompute $\bar{\bar{\Phi}}(k,k+1)$ which smooths back the estimate to t_k. This modified previous estimate is then re-estimated through the prediction and estimation stages of the algorithm. until the estimate converges. This iterated, extended Kalman filter was first

described by Wishner et al (38).

The effect of bias or drift in measurements can be incorporated into the model by relating the predicted value of a measurement y_p to the instrument reading y_m,

$$y_p = y_m + \beta + \gamma t \qquad 2.4.22$$

Goldman and Sargent (20) regard the bias parameter, β , and drift parameter, γ , as state variables and include them in the augmented state vector. Friedland (39) has studied the effects of bias in the state equation and derives a two-level filter algorithm. The state is first estimated as if no bias is present and then this estimate is corrected to account for bias. Computationally, this decoupling of state estimation and bias correction is attractive because the dimension of the state vector is not increased.

In on-line applications of the extended Kalman filter, the non-linear mathematical model is an approximation to the true process behaviour. Consequently, the process noise covariance matrix, Q, cannot be accurately determined. Wells (40), suggests that Q can be taken to represent either uncertainty in the model and the linearisations, or the process noise statistics. In this case, the numerical values assigned to Q depend upon trial and error methods and an intuitive feel for the accuracy of the model.

2.5 Computational Considerations

The computational requirements of the Kalman filter presents a formidable obstacle to its real-time implementation. In systems with a large number of state variables, the sampling frequency of process measurements is limited by both the necessity to minimise numerical error at the prediction stage and by the computation of the matrix inverse at the correction stage. The first fully reported case of real-time non-linear filtering on a minicomputer is by Schmidt et al (41) in which a study of the guidance system of the USAF/ lockheed C5 transport aircraft reveals the practical problems of storage, timing and computation of transition matrix.

In the case of linear systems the transition matrices, $\bar{\Phi}$ and Γ , can be computed a priori from the exponential matrix,

$$\bar{\Phi}(k+1,k) = \exp(A\Delta t) \qquad 2.5.1$$

where A is the plant matrix and $\Delta t = t_{k+1} - t_k$. Buffham and Kropholler (42) review the available methods for the computation of the exponential matrix including the class of "stiff" problems in which the absolute values of the smallest and largest eigenvalues of A differ considerably. Since the estimation error covariance matrix, P, does not depend upon the observations (equations 2.4.5 - 2.4.10), the values of P and K can also be computed a priori. In real time applications this provides a possibility of trading processing time against storage by precomputing P and K and storing K.

In non-linear systems, the matrices $\bar{\Phi}$ and $\bar{M}$ are those of the linearised system and thus may require computation at each filter cycle. The minimum

sampling interval will be increased further by the necessity to reduce the integration step length for the prediction of state variables (equation 2.4.17).

2.5.1 Filter Algorithm

Wells (43) proposes an approximate method for the elimination of matrix inverse for non-linear systems by considering only the diagonal elements of the predicted error covariance matrix, $P(k+1|k)$, (equation 2.4.18). The consequent reduction in processing time and accuracy of estimation is not reported.

Jazwinski (13) and Singer and Sea (44) show how the matrix inversion is reduced by processing the measurement vector one measurement set at a time. When the measurement sets are uncorrelated, the measurement vector can be ordered so that the noise covariance matrix is of the block diagonal form,

$$R(k+1) = \begin{bmatrix} R_1(k+1) & m_1 & & & \\ & & R_2(k+1) & m_2 & \\ & & & \ddots & \\ & & & & R_t(k+1) \quad m_t \end{bmatrix} , \qquad 2.5.2$$

where each $R_i(k+1)$ is an $m_i \times m_i$ covariance matrix and the sum of the dimensions of the lesser matrices equals that of the original $R(k+1)$ matrix. The corresponding measurement vector is partitioned as

$$y(k+1) = \begin{bmatrix} y_1(k+1) \\ y_2(k+1) \\ \\ y_{\dot{t}}(k+1) \end{bmatrix} = \begin{bmatrix} M_1(k+1) \times (k+1) + v_1(k+1) \\ M_2(k+1) \times (k+1) + v_2(k+1) \\ \\ M_{\dot{t}}(k+1) \times (k+1) + v_{\dot{t}}(k+1) \end{bmatrix} \qquad 2.5.3$$

Thus there are $\dot{t}$ uncorrelated measurement sets, the i^{th} set having m_i elements.

The filter algorithm becomes,

Prediction:

1. $$x(k+1|k) = x(k|k) + \int_{t_k}^{t_{k+1}} f(x(k|k), u(k)) \, dt \qquad 2.5.4$$

2. $$P(k+1|k) = \bar{\Phi}(k+1,k) \, P(k|k) \, \bar{\Phi}^T(k+1,k) + Q(k+1) \qquad 2.5.5$$

Estimation:

3. Set $i = 1$

4. $$K_i(k+1) = P(k+1|k) \, \bar{M}_i^T(k+1) \left[\bar{M}_i(k+1) P(k+1|k) \bar{M}_i^T(k+1) + R_i(k+1) \right]^{-1} \qquad 2.5.6$$

5. $$x(k+1|k+1) = x(k+1|k) + K_i(k+1) \left[y_i(k+1) - \bar{M}_i(k+1) \times X(k+1 \, k) \right] \qquad 2.5.7$$

6. $$P(k+1|k+1) = \left[I - K_i(k+1) \bar{M}_i(k+1) \right] P(k+1|k) \left[I - K_i(k+1) \bar{M}_i(k+1) \right]^T + K_i(k+1) \, R_i(k+1) \, K_i^T(k+1) \qquad 2.5.8$$

7. If $i < \dot{t}$ put $i = i + 1$ and return to step 4.

8. Set $k = k + 1$ return to step 1.

In this sequential processing procedure, the inversion of one m x m matrix is replaced by the inversion of $\dot{t}$ matrices of dimensions $m_1 \times m_1$, $m_2 \times m_2$, ..., $m_t \times m_t$. In the special case where all the measurement noises are uncorrelated, ($m = \dot{t}$), the inversions reduce to m scalar divisions.

One column of the gain matrix, $K_i(k+1)$, is formed during each measurement iteration and $M_i(k+1)$ is a row vector. This technique yields the identical solution to the extended Kalman filter algorithm with a theoretical reduction in the computational requirements of the covariance correction equation of over 50% (44). In addition, the iterative nature of the algorithm permits priority and interrupt measurement strategies without disturbing the Kalman filter operation.

2.5.2 Transition Matrix

Accurate prediction of state variables by the state transition method is not possible for non-linear systems and consequently an alternative method (e.g. Runge-Kutta) must be adopted in equation 2.5.4. To predict the state covariance matrix (equation 2.5.5.), some form of transition matrix is required. For the continuous non-linear system,

$$\dot{x}(t) = f(x(t), u(t)), \qquad 2.5.9$$

the transition matrix is expressed as a Taylor series expansion

$$\bar{\Phi}(k+1,k) = I + \Delta t \frac{\partial f(x(t), u(t))}{\partial x}\bigg|_{x = x(k)} + \frac{\Delta t^2}{2} \frac{\partial^2 f(x(t), u(t))}{\partial x_i \partial x_i}\bigg|_{x = x(k)} + \text{higher order terms} \qquad 2.5.10$$

When the series is truncated after the first order term, the transition matrix is that used in the extended Kalman filter, and after second-order terms, in the second-order filter. Clearly the second-order method requires greater computer time and storage, although comparisons of the accuracy of the

methods (35 and 38) do not consider problems of this type. Both methods are susceptible to errors as the sampling interval, Δt, increases and the series may even diverge. Since the transition matrix represents the influence of the model upon the calculation of the filter gain and covariance matrices, these errors must be minimised. This may not be possible in real-time applications, although some trading of computer time and accuracy has been reported (41). One possibility suggested by Wells (40) is to reduce errors by "judicious" selection of the Q matrix. However, no theoretical method has been developed for non-linear systems.

McLean et al (45) derive the transition matrix continuously by solving the state equations with n sets of perturbation equations, each with a unit initial condition on one of the x_i and the remainder zero. As the state equation is solved for each unit initial condition, the corresponding column of the transition matrix is formed. After each filter cycle, the initial conditions are reset to unity or zero and the computation is carried out until the next observation time. This algorithm utilizes all available computer time between observations, but is not suitable for highly non-linear systems where the integration method requires a small step length.

2.5.3 Prediction of State Variables

Selection of a numerical integration method for the state variable prediction stage of the filter algorithm depends upon available computer time, storage and required accuracy. Integration methods have been reviewed by Distefano (46) including the classical Euler and Runge-Kutta methods

and more recent methods for the solution of "stiff" dynamic equations. Wells (40), in an off-line Kalman filter experiment, suggests the Euler method but notes significant increase in error with large step length. Schmidt (41), in a real-time application, applies the transition matrix method of the linear filter and experiences difficulty in deriving a sufficiently accurate $\bar{\Phi}(k+1,k)$.

2.5.4 Observation Interval

In a real-time application, the minimum observation interval is the sum of the times required for measurement, state variable prediction, executions of a filter cycle and output of information and control signals. If the interval is excessive the computation of $\bar{\Phi}(k+1,k)$ will generate significant errors, so that for a highly non-linear system, measurements should be made as frequently as possible. Athans (47), presents an on-line strategy for selecting the best single measurement at any given time so that the measurement policy can be specified in advance. Mehra (48) compares the extended Kalman filter at different measurement rates in the simulation of a balistic re-entry vehicle. The use of measurement averaging during the filter cycle time is studied by Schmidt et al (41). While this averaging process smooths the signal noise as desired, there is a danger of smoothing the signal itself and causing estimation bias.

2.5.5 Storage and Processing Time

The requirements of storage and execution speed of the non-linear filter algorithm are a function of the system order and the number of

measurements. Mendel (49), derives an equation for the computation time of any system based upon the times associated with total number of multiplications, additions and computer logic time. The total storage is reduced by making explicit use of the structure of the system matrices and processing time is reduced by the sequential algorithm (equations 2.5.4 - 2.5.9). Coggan and Wilson (50) have implemented the Kalman filter algorithm on a PDP-8 minicomputer with 4K of core. Inclusive of matrix subroutines, the computer will support a ninth-order system with a filter cycle time of nine seconds. Wells (40) on a more powerful Univac 1108 computer, reports a processing time of 1.8 msec for a sixth order system (compared with 0.6 seconds for the equivalent system on the PDP-8).

2.5.6 Filter Performance

To minimise the quantity of data output during a filter cycle, it is convenient to express the filter performance as a single vector of estimation errors. When a digital simulation is used to generate "plant" data, the actual states x_a are available and the filter performance can be compared on the basis of the following vectors.

1. Root mean square error - Wishner et al (38).

$$c(k) = \sum_{i=1}^{N} \frac{(x_a(k) - x(k|k))^2}{N}^{\frac{1}{2}} \qquad 2.5.12$$

where N is the number of samples in the run.

2. Ratio of scaled variables - Coggan and Noton (5).

$$d(k) = \log_{10} \frac{x(k|k)}{x_a(k)} \qquad 2.5.13$$

In a real application, x_a is never known. The matrix of error covariances, $P(k|k)$, is the only information available (51). For any variable the theoretical estimation error vector can be expressed as,

$$e(k) = \log_{10}\left(1 + \frac{\sigma_f(k)}{\bar{x}} \right) \qquad 2.5.14$$

where $\sigma_f(k)$ is the vector of square roots of the diagonal elements of $P(k\,k)$ and $\bar{x}$ is the vector of state means. If the state is not randomly varying about a mean value the error can be expressed as

$$e(k) = \log_{10}\left(1 + \frac{\sigma_f(k)}{x(k|k)} \right) \qquad 2.5.15$$

but this does not account for bias and drift in the estimate.

If the physical model is accurately described by equations 2.4.11 and 2.4.12, $P(k|k)$, can be used to describe the manner in which the estimates converge to the true state. Examination of $P(k|k)$ element by element is unsatisfactory, since it involves n^2 elements. Sorensen (22), introduces the concept of the error ellipsoids defined as the n-dimensional surfaces of constant probability density. The direction and magnitude of the principal axes of the ellipsoids are defined by the eigenvectors and eigenvalues of $P(k|k)$ which is positive-definite (i.e. complete controllability and observability).

The error ellipsoid is used to characterise the variation of the estimates about the true states. For a given confidence limit, it is possible to integrate the probability density over the surface of the ellipsoid to obtain the probability that the true state will lie within the ellipsoid. When the

magnitude of an axis decreases, the conclusion is that the error in the estimate is decreasing in the direction of that state variable. As the number of filter cycles increases, the magnitudes of the axes decrease, i.e. the filter converges. A two-dimensional example is described diagramatically by Bryson and Ho (52) and by computer animated film by Woodside (53).

2.6 Kalman Filter Applications

2.6.1 General Applications

Since the original classical paper by Kalman (3), linear and non-linear filtering theory has been applied successfully in the aerospace field. Certainly, many of the theoretical and practical advances have been contributed by aerospace and electrical engineering researchers. The first practical application of the extended Kalman filter is by Smith, Schmidt et al to space vehicle guidance (45) and orbit determination (54). The dynamic equations for these systems are well-known from satellite orbit mechanics and the equations of motion. The measurements, based on radar and in-board celestial readings are subject to errors, the statistical characteristics of which can be determined. These applications are reviewed by Schmidt (55) and Sorensen (22). Re-entry vehicle trajectory estimation studied by Athans et al (35) presents a more severe modelling problem - the dominant forces are aerodynamic rather than gravitational. Because of the relatively poor knowledge of atmospheric conditions, these forces cannot be described accurately. Furthermore, the dynamics are much more non-linear than orbit dynamics and may be

expressed in different co-ordinate systems. Mehra (48) proves that bias is reduced by the selection of the least non-linear co-ordinate system and by implementing an iterative filter algorithm.

Most reported results in this field are either concerned with the simulation of known system dynamics corrupted by noise to provide "measurements", or only successful final results are published. The practical application of the Kalman filter on-line to a real process with uncertain dynamics is not extensively reported. A detailed study of the application of the linearised theory to the USAF/Lockheed C-5A aircraft navigation is reported by Schmidt et al (41) including the real-time computational problems of storage, numerical precision, observation interval and linearised transition matrix calculation.

Kalman filtering has become an integral part of the broader field of modern control theory, where accurate state and parameter estimation is required for an optimal control scheme. The theory is included in control textbooks by Åström (56), Bryson and Ho (52) and Sage and Melsa (57).

Outside of the aerospace and chemical engineering fields, Kalman filtering is used by Wheelwright and Makridakis (58) as a technique for preparing short to medium-term economic forecasts, where although more accurate, it is found to be more expensive than conventional time-series analysis. Other recent applications include agricultural pest control by Ford-Livene (59) in predicting the number of pests and optimum pesticide distribution from a pest reproduction model; the surveillance and

control of traffic movements by Szeto (60); harmonic analyis by Sharma et al (61); nuclear reactor control by Godbole (62); the control of a cement mill by Belanger (63) and telescope position estimation by Tse (64).

2.6.2 Chemical Engineering Applications

The identification techniques developed in the aerospace problems are directly applicable to chemical engineering systems. In most processes the system dynamics are non-linear, uncertain and contain unknown parameters and the measurements are affected by noise. Often, when reliable dynamic models are derived, they consist of sets of distributed parameter differential equations too complex for on-line, real-time filtering.

The selection of the Kalman filtering technique for the identification of chemical engineering processes is based upon the following:-

1. Some of the difficulties associated with model building and parameter identification in multivariable systems are overcome. Since the structure of the model is retained and a measure of the accuracy of the estimation is available as $P(k+1|k+1)$, the method lends itself to the development of suitable models and testing of model simplification.

2. The filter is robust in as much as approximate models do not drastically affect the accuracy of estimation.

3. Since the algorithm is sequential in operation and discrete measurements are always made sequentially, existing on-line measurement strategies require no modification.

4. Computationally, the algorithm is attractive for on-line use because previous measurements are not stored. Thus a system with a large number of state variables can be handled by a comparatively small process control computer.

5. Due to erratic disturbances, a chemical process is seldom at steady-state which precludes the use of many alternative identification methods. The Kalman filter can be utilised during normal process operations.

6. The Kalman filter can be extended to include process non-linearites and transport lags.

7. Measurement noise statistics, R, can be derived from separate on-line experiments. The selection of the process noise matrix, Q, is more complex but this problem is by no means specific to chemical engineering applications.

8. Many chemical processes have large time constants so that problems of observation interval and on-line computation time are eliminated. The on-line filter may even be computed via a remote time-sharing terminal.

Chemical engineering applications can be conveniently divided by authors as follows:

Coggan, Noton and co-workers

One of the first chemical engineering applications of the extended Kalman filter is by Noton and Choquette, in Canada, in the identification of a reactor train for The Polymer Corporation. Initially (65), the computer was used in an off-line manner during open-loop control experiments and later (66) during closed loop experiments via a remote time-sharing

computer. Due to commercial secrecy, the mathematical model is not published but reference is made to unmeasured state variables, randomly varying parameters and transport lags. In a chemical engineering context, this on-line work has pioneered the solution of many of the practical problems of applying the filter in real-time. Although not fully computerised (some measurements are input manually via scan switches at the process control room), the overall exercise is successful, in as much as an improvement over manual control is experienced. One theoretical development from this application is the decomposition of high order systems to minimise filter computation time (67). This has particular reference to sparsely coupled subsystems with few stochastic inputs.

In England, the applications are reported by Coggan and Noton (5). This notable paper solves the theoretical problems of large numbers of state variables, parameter state equations and transport lags that are characteristic of chemical processes. An important distinction between two types of state variables is reported -

a. Interdependent state variables: variables which are dependent upon the process and are affected by disturbances either directly or indirectly

b. Non-interdependent state variables: variables which affect, but are not affected by the interdependent variables.

A state variable, x_i, is interdependent if the i^{th} row of the transition matrix contains one or more non-zero off-diagonal elements. The magnitude of the coefficients of interdependent variables in the transition matix has great influence upon observability and is discussed later.

The estimation procedure is applied to simulated systems exhibiting strong non-linearites, intermittent measurements, large random disturbances, unknown parameters, transport lags and unknown initial values. The possibility of trading model simplification for unnecessary numerical accuracy is also discussed. An approach to model reduction, prior to estimation is suggested by Coggan and Wilson (51) to minimise the number of state variables required to describe a system. The filter algorithm is extended to evaluate measurement error statistics and detect the presence of bias. Although the heat exchanger and absorber systems are simulated, feedback of these statistics, within the algorithm, improves the estimation error when the model is erroneous. The authors also report the on-line implementation of the filter algorithm on a minicomputer (50), including an investigation of the computation time per filter cycle for various dimensions of the state vector. These filter cycle times could be improved by use of the sequential processing technique. However, the description of the implementation of the software for a 10^{th} order system on a 4K computer refutes previous assumptions regarding the impracticability of the estimator algorithm.

Sargent and co-workers

The feasibiltiy of using the Kalman filter for on-line state and parameter estimation in chemical engineering systems has been reported by Goldman and Sargent (20). The extended filter algorithm is derived for disturbance-free processes and applied to the identification of a simulated distillation column and a fixed-bed catalytic reactor with superimposed Gaussian or rectangular measurement noise. The extended Kalman filter is shown to be robust in

estimating bias and drift in simulated measurements and the oscillating memory filter is proved to be less sensitive to modelling errors than the classical growing memory filter. It is reported that the convergence of the filter from initial estimates, $x(0|0)$, is accelerated by selecting a high initial estimation error covariance matrix, $P(0|0)$. However, this is only the case for systems assumed to have no process noise and accurate measurements. Klinger (68) investigates the effect of prior information in the estimation of noise free processes and concludes that theoretically unbiased convergence can be achieved from $P(0|0) = \infty . I$.

An extension of the non-linear catalytic reactor study as part of an optimal control scheme is reported by Joffe and Sargent (69) including the effects of input noise disturbance. The non-linear distributed parameter stochastic system is decomposed into a non-linear lumped parameter model. Both the process and control scheme are simulated and found to be insensitive to the statistical assumptions, initial estimates and process noise convariance of the filter algorithm.

Wells

Wells (40) applies the Kalman filter to the identification of states and parameters of a simulated, six-dimensional non-linear well-stirred reactor model. On a large off-line Univac 1108 computer, the filter cycle time is reported as 1·8 msecs, which could be further improved by the sequential processing technique. An important concept, discussed in this paper, is the analogy between the process noise covariance matrix, Q, and process

uncertainty. The magnitude of the Q matrix can be increased for systems that have dynamics that are not well understood or for state equations that represent a model simplification, thus placing more weight upon the measurements. Consequently, an exact description of the process dynamics is not necessary to achieve good estimates. In chemical engineering problems, high numerical accuracy is not required so that some model simplifications and approximations can be attempted with corresponding adjustment of the Q matrix.

Seinfeld and co-workers

Seinfeld (70) has extended the Kalman filter to stochastic systems described by non-linear parabolic and hyperbolic partial differential equations. The computational requirements of the on-line implementation of such a system are prohibitive. Gavalas and Seinfeld (71) reduce a plug flow catalytic reactor problem to a lumped-parameter system and successfully estimate state variables. The equivalent distributed-parameter system is filtered by Seinfeld et al (14), but problems of convergence and observability in distributed-parameter systems remain unsolved. The incorporation of these techniques into a distributed-parameter control problem is studied by Yu and Seinfeld (72) utilising a simulated scalar parabolic system. Since many chemical engineering systems can be only accurately modelled by distributed-parameter systems, there is clearly further useful work to be carried out in this area.

2.7 Heat Exchanger Dynamics

2.7.1 Introduction

The study of the dynamic behaviour of heat exchangers has received increasing amounts of attention from investigators. Considering the great diversity in heat exchange equipment, the endless variety of process applications and the fact that the three basic modes of heat transfer are involved to varying degrees, the field of heat exchanger dynamics is both extremely broad and complex. General reviews of the literature, such as those by Williams and Morris (73) and Williams (74) cite a substantial number of papers dealing with this subject.

This brief review is limited to shell and tube type exchangers involving an isothermal condensing medium. In particular, the dynamics of shell and tube evaporators, similar to the process under study, are considered.

Mathematical models of heat exchangers involving condensible media have been developed for use in control applications. Some researchers use an analytical approach based on a knowledge of the governing laws and the system geometry whereas others develop transfer functions from laboratory test data involving both frequency response and pulse testing methods. Within the accuracy of the assumptions, models developed by the former method are applicable for all types of input disturbance and include process non-linearites. Buckley (75) presents a comprehensive summary of the latter methods which incorporate classical frequency-response methods in the design and testing of heat exchanger control systems.

FIGURE 2.1

IDEALISED HEAT EXCHANGER

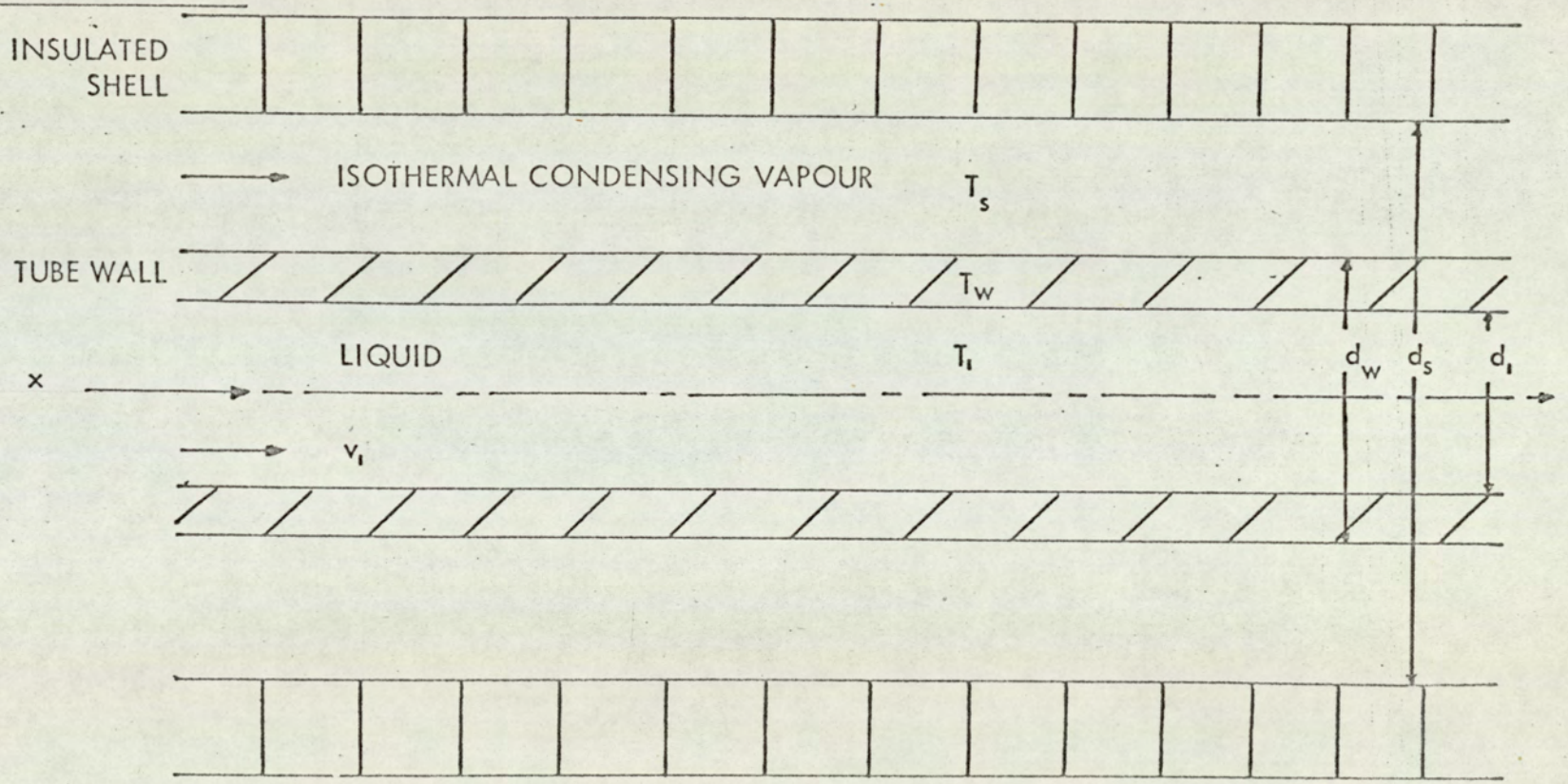

2.7.2 Analytical Methods

Figure 2.1 represents the simple case of liquid flowing through a vapour heated tube of a concentric-tube heat exchanger. An unsteady state heat balance on the process fluid is given by

$$\frac{\partial T_1}{\partial t} + v_1 \frac{\partial T_1}{\partial x} = \frac{4h_1}{\rho_1 c_1 d_1} \cdot (T_w - T_1) \qquad 2.7.1$$

on the tube wall by,

$$\frac{dT_w}{dt} = \frac{4 d_w h_s}{\rho_w c_w (d_w^2 - d_1^2)} \cdot (T_s - T_w) - \frac{4h_1 d_1}{\rho_w c_w (d_w^2 - d_1^2)} \cdot (T_w - T_1) \qquad 2.7.2$$

and on the steam space by

$$V_s \frac{d(\rho_s H_s)}{dt} = \Delta H_s - \frac{4 h_s d_o}{(d_s^2 - d_w^2)} \cdot (T_s - T_w) \qquad 2.7.3$$

where T, h, d, c, ρ and H represent temperature, local heat transfer coefficient, diamater, specific heat, density and specific enthalpy. Subscripts 1, w and s refer to process fluid, tube wall and vapour space respectively. The term ΔH_s of equation 2.7.3 represents the difference in enthalpy between vapour entering the exchanger shell and the vapour and/or condensate leaving. V_s is the shell volume and v_1 is the process fluid velocity.

These equations are formulated subject to the following assumptions:

(1) Temperature and velocity profiles of the fluid are uniform across any diameter, i.e. plug flow, and heat transfer by diffusion in the

direction of flow is negligible both in the process fluid and tube wall.

(2) The thermal conductivity of the wall is infinite in the direction at right angles to the direction of flow and zero in the direction of flow.

(3) There are no heat losses through the heat exchanger outer wall.

(4) Heat transfer at the tube surface is proportional to temperature difference.

(5) The vapour temperature, T_s, is uniform throughout the shellside of the exchanger and any condensate does not lose sensible heat.

(6) Densities, specific heat, cross sections and heat transfer coefficients are constant,

and thus represent a heat exchanger having distributed fluid thermal capacitance.

When the outlet fluid temperature response to disturbances in inlet temperature or vapour temperature is required, these assumptions render equations 2.7.1 - 2.7.3 linear. A general solution can therefore be obtained in terms of the three variables by taking Laplace transformations and solving the resulting differential equation in x for the appropriate boundary conditions, e.g. Finlay (76). The dynamics of a multipass exchange is described by Stainthorp and Axon (77) as a combination of a number of single tube exchangers with each flow reversal chamber assumed to be a first order lag. The mathematical solution is either inverted to give a time-dependent solution, or left as a transfer function from which frequency-response data may be obtained.

In industrial applications, the frequency-response data are more

acceptable in control system design because the frequency-response characteristic can be obtained directly from the transfer function of the system, frequency-response data are compatible and additive, and the techniques are extensively developed. Representative papers are those of Stermole and Larson (78) and Stainthorp and Axon (77).

The assumptions listed are not sufficient to render equations 2.7.1 - 2.7.3 linear when the response to disturbance in flow rate is required and when the shellside is non-isothermal. The non-linearity is a consequence of the dependence of heat transfer coefficient upon fluid velocity and vapour enthalpy and density upon temperature. Standard non-linear correlations, e.g. Dittus-Boelter and Nusselt equations, are available to determine heat transfer coefficients while the temperature dependence of vapour enthalpy and density is usually available in tabular form.

When industrial scale heat exchangers are considered, there are eight non-linear dynamic relationships of interest, namely the response of the tube or shellside outlet temperatures to changes in the inlet temperatures or flow rates of either tube or shellside fluid. The distributed-parameter models derived are exceedingly complex, and numerical evaluation is feasible only with the aid of a high-speed digital computer. Heidemann et al (79) develop the non-linear distributed dynamic model for a simple single-tube heat exchanger based upon experimental heat transfer coefficient correlations and constant shellside vapour pressure.

Distributed-parameter models can be simplified in two ways. Firstly, the distributed-parameter system can be represented by a lumped-parameter

analogy. Thermal capacitance is assumed to act at a point rather than as a continuous function of length. Dependence on position is thus removed and the describing equations have time as the only independent variable. An example of this approach is the work of Fricke et al (80) in which a multi-pass exchanger is represented by 6 lumped sections on the shellside and 24 lumped sections on the tube side in order to fascilitate simulation on an analog computer. The second method of simplification is linearisation of the basic model describing the distributed parameter system e.g. Stermole and Larson (78), which permits the use of Laplace transforms to generate frequency response curves. The converse of the space-lumping simplification, time-lumping, is developed for a parallel flow heat exchanger by Schmidt and Clark (81), and the corresponding computational requirements are found to be less than the conventional method. A simplification by the use of Hermitian polynomials is successfully applied by Dorri (82).

2.7.3 Evaporator Models

Mathematical models of evaporator systems reported in the literature, use both empirical and theoretical approaches. Johnson (83) fits parameters to various models of a falling-film evaporator. Nisenfeld and Hoyle (84) consider simple empirical models for feed-forward control and use two first-order lags and a time delay to represent dynamically a six-effect evaporation process.

The first theoretical derivation is by Anderson et al (85) where a lumped-parameter, sixth order model of single pan-type evaporator effect

is reduced to a third-order system by neglecting vapour space and heat transfer dynamics. In the analysis, only small variations are considered and the equations are linearised in all the variables. Andre and Ritter (86), develop the lumped-parameter dynamic equations of a double-effect evaporator and replace the vapour phase equations with their steady-state counterparts. The computer simulation of the resulting fifth order model gives excellent agreement with experimental data. This dynamic model is used further in evaporator control system design by Ritter and Andre (87) and computer control of an evaporator by Newell (88). The effect of simplification in the development of the same model (86) and alternative control strategies is developed by Newell and Fisher (89). A comprehensive model of 17-effect desalination evaporator is developed by Burdett and Holland (90) and includes the formulation of the heat transfer dynamics of the large cylindrical walls of each effect.

In a recent paper by Hamilton et al (91), the fifth order evaporator model (86) is used further in filtering experiments that provide accurate estimation of state for various control algorithms. The filtering technique does not give optimal estimates because the filter gain matrix is adjusted intuitively rather than by the Kalman algorithm. Since the overall objective of the work is one of evaporator control, rather than estimation, the accuracy and assumptions of this simplified filter is not discussed.

2.8 Chapter Review

Process identification techniques are surveyed with special reference to the technique of Kalman filtering. The computational difficulties of programming the Kalman filter in real time have been considered together with reported applications. Mathematical modelling of heat transfer equipment has been briefly considered and it appears that heat transfer processes of the type under consideration can be modelled by established techniques.

The principle areas for further exploration are:

1. The efficient on-line real-time implementation of the Kalman filter algorithm on a small computer.

2. The analysis of the effect of uncertainty in the mathematical model and noise statistics in non-linear systems.

3. The application of the Kalman filter to the study of heat transfer dynamics, where time constants are small, and hence available computation time is small.

CHAPTER 3

THE DOUBLE-EFFECT EVAPORATOR - COMPUTER SYSTEM

3.1 General

One of the main advantages of linking a digital computer to a chemical engineering process is that the computer is capable of logging or storing numerous measurements at high speed. Furthermore, the measurements can be processed immediately, so that the results of the computation can be made available to the process end of the system. The nature of the information returned to the process depends upon the sophistication of the on-line hardware, ranging from direct digital control to simple teleprinter messages for a process operator.

Figure 3.1 shows the general layout of the evaporator-computer system. From the process instrumentation, a number of analogue signals are connected to the remote cabinet of a two-part data logger situated alongside the process. By means of trunk cabling, the remote cabinet is linked to the main cabinet of the data logger, which is itself connected to the digital computer. Computed information is returned to the communication teletype at the plant end of the system, which facilitates remote control of computer programs and input/output of data.

All logging operations are executed from the digital computer by programmed commands output to the main cabinet. The commands are decoded into data logger instructions to perform operations such as channel scanning, clock reading and amplification. A scan instruction causes the input side of an

FIGURE 3.1

THE EVAPORATOR-COMPUTER SYSTEM

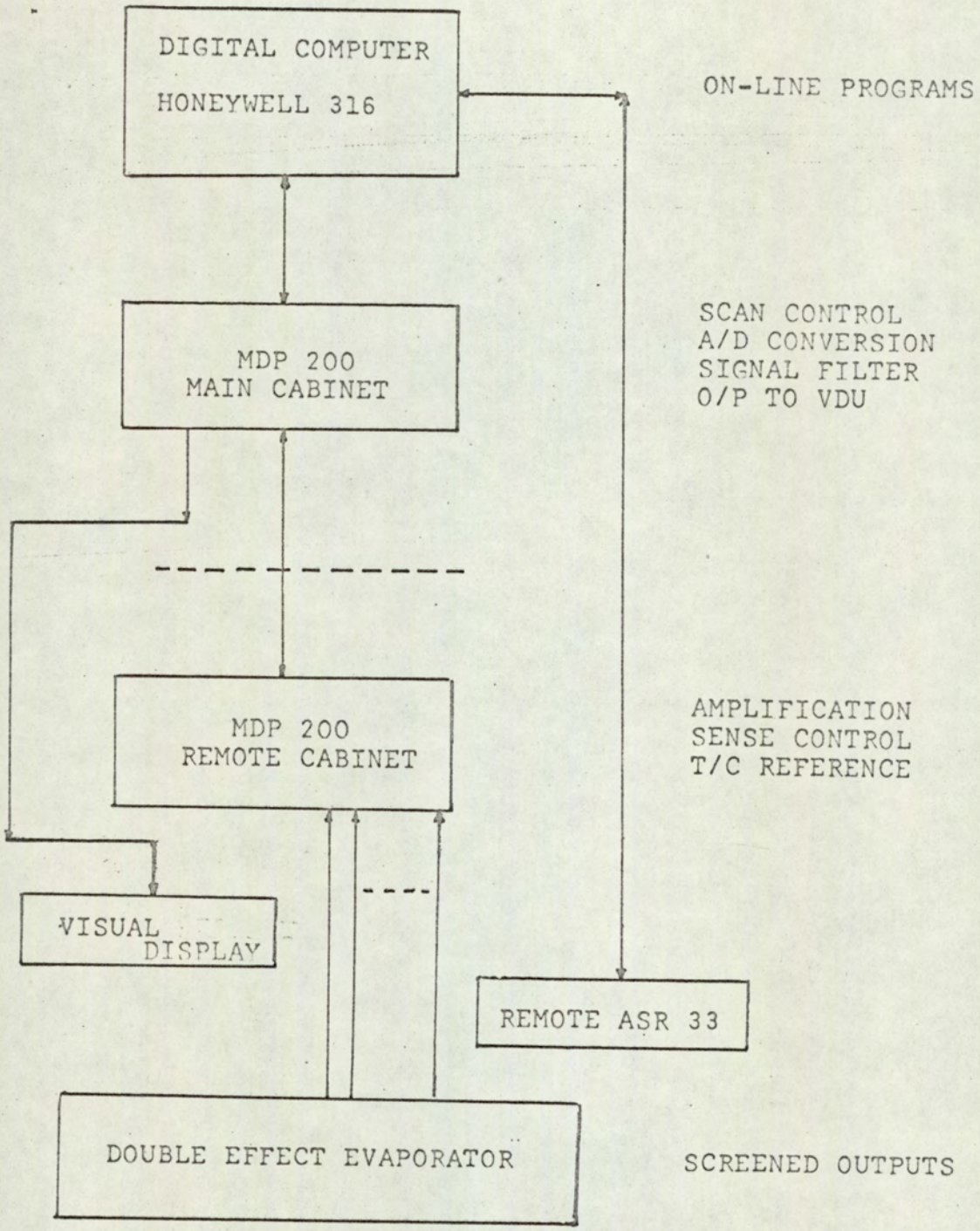

analogue to digital converter (ADC) to be switched to the required analogue channel connected at the remote cabinet. The digital output of the ADC returns to the computer for numerical conversion and processing.

3.2 Double Effect Evaporator

The evaporator was manufactured and erected by Kestner Evaporator and Engineering Company Limited. Originally (92), the plant was designed to operate as either two single or one double effect evaporator with an additional option of vacuum operation. The author has been principally concerned with operation in the double-effect, vacuum state. A summary of the evaporator units is given here; a detailed description of the engineering construction is provided in Appendix 1.

3.2.1 Process Description

A flow diagram of the double-effect evaporator is presented in Figure 3.2.

The first effect of the evaporator is of the Kestner climbing film type (93) and consists principally of a vertical liquor preheater, a climbing film calandria and a tangential cyclone separator. Evaporation is carried out by the climbing film method, in which the liquor is in contact with the steam heated tubes for a short period of time.

The vertical second effect is of the forced circulation type and consists of the heating calandria, the salting-out type separator and the circulation pump. Liquor from the separator is continuously circulated through the tubes of

FIGURE 3.2

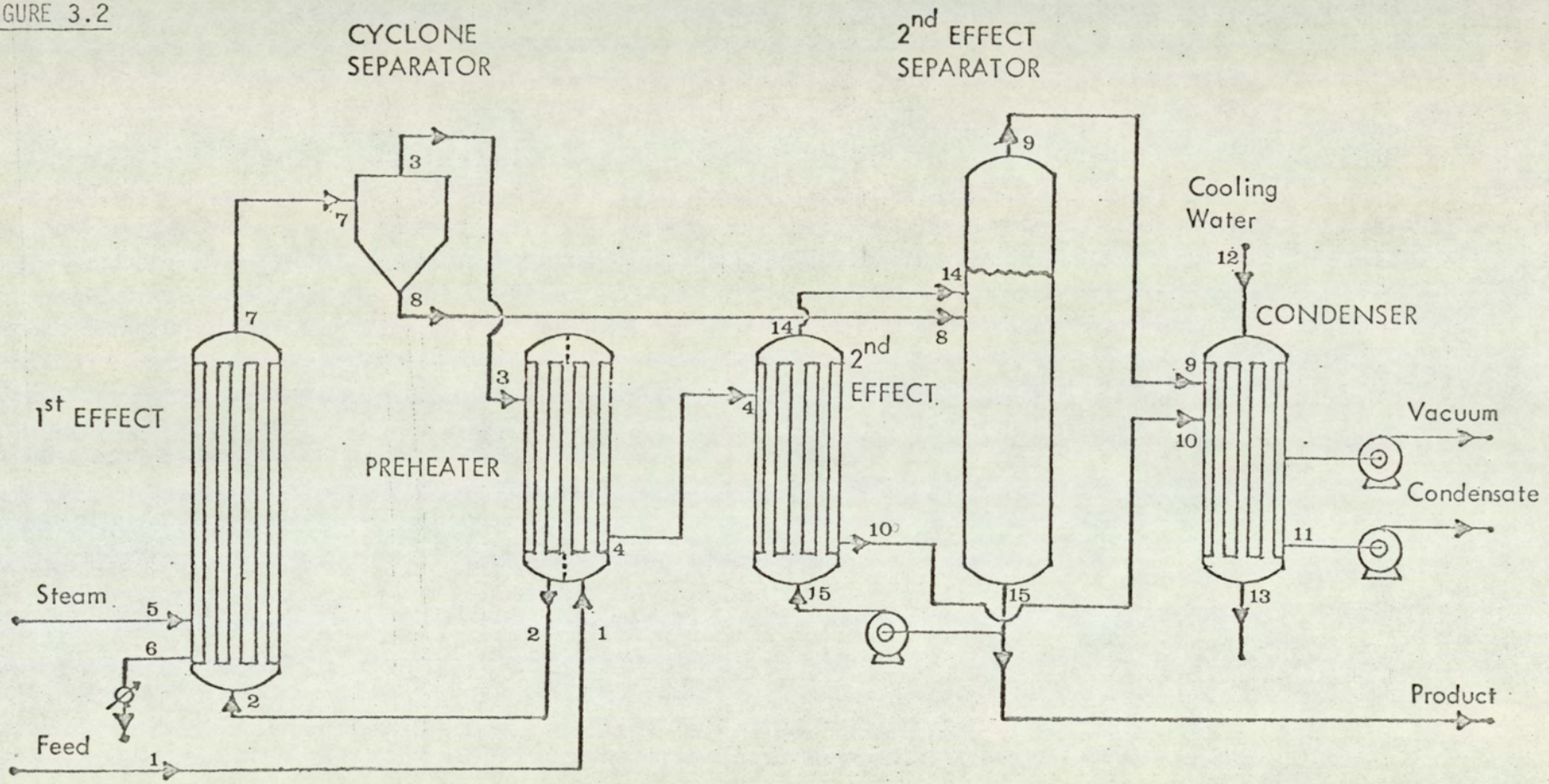

DOUBLE EFFECT EVAPORATOR

the calandria at high velocity and back into the separator. Vapour from the shellside of the preheater is used as heating medium on the shellside of the calandria. The liquid level in the separator is approximately one meter above the top tube plate of the calandria and the resulting static head in the tubes prevents boiling until the liquor enters the separator.

Vapour from the second effect separator and the second effect calandria shell is passed to the shellside of the water cooled, vertical, shell and tube condenser. Under vacuum operating conditions, the vacuum pump draws on the shellside of the condenser.

3.2.2 Process Operation

Cold feed water from storage tanks mounted above the evaporator is gravity fed to the shell and tube preheater, where heat is exchanged with vapour leaving the cyclone separator. From the preheater, the warm feed enters the base of the tubes of the climbing film evaporator, which are heated externally by 240 kNm^{-2} (20 p.s.i.g.) saturated steam. Boiling occurs at the bottom of the tubes and the consequent release of vapour produces two-phase flow conditions throughout the tubes. The mixture of liquid and vapour is then separated by the cyclone separator.

Under vacuum operating conditions, the vapour space pressure throughout the evaporator is maintained constant by the vacuum pump, so that heat transfer from the vapour leaving the preheater shell is then used as heating medium on the shellside of the second effect calandria, where further condensation occurs

as a result of heat transfer. The resulting mixture of liquid and unused vapour is drawn into the shellside of the condenser and joins the condensate stream pumped from the system.

From the base of the cyclone separator the hot liquid flows to the large second effect separator and is mixed by the action of the circulation pump. Since there is no solution being concentrated, the liquid level in the second effect separator varies throughout the operation, according to liquid feed rate and the total thermal load on the system. The vapour produced by boiling in the second effect separator is drawn to the shellside of the condenser by the vacuum pump, which permanently maintains the evaporator pressure at approximately 6 kNm^{-2} (28 inches Hg) vacuum.

The operating conditions of the evaporator may be varied by manual control of feed rate, steam rate or condenser cooling water rate.

3.2.3 Process Notation

Each steam of the double effect evaporator is arbitrarily assigned a reference number, as shown in Figure 3.2. Temperature, liquid flow, vapour flow and enthalpy are assigned the symbols T, M, V and H respectively. Thus T_{11} refers to the temperature of the condensate and M_2 the feed rate to the first effect. Where vapour temperature is measured indirectly by pressure, the symbol T is preferred. The head in the second effect is denoted by H_s.

3.2.4 Process Instrumentation

All process variables measured via the data logger must be provided as analogue D.C. voltages. Furthermore, the analogue signals are susceptible to corruption by electrical noise, so that all cabling must be screened and all screens insulated. The positioning of transducers is shown in Figure 3.3.

Temperature is measured by NiCr/NiAl thermocouples and an isothermal ($0^{\circ}C$) reference chamber incorporated into the remote cabinet of the data logger provides a cold junction for each thermocouple. The flow rates to the first and second effect are measured by variable area magnetic flowmeters. Each flowmeter includes a D.C. potentiometer exhibiting linear flow/current characteristics. Similar types of potentiometer are included in the strain gauges measuring absolute vacuum and the differential pressure cells measuring the head in the second effect and the steam flow through an orifice plate. The flow rate of cooling liquid to the condenser is measured off-line by rotameter.

The transducers are summarised in Table 3.1.

FIGURE 3.3 INSTRUMENTATION

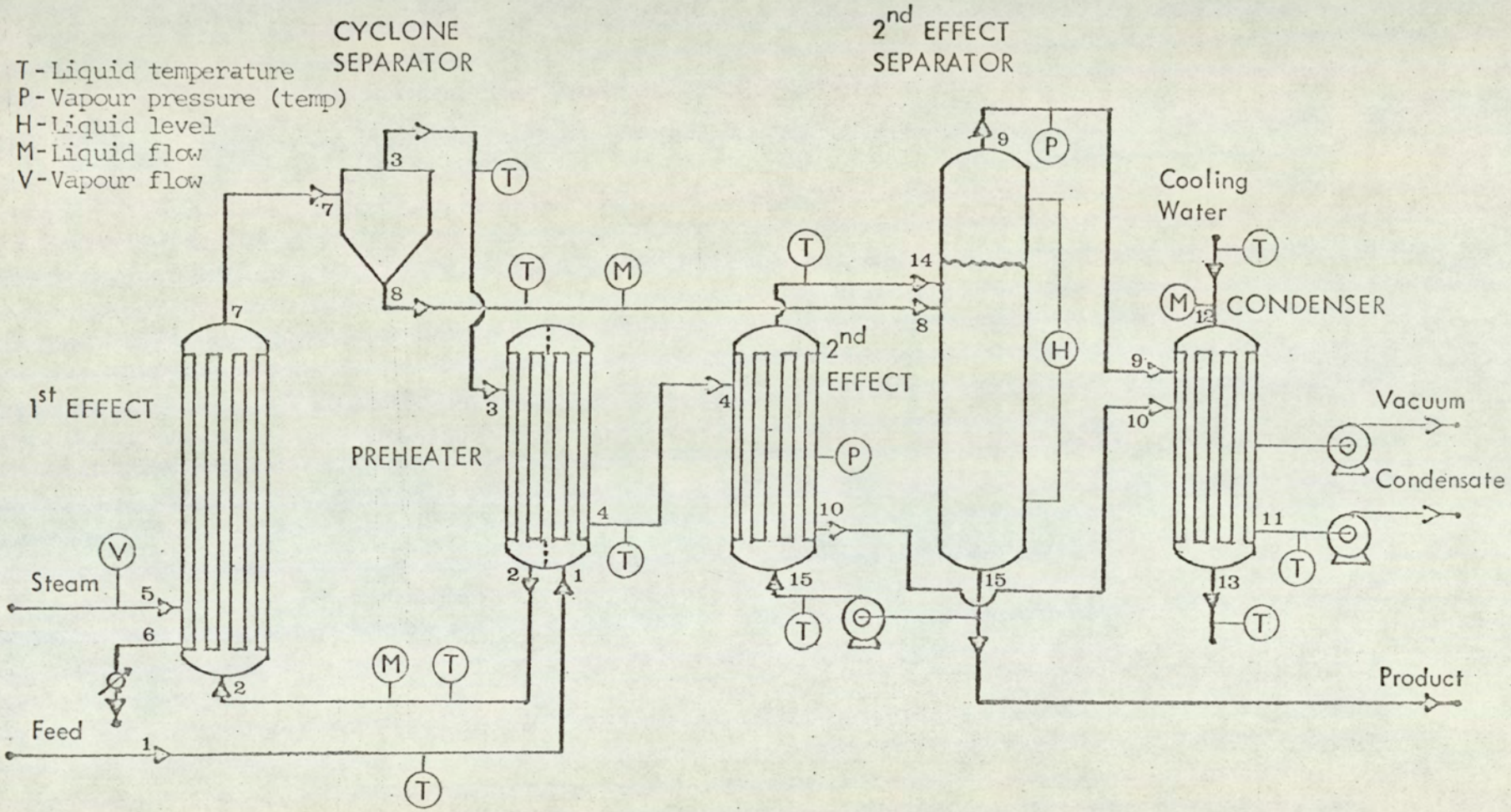

DOUBLE EFFECT EVAPORATOR

Table 3.1 - Double Effect Evaporator Transducers

Variable Name	Channel No.	Measurement Device	Input range	Analogue output range
T_9	14	Strain gauge	4-200 kNm^{-2}	$\pm$ 5 V
T_{10}	15	Strain gauge	4-200 kNm^{-2}	$\pm$ 5 V
M_2	16	Variable area	0-70 gs^{-1}	4-20 mA*
M_8	17	Variable area	0-40 gs^{-1}	"
H_S	18	Differential pressure	0-40 m H_2O	"
V_5	19	Orifice/D.P.	0-20 gs^{-1}	"
T_{12}	20	Thermocouple	0-100 C	0-25 mV
T_{13}	21	"	"	"
T_1	22	"	"	"
T_2	23	"	"	"
T_{15}	24	"	"	"
T_{14}	25	"	"	"
T_8	26	"	"	"
T_{11}	27	"	"	"
T_4	28	"	"	"
T_3	29	"	"	"
M_{12}	—	Rotameter	0-1000gs^{-1}	—

* The milliamp signals on channels 16-19 are converted to analogue voltages by connecting a resistance in parallel across the input terminals of the remote cabinet

3.3 The Digital Computers

3.3.1 The PDS 1020

Originally, the MDP200 data logger was linked to a Pacific Data Systems 1020 digital computer with 4K core and a cycle time of 2.3 ms for input/output of data and commands; the logger and PDS1020 are hardware compatible. Each stores data and instructions as 16 bit, binary coded decimal (BCD) words plus a sign bit. The on-line programming capabilities are restricted to the use of machine code or assembler instructions and examples have been previously reported (12).

3.3.2 The Honeywell 316

Limitations of storage, speed and programming capability have led to the acquisition of a Honeywell 316 computer, shown in Figure 3.4. The H316 system (94) consists of the 1.6 microsecond cycle time CPU, 12K of core, paper tape reader, paper tape punch and ASR33 teletype. Input/output to magnetic tape cassettes provides an option to paper tape reader and punch. The word length is 16 bits (i.e. 5 octal digits plus sign bit) and the CPU includes real time clock and high speed multiply/divide options.

Figure 3.4, a simplified block diagram of the H316 CPU, shows the machine registers, the control limit of the CPU, the I/O bus for input/output of data and the address bus for selection of peripheral device. Data and instructions from memory are transferred to and from the registers through the M-register. The A-register (and its extension the B-register) is the primary arithmetic and logic register of the computer, and the P-register contains the

FIGURE 3.4

THE HONEYWELL 316 SYSTEM

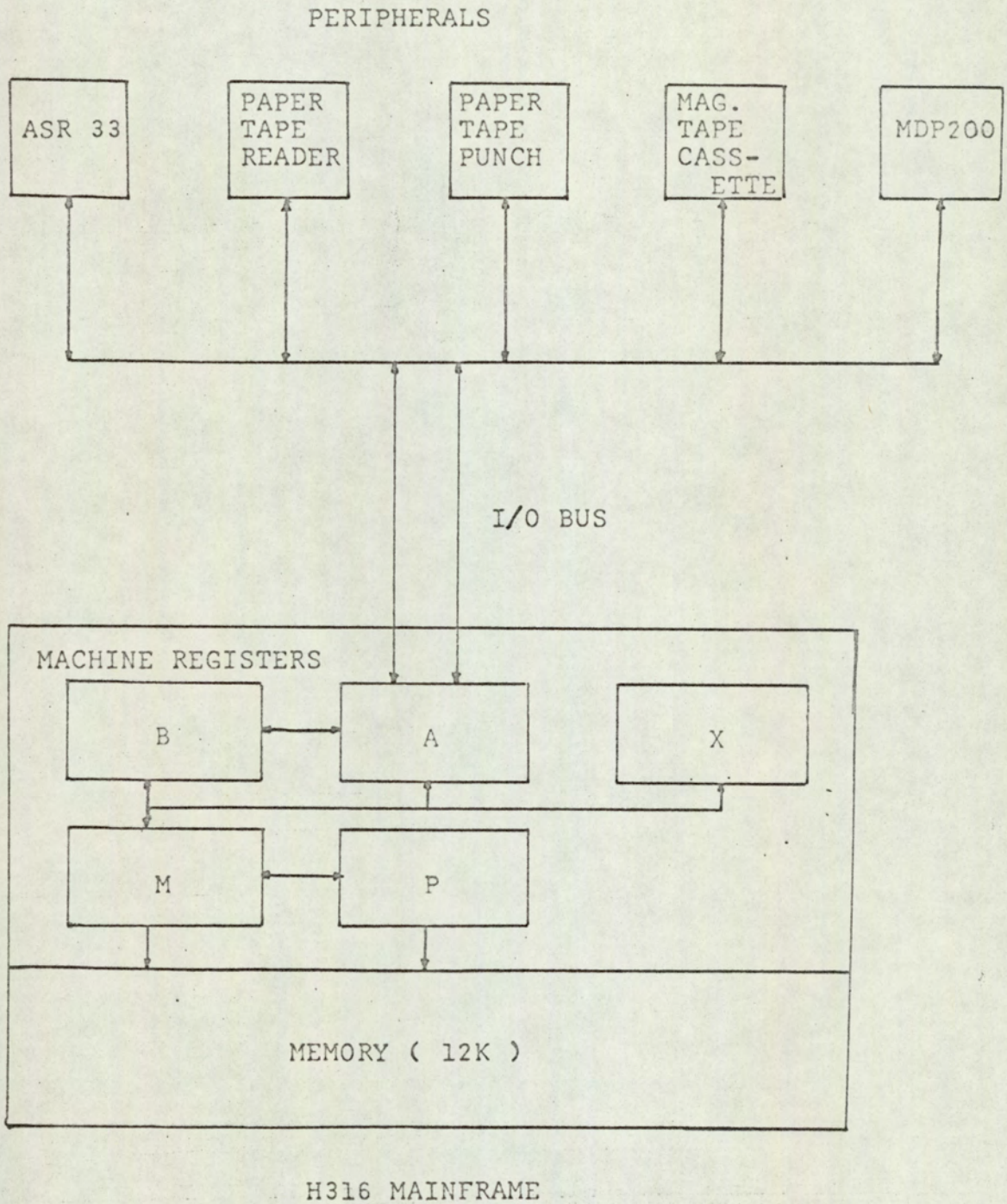

H316 MAINFRAME

location of the next instruction to be executed. All input/output devices are connected to the same I/O bus, which essentially consists of 16 parallel input lines to the A-register. On execution of a programmed I/O instruction the data lines of the required device are directed to the I/O bus by the bit pattern entered into the address bus as part of the instruction. The data is then transferred to or from the A-register during one memory cycle. Under normal off-line working the teletype, reader and punch are connected to the I/O bus in the proximity of the computer. During on-line work the teletype can be removed to the evaporator laboratory to provide remote control of computer programs.

Data words are stored in binary form using two's complement notation to signify negative numbers. The H316 accepts and processes data words in both single and double word length format corresponding to single precision integer and real variables. Instruction words are divided into four types - memory reference, I/O, shift and generic operating on the contents of the appropriate machine registers. The direct address of a memory reference instruction can be modified by the index register to produce a new effective address.

3.4 The MDP 200 Data Logger

The Electronic Associates MDP 200, shown in Figure 3.1, is housed in two sections - the main and remote cabinets. In the main cabinet, located alongside the H316, are the Buffer the Multiplexer, Reed Relay Scanner, Analogue to Digital Converter (ADC), Differential Buffer and Trunk Selector. The remote cabinet, situated by the evaporator, consists of a Scan Control Unit, Reed Relay Trays, Gain Control Patch Panel, Preamplifier and Visual Display

Unit. Also housed in the remote cabinet are a De La Rue Zerac isothermal reference chamber, four manual scan switches and four sense lines - an extension of the H316 sense switches.

Operation of the MDP 200 is initiated by the output of a BCD command from the A-register of the H316 along the I/O bus to the Buffer and Multiplexer. This unit acts as a buffer and translator between the computer and logger, interpreting the command as an instruction to reference either the digital clock, a particular analogue channel or the scan switches. The Digital Clock provides BCD output of either hours and minutes or seconds and tenths of seconds. Scan switches are a set of four manual digi-switches on the remote cabinet which enable decimal numbers to enter the A-register of the computer from the remote cabinet and, in conjunction with the sense lines, are used for remote program control.

Readings from the Digital Clock and scan switches are connected directly through the Buffer and Multiplexer; scanning of analogue input channels is as follows:-

1. From the Buffer and Multiplexer the command to read a particular channel is directed to the Reed Relay Scanner.

2. The Reed Relay Scanner signals the scan control unit to activate the reed relay on the required channel.

3. The incoming analogue signal is amplified by a factor of 1, 10, 100 or 1000; the required gain is set either by program control or manually by patch panel on the remote cabinet.

4. Between the remote cabinet and the main cabinet the analogue signal is transmitted via the screened trunk cabling to the differential buffer in the main cabinet which removes the effect of differences in electrical ground between the cabinets.

5. An optional electronic filter is applied to the analogue signal to remove noise; the filter is selected manually or by program control.

6. Digitisation of the analogue signal takes place in the ADC and when conversion is complete, the 16 bit BCD data word is transferred to the H316 A-register via the I/O bus. At the same time, the digital output of the ADC is displayed at the Visual Display Unit.

Maximum scanning speeds of 30 channels/second (filter out) and 10 channels/second (filter in) are available.

3.5 The MDP200 - H316 Interface

While the PDS 1020 is hardware compatible with the data logger, the link between the H316 and MDP 200 was achieved by the construction of a special purpose hardware interface. The interface is necessary to provide logic level conversion and timing during input/output, so that the H316 can be programmed to emulate the operation of the PDS1020. A detailed explanation of the design and construction of the interface is given in Appendix 2. Each 16 bit BCD data/command word is conveniently passed to and from the A-register via the 16 parallel lines of the I/O bus. However, the additional sign bit provided by the ADC is handled separately. Additional facilities incorporated into the interface design include the extension of the H316 sense switches to the remote cabinet.

3.6 Chapter Review

Chapter 3 describes the components of the experimental system - the double effect evaporator, MDP200 data logger, PDS 1020 and Honeywell 316 digital computers and MDP200-H316 interface. A detailed description of the evaporator heat exchangers and design of the MDP200-H316 interface is provided in appendices 1 and 2. A general view of the evaporator and remote data logger cabinet is shown in Plate 1. The main cabinet and computer hardware are shown in Plate 2.

Following the computer system hardware, it is necessary to describe the computer programs that control data logging operations. This includes both the standard Honeywell software and the programs written specifically for this on-line system.

PLATE 1 - THE DOUBLE EFFECT EVAPORATOR

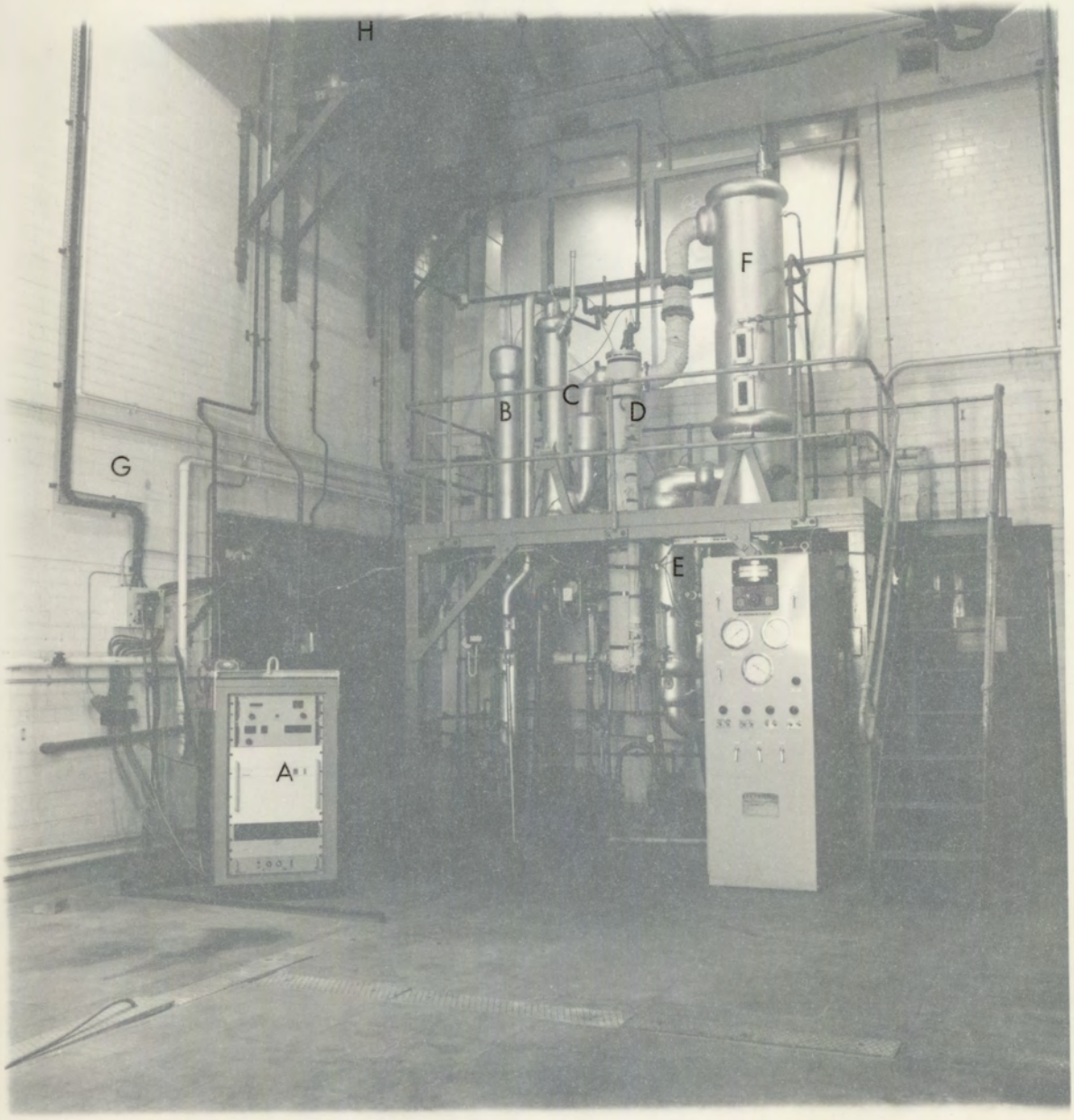

A MDP200 Remote Cabinet
B First Effect
C Preheater
D Condenser
E Second Effect
F Second Effect Separator
G Trunk Cabling to Computer
H Feed Storage

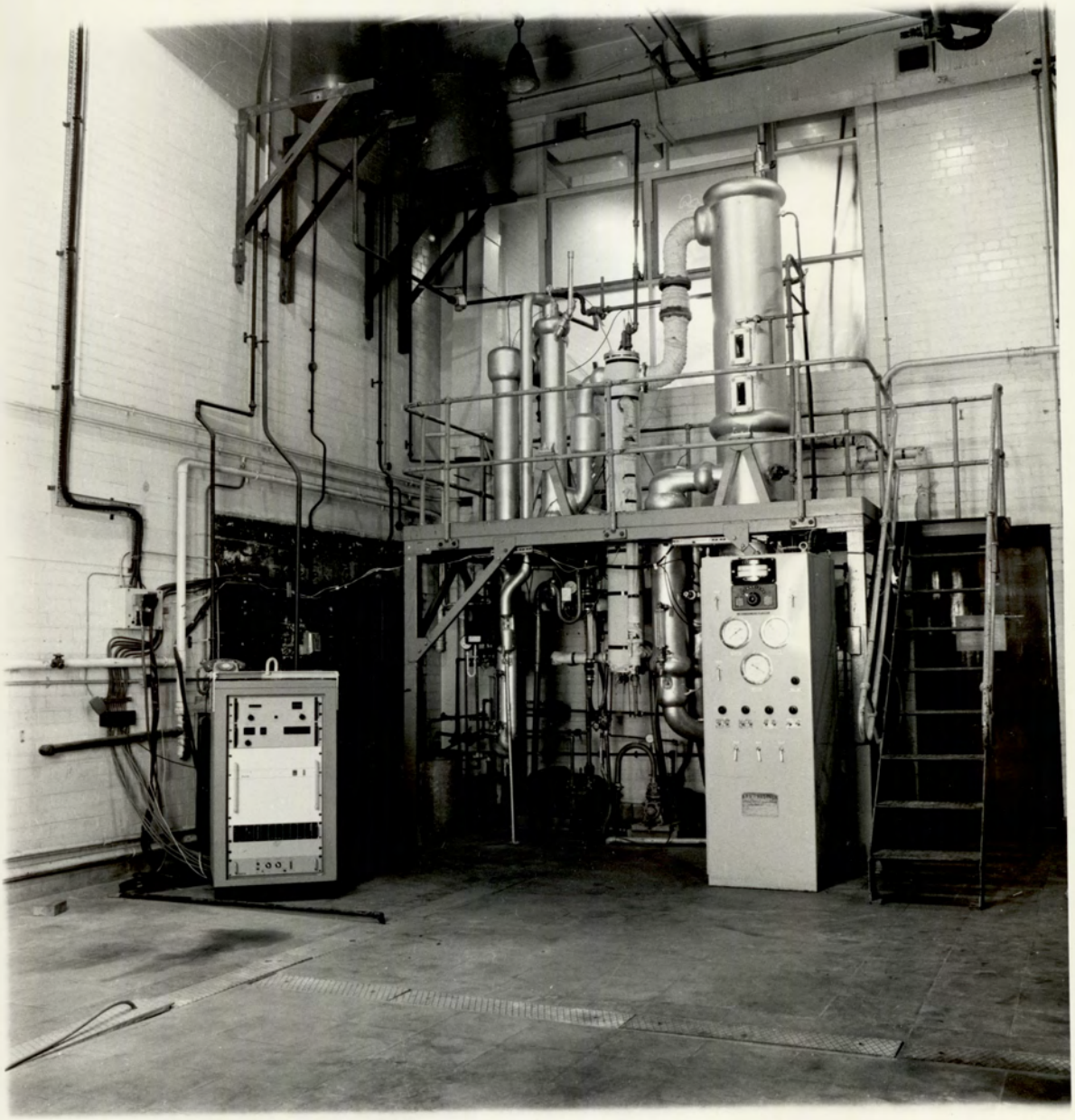

PLATE 2 - THE HONEYWELL 316 COMPUTER

A H316 Mainframe

B Magnetic Tape Cassettes

C Paper Tape Punch

D Paper Tape Reader

E ASR 33 Teletype

F MDP200 Main Cabinet


FORTRAN AND BASIC
ERROR CODES
FIRST AID

CHAPTER 4

THE HONEYWELL 316 SYSTEM SOFTWARE

4.1 General

By comparison with large multi-access computers, the minicomputer is limited in memory size, machine code instruction set and numerical precision. An instruction word of sixteen bits requires 4 bits to represent a sufficient number of operands. An indirect addressing bit and an indexing bit are necessary and consequently, the maximum number of locations that can be accessed by direct addressing is 1024 (2^{10}) or two sectors - the current sector of the instruction and the lowest sector in memory (base sector). By indirect addressing the maximum number is 16384 (2^{14}), since the index and indirect addressing bits are still required. At the expense of computing time, numerical precision is improved by storing data as double or treble length words.

Since the computer system has no backing store, the system does not support multiprogramming and all programs are executed in the batch mode. Running a program commences with the off-line preparation of a source tape for either the DAP-16 assembler or FORTRAN compiler. The result of successful compilation or assembly is an object code tape, which must then be loaded into core and dumped to form a self-loading system tape (SLST). This is achieved by loading a self-loading object tape loader into memory and then utilising the loader to enter the object program. Supporting programmer and/or library subroutines, in object code, are loaded similarly. When all necessary object programs are loaded, the contents of memory are dumped onto paper tape or magnetic tape cassette to form an SLST

and the program is executed. In the event of an execution error, the whole operation may require to be repeated.

During normal off-line processing, the time-consuming compiling and loading procedure is avoided by use of the interactive compiler for the language BASIC. Although execution of interpretative BASIC programs is somewhat slower than FORTRAN or DAP-16, the interactive use during execution and program modification outweighs the disadvantages. The version of the BASIC compiler for the H316 computer, BASIC-16, has a number of non-standard additional refinements. The most important of these is the ability of BASIC to access FORTRAN or DAP-16 subroutines that are permanently resident in core. This means that any repetitive operation or calculation programmed at the FORTRAN or DAP-16 level, can be accessed interactively and with a simple data input/output format. Also, the combination of DAP-16 and BASIC provides the dedicated utility subroutines with the supporting computing power of a high level language.

This technique has been used to produce an interactive, on-line, data logging system (BASELINE) and an interactive digital simulation program (ASP).

4.2 Standard Software

4.2.1 DAP-16 Assembler

To avoid programming directly in machine code, a symbolic assembler, DAP-16, is provided by the manufacturer (95). Each machine operation is assigned a symbolic name and where necessary, each address referenced by an instruction is given a symbolic label. The assembler is a 'one for one' language, i.e. one symbolic instruction corresponds to one machine code operation, except in the case of pseudo-operations, which request action by the

assembler rather than specifying an operation code. The source text, produced off-line on paper tape, is usually assembled in two passes.

The assembler produces two independent outputs. The first is the object code which is punched onto paper tape for further processing by the loader, and the second is the assembly listing which is printed at the teletype. Included in the listing are programmer comments, any error messages and an octal representation of each machine code instruction or data word. Examples of DAP-16 source and assembly listings are included in Appendix 3.

4.2.2 FORTRAN Compiler

The Honeywell FORTRAN IV compiler has been produced for 16 bit computers according to the American Standards Association specification (96). Details of the programming language are well documented (97). Operation of the compiler in the batch mode requires the addition of simple control characters ($\$o$) to terminate each program. Peripheral device codes are dedicated to 1 - teletype and 2 - paper tape reader/punch.

FORTRAN source tapes are prepared off-line on paper tape in the standard format. Object code output is normally directed to the paper tape punch and listings are output to the teletype.

4.2.3 FORTRAN Translator

The FORTRAN translator is a standard, one pass, package which converts FORTRAN source programs into DAP-16 assembly source instructions. This enables DAP-16 source statements to be inter-mixed with FORTRAN statements

in a defined manner, thus increasing the programming scope beyond the machine-independent restrictions of FORTRAN. Source tape preparation is identical to FORTRAN with the exception that an 'A' is inserted into the comment column when a line contains an assembler instruction. Translator output comprises a paper tape and teletype listing of the output DAP-16 source tape. The teletype listing optionally includes the translator source program.

The FORTRAN translator comprises the major part of the FORTRAN compiler with two restrictions. Firstly, doubly subscripted dynamic arrays are not permitted, and secondly, an array which is a dummy argument of a subroutine can have only one dimension. The latter restriction is avoided by the programming technique adopted for the Kalman filter subroutine described in Section 6.6.2.

4.2.4 Object Loader

Object code produced by the DAP-16 assembler or FORTRAN compiler is processed by a loader to form a core image in memory. References to external names such as library or user written subroutines are also resolved. To the loader, object code from both DAP-16 and FORTRAN is identical, so that programs from the two separate sources can be inter-mixed.

There are two modes of operation of the loader. In the first, the desectorising mode, the loader handles all intersector references by generating indirect address links where necessary. These links are usually located in base sector, unless the assembler program specifies a location elsewhere by the SETB (set base) pseudo-operation. The second mode of operation, the load mode, assumes that all intersector links are handled by the assembler program. Where

links exist, they are noted by the loader, thus providing a method of debugging and loading a program when cross-sector references require special treatment.

4.2.5 BASIC-16

BASIC is an interactive, problem-orientated, high-level language with a simple vocabulary and grammar. The language was originally developed at Dartmouth College and general details are well documented (98).

The BASIC compiler is interpretative in operation, i.e. each instruction is translated from source to machine code and executed whenever it is encountered. All constants are stored internally in floating point format but input may be in integer, fixed point or floating point form. The output format is adjusted by BASIC to provide maximum precision from six figure significance.

BASIC-16 is the Honeywell version of BASIC for 16 bit machines with memory size 4K or more. In standard form, communication with BASIC is from the teletype, but a machine code modification to the computer permits input/output via the paper tape reader and punch.

An additional refinement provided in BASIC-16 is the CALL statement, which enables a FORTRAN/DAP-16 subroutine to be accessed from a BASIC program. The general form of the statement is

In CALL (sn, a_1, a_2, ..., a_n)

where In is the line number of the statement

CALL is the statement operator

Sn is the subroutine reference number (1 to 10)

a_1 to a_n are arguments to be passed to the subroutine called.

Unlike the CALL statement in FORTRAN, the subroutine is not assessed by name but by a reference number to an entry in a table stored in the BASIC-16 compiler, containing the starting addresses of up to ten subroutines. The arguments a_1 to a_n correspond to the dummy arguments of the FORTRAN subroutine definition. Since all BASIC variables are real in the FORTRAN sense, the dummy arguments in the FORTRAN subroutine must also be real and any integer numbers required must be converted internally. Where a FORTRAN dummy argument is a subscripted variable, the corresponding BASIC argument is the first subscript required of the array, e.g. CALL (1, X, A(0), B(0,0)).

4.3 Applications Programs

4.3.1 Interactive BASIC/FORTRAN Systems

The two principal advantages of combining FORTRAN or DAP-16 subroutines with BASIC are the capability for interactive programming and the increased speed of execution. In addition, a programmer considers only the correct number and order of arguments and need not be aware of the content of the subroutines. The disadvantage of such a system is the reduction in available core store by duplication of software in the compiler and subroutines.

Production of an interactive system tape is initiated by loading the BASIC compiler and object tape loader into the lower part of memory. Next, the object tape produced from compilation or assembly of the subroutines is loaded into the highest available sector, together with supporting library routines. Cross sector link addresses are stored in a table in base sector within the BASIC compiler. The starting addresses of each subroutine are then manually patched into a dedicated area of the compiler and a permanent copy

of the complete system tape is dumped onto paper tape or magnetic tape cassette.

During initialisation of the compiler, the highest address available for storage of BASIC programs is set to the address immediately below the first subroutine.

4.3.2 BASELINE

BASELINE is the name given to the BASIC/FORTRAN system used for on-line data logging operations (9 9).

The operation of the MDP200 is controlled by a number of subroutines constructed to emulate the action of the PDS1020 digital computer. A detailed description of the FORTRAN and DAP-16 subroutines is given in Appendix 3. A fundamental assembler subroutine creates the logic output pulses and BCD command words to control the operation of the data logger. When the BCD data word is returned to the A-register of H316, another subroutine converts BCD to binary by the ADD-3 algorithm (100).

At the BASIC level the subroutines are as follows:-

(1) The statement CALL (I, N, V, F) causes MDP200 analogue channel number N to be scanned and the variable V to be set equal to the current data value on this channel. If the channel is out of range (i.e. N < 0 or N>39) the flag F is set to unity, otherwise F is zero.

(2) The statement CALL (2,H) causes the variable H to be set equal to the current hours and minutes reading of the MDP200 clock, H is a four

digit value ($0 \leq H \leq 2359$) in which the two leftmost digits represent the hours and the two rightmost represent the minutes.

(3) The statement CALL (3,S) causes the variable S to be set equal to the current seconds reading of the MDP200 clock. S is a four digit value in which the two leftmost digits represent seconds, the third digit represents tenths of seconds and the fourth digit is always zero.

(4) The statement CALL (4,D) causes the variable D to be set equal to the current setting of the four scan switches on the MDP200 remote cabinet.

(5) The statement CALL (5,0) stops the H316 real time clock. This statement is used in association with subroutine 7 when the interrupt facility is used.

(6) The statement CALL (6,T,X) tests the sense switches on the H316 computer or the sense lines on the remote cabinet. If sense switch number T is set, X is set to 2, otherwise X = 1.

(7) The statement CALL (7, I, N1, N2, R, A(0,0), R1,D1, E) causes channels N1 to N2 to be scanned R times and the average of each channel value to be stored in A(N1, D1) to A(N2, D1). This sequence is repeated every I seconds a total number of R times and each time, D1 is incremented by 1. This operation utilises the interrupt facility of the computer, i.e. the computation in progress is suspended and resumed after the scans have been carried out. If interrupt is not required I is set equal to zero. The flag E indicates whether the channels selected are out of range.

4.3.3 ASP

The BASIC compiler is combined with a set of FORTRAN subroutines for numerical integration to form the Aston Simulation Program (ASP), (101,102)

ASP is used in the simulation of continuous dynamic systems and was designed to study dynamic models of the evaporator.

To minimise programming by the user, the COMMON area of memory is used for transmission of variables required only by the subroutines. One result of this organisation is that the BASIC simulation program must be structured in a prescribed manner for initialisation of variables, statement of derivatives and numerical integration. A detailed description of program structure and FORTRAN subroutines is provided in Appendix 4. The BASIC subroutine calls are as follows:-

(1) CALL (1,T) initialises the COMMON area of core and the independent variable, T.

(2) CALL (2, P, E, F1, F2) calls the output control subroutine. The print interval, P, and the final value of independent variable, E, are compared with the current value of T. When the independent variable increases by the print interval, P, flag F2 is returned with the value 2, otherwise, it remains at 1. At the end of the run ($T \geqslant E$), flag F1 is returned similarly.

(3) CALL (3, T, H, R) integrates the independent variable, T, and performs housekeeping operations, through COMMON, for the integration procedure. H is the integration step length, and R, specifies the integration order. R = 2 for the modified Euler method and R = 4 for the Runge-Kutta fourth order method.

(4) CALL (4, X, DX) causes the integration of the dependent variable X from it derivative DX.

(5) CALL (5, A, B, C, W(0), Z(0)) accesses the function generation subroutine. For a given value A of W (where Z = f(W)), a corresponding value

B of Z is computed by linear interpolation. The table of data of Z and W contains a total of C entries.

4.3.4 Kalman Filter Subroutine

To increase processing speed during real time state variable and parameter estimation, the Kalman Filter program is written in FORTRAN and incorporated into BASELINE as an optional eighth subroutine. The implementation of the algorithm is described in Section 6.6. The BASIC statement is:-

CALL (8, P(0,0), Q(0,0), R(0,0), M(0,0), F(0,0), X(0), Y(0), E1,
S(0,0), K(0,0), N, M)

where P is the transition matrix (input).

Q is the process noise matrix (input).

R is the measurement noise matrix (input).

M is the measurement matrix (input).

F is the estimation error covariance matrix (input/output).

X is the state variable vector (input/output).

Y is the measurement vector (input).

E1 is the filter convergence factor (input).

S is the predicted residual covariance matrix (output).

K is the filter gain matrix (output).

N is the number of state variables (input).

M is the number of measurements (input)

4.4 Chapter Review

Chapter 4 describes the computer programs available for the H316 - evaporator system. This includes the standard software-DAP-16 assembler, FORTRAN IV compiler, FORTRAN translator and BASIC-16 compiler, and the applications software-BASELINE and ASP. The latter are constructed from a combination of standard software and special purpose subroutines to provide interactive programming facilities for on-line data logging and dynamic simulation. Once constructed, the applications packages are available to any programmer with a knowledge of BASIC.

Having described the system hardware and software, it is next necessary to formulate mathematical models of the steady state and dynamic behaviour of the evaporator. The on-line implementation and solution of the models is effected by use of the software applications packages.

CHAPTER 5

MATHEMATICAL MODELS

5.1 General

Mathematical models of process plant often contain many more variables than those of aerospace systems, which represent the most common application of Kalman filtering. Detailed models of evaporators can be formulated as distributed-parameter equations but in the case of the double-effect evaporator, this means a large number of state variables and insufficient computer time and storage for implementation of the filter algorithm. Thus, some form of simplified model must be developed so as to reduce computational requirements yet still retain the essential characteristics of a detailed model. This is usually achieved by transforming the equations to a lumped-parameter form. Further simplifications can be made by making realistic assumptions based upon a detailed understanding of the operation of the evaporator. Such an understanding is achieved by both visual observation of normal process operating conditions and by performing on-line steady state experiments to determine unknown parameters such as overall heat transfer coefficients.

Steady-state experiments, over the whole range of operation of the evaporator, produce data for the formulation of steady-state correlations relating unknown parameters to operating conditions. This provides a comparison with existing correlations, developed for similar equipment, and numerical values for unknown coefficients in the dynamic model. Due to random disturbances, the evaporator is never at true steady state so that the experimental data are combined to form the best available correlations. The

accuracy of correlations and simplifying assumptions is determined by simulating the dynamic model and comparing the simulated results with real plant data.

5.2 Steady-State Model

The steady state model consists of mass and energy balances over each unit of the evaporator and the determination of overall heat transfer coefficients based upon heat transfer in each exchanger. In some cases, the flows and enthalpies of each stream can be calculated directly from measurements, while in all other cases the mass and energy balance equations must be solved.

The stream notation described in Section 3.2.2 is used throughout the derivations. The symbols M, V, T and H represent liquid flow, vapour flow, temperature and enthalpy respectively. Figure 5.1 shows double effect evaporator with stream numbers, mass flows and instrumentation.

5.2.1 Mass Balances

At the preheater, second effect and condenser shells there is a change of phase as vapour condenses

$$V_3 = V_4 + M_4 \qquad 5.2.1$$

$$V_4 + M_4 = V_{10} + M_{10} \qquad 5.2.2$$

$$V_{10} + M_{10} + V_9 = M_{11} \qquad 5.2.3$$

Within the tubes of the climbing-film first effect the liquid feed is partially vaporised,

FIGURE 5.1 INSTRUMENTATION AND MASS FLOWS

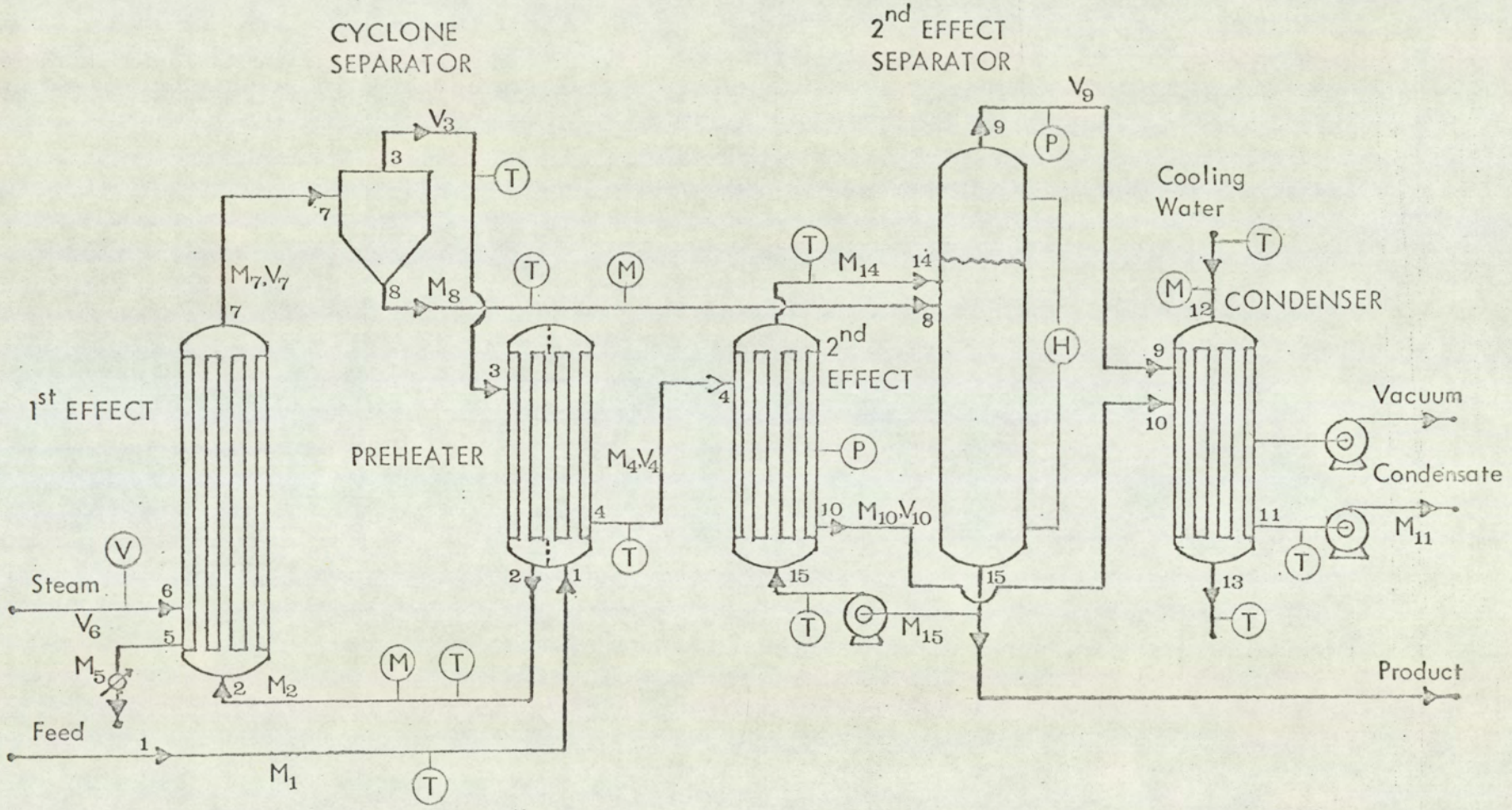

DOUBLE EFFECT EVAPORATOR

$$M_2 = M_7 + V_7 \qquad 5.2.4$$

and the resulting vapour/liquid mixture is separated at the cyclone

$$M_7 + V_7 = M_8 + V_3 \qquad 5.2.5$$

The liquid heated in the forced-circulation second effect is vaporised in the second effect separator where there is an accumulation of liquid, denoted by M_A,

$$M_8 + M_{14} = M_{15} + V_9 + M_A \qquad 5.2.6$$

For completeness, the continuity equations not involving phase change are stated. At the preheater tubes,

$$M_1 = M_2 \qquad 5.2.7$$

and the first effect shell, where all steam supplied is condensed,

$$V_5 = M_6 \qquad 5.2.8$$

and at the second effect and condenser tubes,

$$M_{14} = M_{15} \qquad 5.2.9$$

$$M_{12} = M_{13} \qquad 5.2.10$$

5.2.2 Energy Balances

The energy balances over each unit are derived to obtain the enthalpy of each steam subject to the following assumptions:-

1. There are no heat losses in the system.

2. Where vapour and liquid/vapour mixtures exist they are at the saturated vapour temperature at the operating pressure.

3. The heat exchanger shells are well-mixed so that the exit and shell temperatures are equal.

Again, using the stream notation of Section 3.2.3, the following equations are derived:-

Preheater

$$H_1 + H_3 = H_2 + H_4 \qquad 5.2.11$$

1st Effect

$$H_2 + H_5 = H_7 + H_6 \qquad 5.2.12$$

Cyclone

$$H_7 = H_8 + H_3 \qquad 5.2.13$$

2nd Effect

$$H_4 + H_{15} = H_{14} + H_{10} \qquad 5.2.14$$

2nd Effect Separator

$$H_8 + H_{14} = H_9 + H_{15} + H_A \qquad 5.2.15$$

Condenser

$$H_{12} + H_9 + H_{10} = H_{13} + H_{11} \qquad 5.2.16$$

Based on the above assumptions and taking the datum temperature as $0^{\circ}C$, the enthalpy terms are defined by

$$H_1 = M_1 C_p T_1 \qquad 5.2.17$$

$$H_2 = M_2 C_p T_2 \qquad 5.2.18$$

$$H_3 = V_3 g(T_3) \qquad 5.2.19$$

$$H_4 = V_4 g(T_4) + M_4 C_p T_4 \qquad 5.2.20$$

$$H_5 = V_5 g(T_5) \qquad 5.2.21$$

$$H_6 = M_6 C_p T_6 \qquad 5.2.22$$

$$H_7 = V_7 g(T_7) + M_7 C_p T_7 \qquad 5.2.23$$

$$H_8 = M_8 C_p T_8 \qquad 5.2.24$$

$$H_9 = V_9 g(T_9) \qquad 5.2.25$$

$$H_{10} = V_{10} g(T_{10}) + M_{10} C_p T_{10} \qquad 5.2.26$$

$$H_{11} = M_{11} C_p T_{11} \qquad 5.2.27$$

$$H_{12} = M_{12} C_p T_{12} \qquad 5.2.28$$

$$H_{13} = M_{13} C_p T_{13} \qquad 5.2.29$$

$$H_{14} = M_{14} C_p T_{14} \qquad 5.2.30$$

$$H_{15} = M_{15} C_p T_{15} \qquad 5.2.31$$

$$H_A = M_A C_p T_A \qquad 5.2.32$$

where C_p is the liquid heat capacity and $g(T)$ is the saturated vapour enthalpy function defined by

$$g(T) = C_p T + \lambda_T$$

where λ_T is the latent heat of vaporisation at temperature T.

The energy balance equations can be further simplified by assuming the cyclone separates liquid and vapour isothermally,

$$T_3 = T_8 \qquad 5.2.33$$

$$T_3 = T_7 \qquad 5.2.34$$

the steam feed to the first effect shell loses heat by condensation only,

$$T_5 = T_6 \qquad 5.2.35$$

and the liquid in the second effect separator is well-mixed and at constant temperature

$$T_A = T_{15} \qquad 5.2.36$$

5.2.3 Solution of Equations

Equations 5.2.1 - 5.2.36 represent 36 equations in 51 unknowns. In addition the 17 measurements are made:

mass flows : $M_1, M_8, M_A, V_5, M_{12}$

liquid temperatures : $T_1, T_2, T_8, T_{11}, T_{12}, T_{13}, T_{14}, T_{15}$

vapour pressure (temperatures) : T_4, T_6, T_{10}, T_9,

giving a redundancy of 2 when all measurements are weighted equally. The redundancy is used to calculate the steam feed rate to the first effect, V_5, which is known to be an unreliable measurement and the condenser cooling water rate, M_{12}, so as to give a measure of total system heat loss. The controlled variables are M_1, T_1, V_5, T_5, M_{12}, T_{12}, M_{14} and the condenser vacuum temperature, T_{vac}.

In practice, the solution of the complete set of 36 equations can be simplified by not stating explicitly the simple mass and energy balances (equations 5.2.7 - 5.2.10 and 5.2.33 - 5.2.36) and thus reducing the required programming (Section 6.3.3).

5.3 Dynamic Model

As shown in the literature review, Section 2.7, the heat transfer dynamics of exchangers can be accurately described by distributed-parameter models. Simplification of these exact models is principally effected by space lumping the equations into a number of discrete well-mixed regions. The objective of this modelling exercise is to produce a set of ordinary differential equations suitable for use in the real-time application of the Kalman filter algorithm. Consequently, the total number of equations is reduced by space lumping the shell and tubes of each exchanger. The assumptions are as follows:

1. The heat exchanger shells are well mixed regions so that the exit and shell temperatures are equal. Where vapour and liquid mixtures exist, the temperature is that of the saturated vapour at the operating pressure.

2. In the majority of the heat exchanger tubes, liquid is the plug flow regime. A lumped liquid temperature is approximated by the arithmetic mean of liquid inlet and outlet temperatures.

3. In the tubes of the climbing film first effect, the liquid and vapour are assumed to be well mixed.

4. The exchanger tubes have zero thermal resistance.

5. The temperature driving force is given by the arithmetic mean of the inlet and outlet temperature differences.

6. There are no heat losses.

The volume fraction of vapour (where vapour and condensate exist together) is denoted by Y, the shell and tube volume by W_s and W_t, the overall heat transfer coefficient by U, the heat transfer area by A, liquid density by ρ_L, vapour density and latent heat by ρ_N and λ_N where N refers to the stream number and hence temperature at which the vapour density or latent heat is calculated. The subscripts c, e, f and g refer to the condenser, first effect, second effect and preheater respectively. C_p and H_s represent the liquid specific heat and liquid head in the second effect separator. The relationship between vapour density and temperature is assumed to be of the form $\rho_N = \alpha(T_N)$. Again, the stream notation of Section 3.2.3 is adopted.

A detailed derivation of the dynamic model is given in Appendix 5, and is summarised overleaf.

5.3.1 Preheater

$$\frac{W_{tg}}{2}\frac{L\,dT_2}{dt} = M_1 C_p T_1 - M_2 C_p T_2 + U_g A_g\left(T_4 - \frac{(T_1 + T_2)}{2}\right) \qquad 5.3.1$$

$$W_{sg}\left(C_p(1 - Y_g)\rho_L \frac{dT_4}{dt} + Y_g \lambda_4 \frac{d\rho_4}{dt}\right) \qquad 5.3.2$$

$$= V_3 C_p (T_3 - T_4) + V_3 \lambda_3 - V_4 \lambda_4 - U_g A_g\left(T_4 - \frac{(T_1 + T_2)}{2}\right)$$

$$\frac{dY_g}{dt} = \frac{V_3 - M_4 - V_4 - W_{sg} Y_g \frac{d\rho_4}{dt}}{W_{sg}(\rho_4 - \rho_L)} \qquad 5.3.3$$

$$\frac{d\rho_4}{dt} = \frac{d\alpha(T_4)}{dT_4} \cdot \frac{dT_4}{dt} \qquad 5.3.4$$

$$\frac{dM_4}{dt} = \frac{A_g U_g + V_3 C_p}{\lambda_4} \cdot \frac{dT_4}{dt} - \frac{A_g U_g}{2\lambda_4} \cdot \frac{dT_2}{dt} - \frac{V_3 C_p}{\lambda_4} \cdot \frac{dT_3}{dt} \qquad 5.3.5$$

$$\frac{dV_4}{dt} = \frac{dV_3}{dt} - \frac{dM_4}{dt} \qquad 5.3.6$$

5.3.2 First Effect

$$W_{te}\left(C_p(1 - Y_e)\rho_L \frac{dT_7}{dt} + \lambda_7 Y_e \frac{d\rho_7}{dt}\right) \qquad 5.3.7$$

$$= M_2 C_p (T_2 - T_7) - V_7 \lambda_7 + A_e U_e (T_5 - T_7)$$

$$\frac{dY_e}{dt} = \frac{M_2 - M_7 - V_7 - W_{te} Y_e \frac{d\rho_7}{dt}}{W_{te}(\rho_7 - \rho_L)} \qquad 5.3.8$$

$$\frac{d\rho_7}{dt} = \frac{d\alpha(T_7)}{dT_7} \cdot \frac{dT_7}{dt} \qquad 5.3.9$$

$$\frac{dV_7}{dt} = - \frac{(A_e U_e + M_2 C_p)}{\lambda_7} \cdot \frac{dT_7}{dt} + \frac{M_2 C_p}{\lambda_7} \cdot \frac{dT_2}{dt} \qquad 5.3.10$$

$$\frac{dM_7}{dt} = \frac{dM_2}{dt} - \frac{dV_7}{dt} \qquad 5.3.11$$

$$T_5 = \text{constant} \qquad 5.3.12$$

5.3.3 Cyclone Separator

$$T_7 = T_3 = T_8 \qquad 5.3.13$$

$$\frac{dT_7}{dt} = \frac{dT_3}{dt} = \frac{dT_8}{dt} \qquad 5.3.14$$

$$M_7 = M_8 \qquad 5.3.15$$

$$\frac{dM_7}{dt} = \frac{dM_8}{dt} \qquad 5.3.16$$

$$V_7 = V_3 \qquad 5.3.17$$

$$\frac{dV_7}{dt} = \frac{dV_3}{dt} \qquad 5.3.18$$

5.3.4 Second Effect

$$W_{tf} C_p \rho_L \frac{d}{dt}\left(\frac{T_{14} + T_{15}}{2}\right) = M_{15} C_p T_{15} - M_{14} C_p T_{14} + U_f A_f \left(T_{10} - \frac{(T_{14} + T_{15})}{2}\right) \quad 5.3.19$$

$$W_{sf}\left(C_p (1 - Y_f)\rho_L \frac{dT_{10}}{dt} + Y_f \lambda_{10} \frac{d\rho_{10}}{dt}\right) \quad 5.3.20$$

$$= (V_4 + M_4) C_p (T_4 - T_{10}) + \lambda_4 V_4 - \lambda_{10} V_{10} - U_f A_f \left(T_{10} - \frac{(T_{14} + T_{15})}{2}\right)$$

$$\frac{dY_f}{dt} = \frac{V_4 + M_4 - M_{10} - V_{10} - W_{sf} Y_f \frac{d\rho_{10}}{dt}}{W_{sf}(\rho_{10} - \rho_L)} \quad 5.3.21$$

$$\frac{d\rho_{10}}{dt} = \frac{d\alpha(T_{10})}{dT_{10}} \cdot \frac{dT_{10}}{dt} \quad 5.3.22$$

$$\frac{dM_{10}}{dt} = \frac{A_f U_f + (M_4 + V_4) C_p}{\lambda_{10}} \cdot \frac{dT_{10}}{dt} - \frac{A_f U_f}{2\lambda_{10}}\left(\frac{dT_{14}}{dt} + \frac{dT_{15}}{dt}\right) \quad 5.3.23$$

$$- \frac{(M_4 + V_4)}{\lambda_{10}} \cdot \frac{dT_4}{dt}$$

$$\frac{dV_{10}}{dt} = \frac{dV_4}{dt} + \frac{dM_4}{dt} - \frac{dM_{10}}{dt} \quad 5.3.24$$

5.3.5 Second Effect Separator

$$A_s \rho_L C_p H_s \frac{dT_{15}}{dt} = M_{14} C_p (T_{14} - T_{15}) + M_8 C_p (T_8 - T_{15}) - V_{9\ 15} \qquad 5.3.25$$

$$A_s \rho_L \frac{dH_s}{dt} = M_{14} + M_8 - M_{15} - V_9 \qquad 5.3.26$$

$$\frac{dV_9}{dt} = \frac{1}{\lambda_{15}} \left((T_8 - T_{15}) C_p \frac{dM_8}{dt} + M_8 C_p \frac{dT_8}{dt} - (M_{14} + M_8) C_p \frac{dT_{15}}{dt} + M_{14} C_p \frac{dT_{14}}{dt} \right) \qquad 5.3.27$$

5.3.6 Condenser

$$\frac{W_{tc} \rho_L C_p}{2} \frac{dT_{13}}{dt} = M_{12} C_p T_{12} - M_{13} C_p T_{13} + U_c A_c \left(T_{vac} - \frac{(T_{12} + T_{13})}{2} \right) \qquad 5.3.28$$

$$T_{11} = \frac{V_9 (C_p T_{15} + \lambda_{15}) + M_{10} C_p T_{10} + V_{10} (C_p T_{10} + \lambda_{10}) - U_c A_c \left(T_{vac} - \frac{(T_{12} + T_{13})}{2} \right)}{M_{11} C_p} \qquad 5.3.29$$

$$M_{11} = V_9 + M_{10} + V_{10} \qquad 5.3.30$$

5.3.7 Discussion of Model

Equations 5.3.1 to 5.3.30 describe the dynamics of all uncontrolled variables in the double effect evaporator. The overall heat transfer coefficients are assumed to be known from steady-state correlations. The principal uncertainty in the development of the model, is the dynamics describing the behaviour of vapour pressure throughout the system. The dynamic characteristics of the vacuum pump are unknown, and the effect of hydrostatic heads and two-phase conditions is not measurable with pilot scale equipment. Consequently, the dynamic model contains terms involving variation in vapour temperature and density which, if the vacuum pump and vapour phase characteristics were known, would otherwise be unnecessary.

A simulation of the above model contains no pressure constraints apart from through T_{vac} in the condenser shell. The relationship between vapour phase temperatures T_{vac}, T_{15}, T_{10}, T_4, and T_7, cannot be deduced from steady-state experiments because of the random nature of the vacuum pump operation and the uncertain pressure differences caused by mixtures of vapour and liquid in the pipe-lines to and from the preheater and second effect shells. However, the steady-state operating equations approximate the dynamic behaviour of vapour temperature around steady-state conditions.

If the vapour pressures are assumed to be controlled variables, varying slowly under the influence of the vacuum pump, then the dynamic model can be simplified to consider only the liquid phase temperature dynamics. Furthermore, since the vapour side equations time constants are very much smaller than the liquid phase, the vapour side equations can be replaced by the equivalent steady-state equations.

5.4 Reduced Model

For the application of Kalman filter theory, the definition of complex system model is not necessary. Huddle and Wismer (27), indicate that unavoidable modelling errors and simplifications can be considered but any reduced model must include those state vector components of dominant or special interest to the designer. The effect of errors and simplifications can be lumped into the process noise covariance matrix.

A simplified dynamic model is obtained from equations 5.3.1 to 5.3.30 by assuming the vapour temperatures are controlled variables. All other previous assumptions are inherent in this simplification.

5.4.1 Preheater

At the preheater tubes, there is no vapour phase and thus the liquid temperature dynamic equation is unchanged,

$$\frac{W_{tg}\rho_L}{2}\frac{dT_2}{dt} = M_1 C_p(T_1 - T_2) + U_g A_g\left(T_4 - \frac{(T_1 + T_2)}{2}\right) \qquad 5.4.1$$

and at the shellside, when T_4 is a controlled variable, the steady-state equations defining the vapour the liquid rate leaving are,

$$V_4 = \frac{V_3 C_p(T_3 - T_4) + V_3\lambda_3 - U_g A_g\left(T_4 - \frac{(T_1 + T_2)}{2}\right)}{\lambda_4} \qquad 5.4.2$$

$$M_4 = V_3 - V_4 \qquad 5.4.3$$

5.4.2 First Effect

Both the shellside and tubeside of the first effect contain vapour/liquid mixtures at controlled temperatures T_5 and T_7. The steady-state equations are

$$V_7 = \frac{M_2 C_p (T_2 - T_7) + A_e U_e (T_5 - T_7)}{\lambda_7} \qquad 5.4.4$$

$$M_7 = M_2 - V_7 \qquad 5.4.5$$

5.4.3 Cyclone Separator

The cyclone separator is assumed to act isothermally and at steady-state,

$$T_7 = T_3 = T_8 \qquad 5.4.6$$

$$M_7 = M_8 \qquad 5.4.7$$

$$V_7 = V_3 \qquad 5.4.8$$

5.4.4 Second Effect

At the tubes of the second effect, there is no change of phase and the liquid inlet temperature, T_{15}, is the controlled boiling temperature in the second effect separator. The dynamic energy equation becomes

$$\frac{W_{tf} C_p \rho_L}{2} \frac{dT_{14}}{dt} = M_{15} C_p (T_{15} - T_{14}) + U_f A_f \left(T_{10} - \frac{(T_{14} + T_{15})}{2} \right) \qquad 5.4.9$$

and the shellside steady-state equations (T_{10} controlled) are

$$V_{10} = \frac{(V_4 + M_4) C_p (T_4 - T_{10}) + \lambda_4 V_4 - U_f A_f \left(T_{10} - \frac{(T_{14} + T_{15})}{2} \right)}{\lambda_{10}} \qquad 5.4.10$$

$$M_{10} = M_4 + V_4 - V_{10} \qquad 5.4.11$$

5.4.5 Second Effect Separator

The boiling point in the second effect separator is assumed to be controlled at T_{15}. An unsteady state energy balance gives,

$$A_s \rho_L C_p T_{15} \frac{dH_s}{dt} = M_{14} C_p (T_{14} - T_{15}) + M_8 C_p T_8 - V_9 (C_p T_{15} + \lambda_{15}) \qquad 5.4.12$$

and the unsteady state mass balance

$$V_9 = M_8 - \rho_L A_s \frac{dH_s}{dt} \qquad 5.4.13$$

hence from substitution,

$$\rho_L A_s \lambda_{15} \frac{dH_s}{dt} = M_{14} C_p (T_{15} - T_{14}) + M_8 C_p (T_{15} - T_8) + M_8 \lambda_{15} \qquad 5.4.14$$

5.4.6 Condenser

In the detailed model, the vapour side temperature T_{vac} was assumed to be controlled. Thus the simplified equations are the same.

$$\frac{W_{tc}\rho_L C_p}{2}\frac{dT_{13}}{dt} = M_{12}C_p(T_{12} - T_{13}) + U_c A_c\left(T_{vac} - \frac{(T_{12} + T_{13})}{2}\right) \quad 5.4.15$$

$$T_{11} = \frac{V_9(C_p T_{15} + \lambda_{15}) + M_{10}C_p T_{10} + V_{10}(C_p T_{10} + \lambda_{10}) - U_c A_c\left(T_{vac} - \frac{(T_{12} + T_{13})}{2}\right)}{M_{11}C_p} \quad 5.4.16$$

$$M11 = V_9 + M_{10} + V_{10} \quad 5.4.17$$

5.4.7 Discussion of Reduced Model

Equations 5.4.1 to 5.4.17 represent the reduced dynamic model of the evaporator. There are four differential equations; three describing variation of liquid temperature at exchanger tube outlets and one describing the behaviour of head in the second effect separator. The vapour side temperatures are assumed to be controlled via the vacuum pump at the condenser. The effect of all types of assumptions is tested by simulation and comparison with experimental data.

5.5 Chapter Review

Chapter 5 describes the development of the steady state and dynamic models of the double effect evaporator. A reduced dynamic model is derived by assuming the vapour pressure is controlled. This simplified model is suitable for implementation in the real-time Kalman filter algorithm.

Following the derivation of the mathematical models, it is necessary to describe their on-line implementation together with off-line simulation experiments.

CHAPTER 6

SIMULATION AND ON-LINE EXPERIMENTS

6.1 Introduction

In previous chapters, the development of the hardware, software and mathematical models for the on-line system is described. The combination of on-line (BASELINE) and off-line (ASP) interactive program packages with the steady state and dynamic models provides a basis for the on-line investigation into the operation of the double effect evaporator. The objective of this chapter is to describe the experiments that comprise this investigation.

During recent years, the development of process control computers has reached a high degree of sophistication; currently a complete central processor and memory can be accommodated on a single printed circuit board - thus drastically reducing hardware costs. Data logging equipment has also developed rapidly with the introduction of solid-state components offering high -speed scanning and analogue to digital conversion. One unobvious drawback to the acquisition of such hardware is the availability of software and a mathematical description of the process. In any on-line experimentation, the computer programs provide the essential links between computer, plant and operator. The scope of on-line operations depends upon the flexibility of such programs and the extent of mathematical modelling.

At the simplest level, an on-line computer can be programmed in machine code to control a data logger and print or store the digital values derived from analogue measurements. This type of application represents the minimum

improvement over conventional 'stand-alone' logging systems and fails to utilize the programming potential of the modern, high-speed, digital computer. A minor improvement is effected by storing the instrument calibration constants in core so that the plant measurements can be presented in standard engineering units. Only by excessively time consuming machine code programming can more complex applications be achieved.

When the machine code data acquisition programs are linked to a high-level language compiler to form a package such as BASELINE, the whole range of operations usually associated with off-line computing becomes available for on-line usage. Logical operations, data input/output handling and numerical techniques such as matrix arithmetic and calculation of standard functions can be included with on-line programs to provide extensive programming capabilities. Another advantage, apparent with the use of BASELINE, is the interactive operation of BASIC in the development, testing and editing of programs. Algorithms of the complexity of the non-linear Kalman filter can be programmed and tested in a fraction of the time required for their development in machine code. Furthermore, any programming errors are detected either before execution or while running under control of the BASIC compiler, thus avoiding the possibility of corrupting the contents of the computer memory. Although the interpretitive nature of BASIC represents an addition to program execution time, in most cases the advantages of high level programming outweigh the disadvantage of a reduction in processing speed.

The principle requirements of on-line programs that are not apparent when writing conventional off-line programs are as follows:

1. Program Timing During on-line experiments, measurements are required at definite times. Consequently any other processing must cease when a measurement time occurs so that the computer can be dedicated to data logger control. By means of the hardware interrupt facility connected to the H316 real time clock, any program may be temporarily suspended while on-line operations are performed. Updated variables, derived from measurements are then stored into the appropriate area of the background program before control is returned. The quantity of processing between each instrument sampling is governed by the maximum measurement frequency for a given application and the rate of operation of the data logger under computer control. Where the sampling frequency is critical, as in the case of on-line Kalman filtering, timing experiments are required a priori.

2. Program Control Unlike batch off-line processing, the timing and execution of on-line programs requires control from the process end of the system. In industrial computer control applications, this means the incorporation of a special-purpose plant operators console into the computer system. Since the BASIC compiler is interactive in operation, program editing and initiation for the evaporator system can be carried out via the remote teletype. Control of BASIC programs during execution is effected by use of the sense switches and their extensions located in the MDP200 remote cabinet.

3. Results Output During the course of an on-line experiment vast quantities of information may be processed which in an off-line program could be printed at a teletype. The output of even minor quantities during on-line

experiments may be excessive in terms of computer time usage. Consequently, the results of on-line experiments are either stored in the computer so that they can be dumped at the teletype when CPU time is no longer at a premium, or the quantity of output is reduced to a minimum by further processing. When the results of computations cannot be checked as they are performed, special precautions must be taken during the development of programs to ensure complete accuracy (and hence confidence) before running on-line.

Compared with conventional experimentation, the operation and instrumentation of the double effect evaporator is straightforward except in the type of transducers selected to transmit analogue signals to the data logger. All measurements are converted to a d.c. voltage by linear transducers and are susceptible to corruption by electrical noise. This effect is not apparent with conventional instrumentation where the results of high frequency background voltages are damped out within continuous recording equipment. The analogue voltages input to the data logger are sampled at discrete times by the ADC and thus the effect of noise becomes evident. This problem is overcome, in part, by electronic filtering at the ADC - but only at the expense of an increase in the logger sampling time per channel. Numerical smoothing is obtained by repetitive scanning of each channel at each sampling interval to obtain an ensemble average based upon the state of the instruments over a few seconds rather than at a single instant. An investigation into the effect of noise on the MDP200 ADC is reported by Chard (103). The total resulting signal fluctuation is the sum of the effects of background and MDP200 reed relay noise. During instrument calibration, both effects are considered by operating on-line to the computer.

Like many other experimental systems, the time-consuming operations are concerned with hardware rather than computer programs. The maintenance of process plant, instruments and data logger during on-line experiments, while requiring greater effort than program control, form a necessary part of experimentation and highlight the more realistic problems not experienced by theoretical studies reported in the literature.

The sequence of simulation and on-line experiments is as follows:

1. Instrument Calibration This is carried out on-line to the computer to take into account normal instrument noise.

2. Steady State Operations On-line steady-state experiments are performed over the whole range of operation of the evaporator and the mathematical model is solved to determine unmeasured variables. Further off-line processing is used to analyse all steady-state results to determine correlations for the heat transfer coefficients.

3. Dynamic Logging Between successive steady state conditions the transient state of each instrument is recorded for later comparison with the results of dynamic simulations. The logs include the response of all plant measurements to step changes in plant control variables (preheater feed rate and steam rate to the first effect).

4. Dynamic Simulation The dynamic models, including correlations for heat transfer coefficients are simulated using the ASP package. Comparison of the simulated response with the dynamic logs provides a qualitative indication of the 'fit' of the mathematical model.

5. Kalman Filtering The non-linear mathematical model is incorporated into the Kalman filter algorithm. The following experiments are performed

a) On-line, real time state variable and parameter estimation

b) Off-line estimation based on real plant data, to determine the effects of measurement and model error statistics on the performance of the filter.

The teletype listings of all computer programs are combined in Appendix 6. Block diagrams defining the general structure of programs are included in this chapter and reference is made to the appropriate program in the Appendix.

6.2 General Operations

In all on-line and simulation experiments, a computational algorithm is derived from the mathematical model and translated into the BASIC language. The use of the interactive packages BASELINE and ASP requires programs to be structured in a definite manner to utilize the supporting FORTRAN and assembler subroutines. In all cases, at the BASIC programming level, calibration constants, temperatures, flows etc. are stored in arrays - each subscript corresponding to the appropriate channel or stream number. Correlations, determined from steam tables, relating the physical properties of saturated steam to temperature are stored in BASIC as either standard functions or subroutines for convenient reference from within programs.

6.2.1 On-line Program Structure

Figure 6.1 shows a block diagram of the general structure of an on-line

FIGURE 6.1

GENERAL STRUCTURE OF ON-LINE PROGRAMS

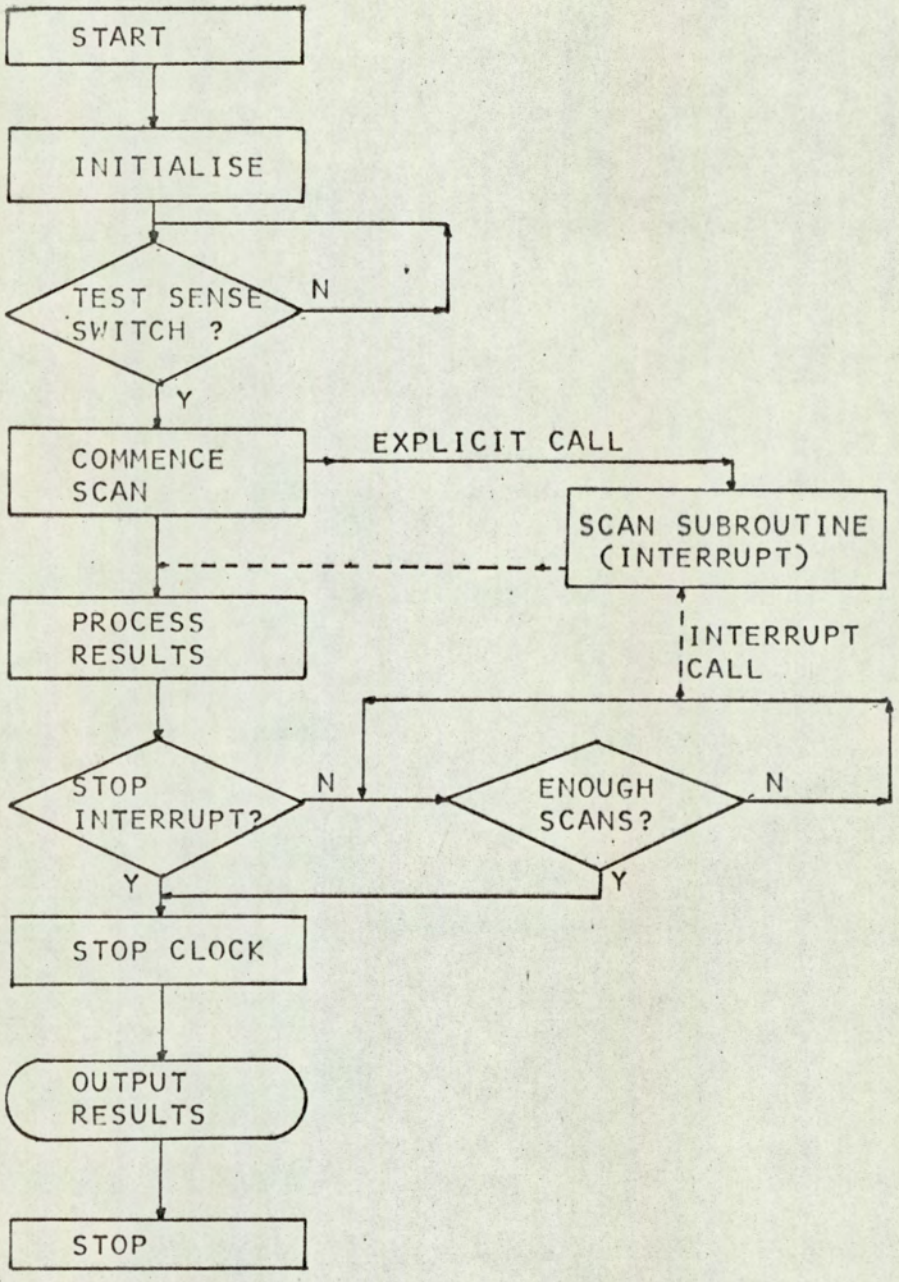

program. Execution commences with the program stored in the computer and the BASIC compiler requesting a programmer operation by printing a question mark character at the remote teletype. On receiving the appropriate command, RUN, the program initialisation section is executed to enable input of run time data. The program then cycles around a test of sense switch using the sixth BASELINE subroutine,

CALL (6, 2, L1)

until, in this case, the second sense switch is depressed and the numerical state of the flag L1 is incremented from unity. Effectively, this forces the execution of the program to wait for remote operation of the switch when plant logging operations can commence.

The principal data logging operation of scanning consecutive channels is performed by the seventh subroutine,

CALL (7, I , N1, N2, E, A(0,0), S, T, E1)

where I is the interval, in seconds, at which the scanning operation is repeated;

N1 and N2 are the first and last channels in the scanning sequence ;

E is the number of samples taken to form an ensemble average at each sampling time ;

A(0,0) is the first element of the BASIC array into which the digitised, averaged analogue recordings are stored;

T is the total number of interrupts required during a given experimental run;

S is a record of the number of interrupts performed up to the current time;

E1 is an error flag indicating whether N1 or N2 are out of range of the available channel numbers.

When logging operations commence, this subroutine is called explicitly to set up the interrupt frequency for the computer real time clock and the link addresses between the machine code subroutines and the BASIC compiler for the variable names. In particular, the array A is used to store the ensemble averages of the ADC output from A(N1, S) to A(N2, S).

Subsequent explicit calls to this subroutine are not necessary since it is accessed automatically every I seconds by means of the computer real time clock. Each time the subroutine is serviced on interrupt the data values are copied into the array A so that they can be further processed by BASIC programs. Once initialised interrupt continues until either S=T, the fifth BASELINE subroutine is called,

CALL (5, 0)

or program control is returned to the teletype by manual intervention or a program execution error.

When logged data are available to the BASIC compiler, the information is processed and relevent results are output or stored. The nature of the processing depends upon the specific application and varies in complexity from simple conversion of raw data by calibration constants to execution of the Kalman filter algorithm. Following processing,a further sense switch test determines whether the interrupt logging operations are terminated. If the operations are continued the program waits for the next interrupt by testing the state of the variable S in the argument list of the seventh subroutine . When all logging operations are complete or the sense switch is depressed, the complete results are output to the teletype. Following output, the computer returns to the programmer request mode by printing the question mark character.

Although Figure 6.1 shows the processing of a single batch of data between each interrupt, the seventh subroutine is written to permit interrupt during the processing of a batch. This requires storage of data in the array A while processing of previous batches is completed. Consequently, the depth to which successive processing can be interrupted is governed by the available storage in the BASIC compiler.

A detailed description of the BASELINE subroutines and their method of operation is given in Appendix 3.

6.2.2 Simulation Program Structure

Dynamic models are simulated using the ASP package (101,102). This is constructed to minimise programming effort by using the COMMON area of memory for transmission of variables required only by the FORTRAN simulation subroutines. BASIC programs, using the ASP subroutines, must be written according to the structure shown in Figure 6.2. There are three sections, as follows.

1. Initialisation Section In this section, the program data are input including the initial values of the dependent variables in the differential equations. Also the first ASP subroutine is called,

CALL (1, T)

to zero the independent variable T and to initialise the COMMON area of core.

2. Derivative Section This section contains the derivative and algebraic expressions that comprise the dynamic model, translated into BASIC and arranged

FIGURE 6.2

STRUCTURE OF ASP PROGRAMS

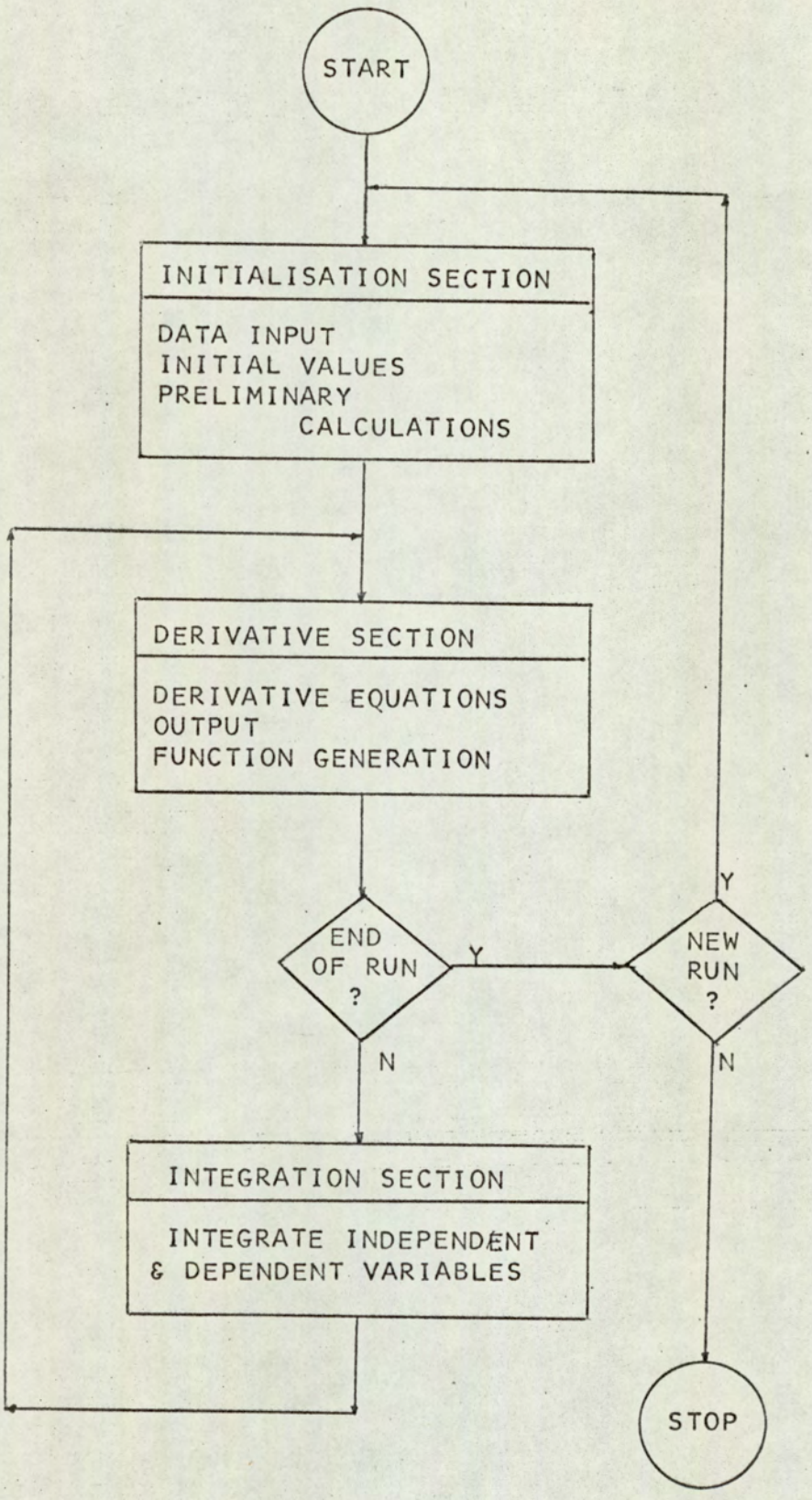

into the correct order. At the end of this section the second ASP subroutine is called to control output of information.

CALL (2, P, E, F1, F2)

The flag F2, is set whenever the independent variable becomes equal to the value specified by the print interval, P, and the flag F1 when the independent variable becomes equal to the terminal value E. Control of the output of the dependent variables is carried out by tests on the numerical values of the flags in the BASIC program.

3. Integration Section This section commences with a call to the third subroutine

CALL (3, T, H, R)

to increment the independent variable, T, by the step length, H.. R determines the order of integration of the dependent variables - either 2 (Modified Euler) or 4 (Runge-Kutta). This is followed by a list of calls to the fourth subroutine

CALL (4, X, D1)

which integrates the derivative D1 over the step length to give the dependent variable X. The length of the list of CALL statements is fixed by the number of first order differential equations to be integrated. At the end of the integration section, program control is unconditionally transferred to the start of the derivative section.

In addition to the integration subroutines, a function generation subroutine is included in the ASP package,

CALL 5(A, B, C, X(0), Y(0))

where from a table of data Y = f(x) stored in the BASIC compiler and containing

C entries, a value B of Y is computed from a value A of X by linear interpolation.

The principal advantage of ASP is that the user need not be aware of the FORTRAN subroutines providing the program is correctly structured. As with BASELINE, the writing and editing of programs is simplified by the interactive operation of the BASIC compiler.

A detailed description of the FORTRAN subroutines and their incorporation into the BASIC compiler is given in Appendix 4.

6.2.3 General Correlations

Continual reference to tables or charts for evaluation of non-linear functions can be avoided by representing the data by some approximate algebraic function. In the worst case, this may represent the development of an iterative algorithm while at the simplest level the data may be approximated by a linear equation.

In on-line steady state and dynamic experiments, it is necessary to obtain a correlation relating the temperature of saturated steam to its pressure. This is because all vapour side measurements are made with pressure transducers. An algorithm has been developed by Richards (104) where the pressure P (kNm^{-2}) is related to temperature T (^{o}K) by the function,

$$P = P_s \exp (13.3185\ \bar{T} - 1.976\ \bar{T}^2 - 0.6445\ \bar{T}^3 - 0.1299\ \bar{T}^4) \qquad 6.2.1$$

where $\bar{T} = 1 - \frac{T_s}{T}$ 6.2.2

and T_s, P_s is the temperature and pressure of saturated steam at atmospheric pressure ($373.15\ ^{o}K$ and $101.325\ kNm^{-2}$).

To calculate T when P is given, a first estimate of $\bar{T}$ is formed by ignoring all but the first term of the polynomial in equation 6.2.1

$$\bar{T}(1) = \frac{\ln\left(\frac{P}{101.325}\right)}{13.3185} \qquad 6.2.3$$

and successively more accurate estimates are obtained by recursively calculating

$$\bar{T}(n+1) = \frac{\bar{T}(1) + ((0.1299\bar{T}(n) + 0.6445)\bar{T}(n) + 1.976)\bar{T}(n)^2}{13.3185} \qquad 6.2.4$$

When, for some small value of n, $|\bar{T}(n+1) - \bar{T}(n)| \leq E$ where E is a small constant, the desired estimate of T (^{o}C) is found from equation 6.2.1 by

$$T = \frac{373.15}{(1 - \bar{T}(n+1))} - 273.15 \qquad 6.2.5$$

Program 1 of Appendix 6 shows the above algorithm translated into a BASIC subroutine. It is important to differentiate between BASIC subroutines (the GOSUB statement) and FORTRAN subroutines that are called from BASIC (the CALL statement). The variable names in a BASIC subroutine are not dummy names transferred as arguments in the FORTRAN sense, and thus must correspond to variable names within the main program. Program 1 contains the listing of the iterative subroutine and a test program comparing the calculated values with data obtained from steam tables (105). The execution commands and results are included as an example of BASIC operations.

For simulation of the dynamic model, further correlations relating latent heat and enthalpy to temperature are advantageous. The relationship between vapour density and temperature is required for simplification of the vapour side equations in the dynamic model. Correlations are obtained by carrying out

linear regression on data obtained from steam tables using a standard Honeywell program - statistical least squares (SLS). The data for the SLS program is selected to be in the region of vacuum operation of the double effect evaporator. The results of the regression analysis are described in Section 7.1.2, the correlations are as follows

Enthalpy	:	$g(T) = 4.1868T + \lambda(T)$	6.2.6
Latent heat	:	$\lambda(T) = -2.4068T + 2501.6$	6.2.7
Density	:	$\log \rho_v(T) = 1.93 \log T - 3.1487$	6.2.8

6.2.4 Calibrations

Where mechanical/electrical transducers operate in a pilot plant environment, frequent calibration is required in order to maintain consistent on-line results. Since the electrical signals are corrupted by noise, the calibrations are carried out on-line to the computer so that the common mode rejection facility of the MDP200 data logger is utilized. On-line operation further enables the same channel to be scanned rapidly so that large sample sizes can be averaged - thus filtering numerically.

The on-line calibration program follows the form of Figure 6.1. The channels are calibrated singly using the first BASELINE subroutine,

CALL (1, N, V, F)

which causes channel number N to be scanned once and the data value to be stored in BASIC as the variable V. The flag F is set if the channel is out of the range of available numbers. Interrupt and repetitive processing is not required.

The program is initialised by inputting the number of the channel to be

calibrated and the execution sequence waits for manual intervention by testing the state of sense switch 2. When the switch is depressed logging operations begin and the channel is scanned continuously until the switch is released, the average of all the scans is then printed at the teletype and the computer returns to the waiting state. If a new channel is required, the program is reinitialised by pressing sense switch 3 after a print out. Program 2 shows the on-line calibration program together with an example of normal output. During continuous scanning, measurements of flow, temperature or pressure are taken manually at the evaporator.

Measurement of temperature by thermocouple is considerably more accurate than alternative methods against which to calibrate, particularly when an isothermal reference chamber is available as a cold junction. Consequently, the calibration procedure described above serves only as a check against manufacturers calibration data. The flow meters are calibrated against flows recorded with measuring cylinder and a stop-watch, and pressure transducers against a mercury manometer.

When sufficient data sets are collected, a linear regression is carried out with the SLS program. The calibration of the differential pressure gauge on the main steam feed orifice plate requires a polynomial regression. Again a standard Honeywell program is available.

6.3 Steady State Experiments

On-line operation of the double-effect evaporator at steady state provides a broad insight into the complexities of the computer/plant system. Furthermore,

when the on-line measurements are used to solve the steady-state model (equations 5.2.1 to 5.2.36), the unmeasured process variables can be calculated so that the state of each process stream is available. From further off-line analysis of steady-state data the heat transfer coefficients of each heat exchanger can be calculated. From sets of data based on steady state runs over the whole range of operation of the evaporator, the correlations relating heat transfer coefficients to plant operating conditions are computed. The correlations are then available for the simulation of dynamic models and in the real time application of the Kalman filter.

One observation of both off-line and on-line experiments is that the plant is never at true steady state. The effects of random disturbances on feed liquor flow and temperature, the unknown performance characteristics of the vacuum pump and the accummulation in the second effect represent constant dynamic disturbances and at best the plant attains a pseudo steady state condition By means of the seventh subroutine of the BASELINE package, a BASIC program is written to scan the instruments at pseudo steady state over a period of one half hour. The effects of any major dynamic disturbances are reflected in the standard deviations of the analogue signals. When the deviations are large, the steady state mass and energy balances are not executed and further time is allotted to enable the plant state to settle before recommencing on-line logging.

6.3.1 On-line Program

The on-line steady state program (Program 3 of Appendix 6) follows the form outlined in Figure 6.1.

When the program is entered at the BASIC level, the starting time of operations is recorded by reading the MDP200 24 hour clock by the second BASELINE subroutine,

CALL (2, T9)

and the variable T9 is returned with the current time. Run time data are then entered from the teletype as follows.

1. Sampling interval - the time between successive interrupts and hence the execution of subroutine 7

2. Samples required - the total number of samples in the steady state run

3. Ensemble - the number of scans at each sampling interval taken to form the ensemble average

4. Steam valve position - since the steam flow calibration is known to be unreliable, the valve position is recorded to assist in reconciling differences between measured and calculated steam rates.

5. Water flow rate. As the cooling water flow rate to the condenser is not measured on-line, the rotameter reading is converted to the appropriate flow rate and input to the program via the teletype.

6. The temperature of the steam in the feed line to the first effect calandria is input by the scan switches at the MDP200 remote cabinet. By means of the fourth BASELINE subroutine,

CALL (4, W1)

the four digit value set at the scan switches is stored into the BASIC variable W1. Although the steam pressure is regulated during normal operations, the pressure fluctuates according to the quantity of condensate in the steam supply lines and the requirements of other users in the laboratory.

When all run data are input, the computer waits for manual control of sense switch 3 at the remote cabinet and when the switch is depressed, on-line steady state experiments are executed as follows.

1. In order to measure the accummulation in the second effect, the differential pressure transducer recording liquid head is scanned rapidly 200 times and an accurate reading of time is taken from the MDP200 clock. The time and the average of the scans are stored for comparison with similar readings at the end of the run.

2. The interrupt scanning operations are initiated by calling the seventh BASELINE subroutine. Following this call, computer operations are temporarily suspended at each sampling interval and subroutine seven is executed. The total number of interrupts is given by the 'samples required' input during program initialisation.

3. The results of scanning the analogue values are stored as continuous sum and sum of squares for later computation of mean and standard deviation.

4. The program then tests sense switch 4 for manual run termination before the required number of samples is achieved (e.g. in the case of plant breakdown). If the test is positive, the real time clock is stopped by a call to the fifth subroutine. If the test is negative, the program waits for interrupt to occur at the next sampling interval by testing the state of the 'scans done' flag in the argument list of subroutine seven.

5. On return from interrupt, the 'scans done' flag is incremented and program control returns to step 3 above.

6. When the total number of samples is achieved or when sense switch 4 is manually set, the head in the second effect is again scanned rapidly 200 times

and an accurate time reading is taken so that the accummulation can be calculated.

7. The analogue values are averaged and the standard deviations computed. If the standard deviations are large, the complete steady state run is terminated by pressing sense switch 1 which creates a BASIC program break.

8. The results of the calculations are printed in the analogue output section which lists the mean and standard deviation of each channel. The mean values are then converted into SI units by the calibration constants and the resulting vapour pressures converted to temperature by the subroutine described in Section 6.2.3. The steady state mass and energy balances are solved to determine unmeasured variables. When the mass flow, temperature and enthalpy of each stream have been computed, a comprehensive converted output is printed at the teletype.

6.3.2 Experimental Procedure

Steady state operations commence when plant conditions are steady following start up. Since the plant is never at true steady state, the best pseudo steady state conditions are achieved by adjusting either the steam rate to the first effect or liquid feed rate to the preheater and allowing sufficient time for the major dynamic effects to settle. During this time, each instrument is scanned and the digital output of the ADC is observed at the visual display unit of the MDP200 remote cabinet. This provides a check on instrument and logger operation before each on-line run is initiated.

When the plant is settled and the instruments are checked, the BASIC program is entered by the RUN command. The current time is immediately printed

for later reference and the run-time values of sampling interval, samples required, ensemble, steam valve position and condenser cooling water rate are input. The temperature of the steam in the feed line to the first effect is set on the scan identification switches; the numerical value is derived from pressure guage observations and the use of steam tables. Logging commences as soon as sense switch 3 is depressed and the ADC output for any channel can be displayed at the VDU, thus providing a continuous check on the performance of the MDP200 main cabinet.

As logging continues, the steam condensate from the shellside of the first effect is collected for comparison with the computed steam rate. In the event of a plant or logger breakdown, logging operations are terminated by manual operation of sense switch 4 when program execution is immediately directed to the analogue output section so that the cumulative effects of errors can be observed. Prior to the analogue output section, the MDP200 clock is read and the current time output. Under normal running conditions logging continues until the total number of samples required is achieved. During the subsequent computation and output, the operating conditions of the plant are changed in anticipation of a further steady state run. When the plant is settled again, the program is re-entered.

6.3.3 Implementation of the Steady State Model

When the steady state analogue output section is complete, the raw data are converted to SI units so that the mass and energy balances can be solved. The converted measurements are stored in a BASIC array, each subscript

corresponding to the instrument channel number. Figure 5.1 shows the pilot plant including stream numbers and instrument readings. In the steady state model, (equations 5.2.1 to 5.2.36) equations 5.2.7 - 5.2.10 and 5.2.33 - 5.2.36, the simple mass and energy balances are included for completeness only and thus it is unnecessary to program every equation when simple relationships can be implied. The stream notation of Figure 5.1 is adopted in stating the calculation order.

After the accumulation in the second effect (M_A) is calculated, the enthalpies of some streams can be computed directly from measurements, (datum of $0^{\circ}C$ is assumed),

$$H_1 = M_1 C_p T_1 \qquad 6.3.1$$

$$H_2 = M_1 C_p T_2 \qquad 6.3.2$$

$$H_3 = (M_1 - M_8)\, g(T_3) \qquad 6.3.3$$

$$H_8 = M_8 C_p T_8 \qquad 6.3.4$$

$$H_9 = (M_8 - M_A)\, g(T_9) \qquad 6.3.5$$

$$H_{11} = (M_1 - M_A)\, C_p T_{11} \qquad 6.3.6$$

$$H_{12} = M_{12} C_p T_{12} \qquad 6.3.7$$

$$H_{13} = M_{13} C_p T_{13} \qquad 6.3.8$$

$$H_A = M_A C_p T_{15} \qquad 6.3.9$$

where $g(T)$ is the vapour enthalpy function.

An energy balance on the cyclone separator (equation 5.2.13) gives

$$H_7 = H_8 + H_3 \qquad 6.3.10$$

and hence the temperature of the liquid/vapour mixture leaving the first effect tubes can be calculated by solving

$$g(T_7)(M_1 - M_8) + M_2 C_p T_7 = H_7 \qquad 6.3.11$$

for T_7. This requires the enthalpy correlation (equation 6.2.6)

$$g(T) = 4.1868T + \lambda(T) \qquad 6.3.12$$

where $\lambda(T) = -2.4068T + 2501.6 \qquad 6.3.13$

and rearrangement to give

$$T_7 = \frac{H_7 - 2501.6\,(M_1 - M_8)}{1.78(M_1 - M_2) + M_2 C_p} \qquad 6.3.14$$

from an energy balance on the first effect (equation 5.2.12) the steam rate can be calculated. Assuming the steam loses heat by condensation only,

$$V_5 = M_6 = \frac{H_7 - H_2}{g(T_5) - C_p T_6} \qquad 6.3.15$$

and hence the enthalpies of the steam and condensate streams follow directly.

$$H_5 = V_5\, g(T_5) \qquad 6.3.16$$

$$H_6 = V_5 C_p T_6 \qquad 6.3.17$$

From the energy balance on the preheater (Equation 5.2.11) the rate of condensation in the preheater shell is determined,

$$M_4 = \frac{H_2 - H_1 + (M_1 - M_8)(g(T_3) - g(T_4))}{\lambda(T_4)} \qquad 6.3.18$$

and hence

$$H_4 \text{ (liquid)} = M_4 C_p T_4 \qquad 6.3.19$$

$$H_4(\text{vapour}) = (M_1 - M_8 - M_4)\, g(T_4) \qquad 6.3.20$$

The circulation rate from the second effect separator through the second effect is found from an energy balance on the separator (Equation 5.2.15),

$$M_{15} = \frac{H_8 - H_9 - H_A}{C_p (T_{15} - T_{14})} \qquad 6.3.21$$

and hence

$$H_{14} = M_{15} C_p T_{14} \qquad 6.3.22$$

$$H_{15} = M_{15} C_p T_{15} \qquad 6.3.23$$

From the energy balance on the second effect (equation 5.2.14) the rate of condensation in the second effect shell is determined,

$$M_{10} - M_4 = \frac{H_{14} - H_{15} - (M_1 - M_8 - M_4)(g(T_4) - g(T_{10}))}{\lambda (T_{10})} \qquad 6.3.24$$

and hence,

$$H_{10}(\text{liquid}) = M_{10}\, C_p T_{10} \qquad 6.3.25$$

$$H_{10}(\text{vapour}) = (M_1 - M_8 - M_{10}) g(T_{10}) \qquad 6.3.26$$

From the energy balance on the condenser (equation 5.2.16), the cooling water rate in the condenser can be calculated,

$$M_{12} = \frac{H_{11} - H_9 - H_{10}(\text{liquid}) - H_{10}(\text{vapour})}{C_p (T_{12} - T_{13})} \qquad 6.3.27$$

The above equations together with the measurements and the implied simple mass balances define the flow, temperature and enthalpy of each stream. The redundancy in the model (2) is used to calculate the steam flow to the first

effect shell and the condenser cooling water rate - the latter providing a measure of total system heat losses when compared with the measured flow rate.

6.3.4 Results Output

Figure 6.3 shows a typical teletype listing resulting from a steady state run. When logging is complete, raw data are output to the teletype in the analogue output section. During normal vacuum operations, the analogue signals are arranged to be negative voltages so that major hardware faults can be detected visually by a change in sign. If the analogue results are acceptable the program performs the heat and mass balances and presents the results in a comprehensive converted output section. For each unit of the evaporator the temperature, flow rate and enthalpy are printed for each stream, as shown in Figure A7.8. Following the converted output, the following computed flows and data are printed for later reference during off-line analysis.

1. Second effect pump circulation rate.
2. Input and calculated condenser cooling water rates.
3. The measured accumulation in the second effect
4. Calculated steam rate to the first effect
5. Steam valve position

6.4 Dynamic State Logging

On completion of a successful steady state run, the control variables - preheater feed and first effect steam rate - are manually adjusted. When the plant settles to a new steady state another run is commenced. During the settling time, the dynamic state of the plant is recorded for later comparison with

FIGURE 6.3 - STEADY STATE PROGRAM : ANALOGUE OUTPUT SECTION

```
 STEADY STATE LOGGING PROGRAM

START TIME  1614  HRS
SAMPLING INTERVAL 130
SAMPLES REQUIRED 120
ENSEMBLE          112
STEAM VALVE POSITION 1.375
WATER FLOW RATE 1742
READY


FINISH TIME 1624  HRS


   19  SCANS DONE

ANALOGUE OUTPUT

CHANNEL NO        MEAN          ST DEV

   12          -233.355        2.06155
   13            -9.66667       .582398
   14          -3854.17        3.74166
   15          -1729.72        1.87083
   16          -5823.73        4.89898
   17          -3464.96        2.82843
   18          -5136.56        8.7178
   19          -7259.59       45.0777
   20           -517.32         .559017
   21           -848.658       4.15331
   22           -613.206        .829156
   23          -1693.97        5.2915
   24          -1373.03        2.39792
   25          -1445.8         2.34521
   26          -1942.2         4.30116
   27           -938.175       4.89898
   28          -1840.83        7.17635
   29          -1898.23        7.31437
```

simulated results. The data represents the response of the plant to a step change in control variable settings.

6.4.1 Dynamic Log Program

Figure 6.1 shows the layout of the dynamic state log program; this is incorporated into the steady state logging program from statement 4000 (Program 3, Appendix 6). Once the program is initiated, a variable code is input as a reference for the type of step change. The codes are 1-change in preheater feed rate, 2-change in steam rate to the first effect. The program then waits for sense switch 3 to be depressed so that logging operations can commence. The manual operation of the switch coincides with the exact time of disturbing plant operations. Logging begins immediately and is repeated every minute by the interrupt facility of BASELINE subroutine 7. Each time the ensemble averaged analogue data are available, they are converted to SI units by the calibration constants and stored in a two-dimensional BASIC array. In the event of a plant or logger breakdown, logging operations are terminated when sense switch 3 is reset.

Theoretically, the program will continue to log and store data until manual intervention. However, the total quantity of data that can be stored in the array is limited by the available free storage in the BASIC compiler. Consequently, the total number of stored values for each channel is restricted to 30 (i.e. 30 minutes of dynamic logging).

6.4.2 Dynamic Log Output

After 30 minutes logging or following manual intervention, the stored converted measurements are printed as shown in Figure A7.48. Firstly, the control variable code is translated into either the steam rate or liquid feed rate and output to the teletype. Then for each channel, the measurements, based on averaging over each minute, are printed in the following order and units,

Channels	12 - 15	in	kNm^{-2}
"	16, 17		gs^{-1}
"	18		m
"	19		analogue value
"	20 - 29		^{o}C.

6.5 Simulation Experiments

6.5.1 General

Digital simulation has become an increasingly popular technique in the analysis of continuous systems. Nevertheless, it is important to realise the objectives and limitations of simulating dynamic models in isolation from real plant data. The reasons for using digital simulation are twofold. Firstly, a dynamic model may be developed before a process is constructed or when process experiments cannot be carried out. In this case, the simulation results provide an accurate response of the model only and any comparison between the numerical results and the real process is purely qualitative. Secondly, a dynamic model may be simulated when some accessible process measurements exist. The results of simulation can be compared with real data and the model may be modified to 'fit' the data so that the results of further simulation

experiments are comparatively reliable. Kalman filtering can be seen as a technique for continuously updating variables and parameters (estimation) based on simulated (predicted) and measured variables.

The objectives of the simulation experiments are as follows

1. To compare the numerical solution of the comprehensive model (equations 5.3.1 - 5.3.30) with on-line data from dynamic logging. This requires that the initial conditions of the numerical integration are the same as those of the real plant, i.e. the previous steady state values recorded prior to disturbance of the evaporator.

2. To ascertain the suitability of the mathematical model in on-line, real-time Kalman filtering. System order and available computer time at the filter prediction step (equation 2.5.4) are important factors in achieving this objective. Clearly the storage and integration time required for the 18th order comprehensive model are impractical in a real-time application and the 4th order reduced model (equations 5.4.1 - 5.4.17) can be utilised if the filter is insensitive to model simplification (27). Since one of the principal objectives of the research is to implement the Kalman filter algorithm in real time it is apparent that without such a technique an on-line study of the evaporator dynamics, is not feasible.

3. To justify the reduction in the order of the model by simulation and comparison with the results of dynamic logs. The reasons for such simplifications are twofold. In addition to the necessity to devise a simple model suitable for implementation of the filter algorithm, the dynamic characteristics of the vapour phase of the evaporator are uncertain. During the

theoretical derivation of the comprehensive model (Section 5.3.7) it was noted that the vacuum pump controls the vapour pressure throughout the evaporator and that the dynamics of the pump and the liquid heads in connecting pipework are not known. Furthermore, the time constants of the vapour phase differential equations are small in comparison to those of the liquid. This suggests that the vapour phase dynamic equations can be replaced by their steady state counterparts and the effect of the vacuum pump be treated as a control variable which is either constant or varying in a known manner.

6.5.2 Simulation Programs - General

One of the principal achievements in the development of the ASP package (Appendix 4) is that the programming effort required of the user is minimised. When a simulation program is structured in the format of Section 6.2.2, a knowledge of numerical integration methods is not required. Thus the simulation of the comprehensive and reduced dynamic models is simply performed by programming the derivative equations in the correct order in BASIC, calling the appropriate subroutines and determining a suitable integration step length by trial and error.

Although the evaporator never attains true steady state conditions, it is assumed that it has reached such a state at the end of a 'steady state' run. Consequently, for simulation purposes, the derivative expressions are forced to zero when the plant measurements are input as initial conditions. This is effected by evaluating a constant loss term for each derivative equation during the initialisation section of a simulation program, such that the derivative is zero.

The loss term remains constant in the dynamic equation throughout a complete simulation run. In practice, the loss term represents the sum of the following effects.

1. Plant heat losses which are not accounted for in the derivation of the dynamic model .

2. Errors due to the transient state of the plant which is assumed to be at steady state .

3. Errors in the evaluation of heat transfer coefficients from the steady state correlations (Section 7.3).

4. Errors in the steady state solution of the dynamic model due to assumptions in the mathematical derivation e.g. space lumping, perfect mixing, etc.

One exception to the calculation of zero derivatives is the equation defining the rate of change of the liquid level in the second effect separator. The liquid head varies throughout all plant operations and so the derivative expression is always finite (except at the unique state when the accumulation is zero) and requires computation at the start of a simulation run.

The unknown parameters in the model are the overall heat transfer coefficients. Section 7.3 describes the calculation of the correlation for a general heat exchanger with an isothermal vapour shell and liquid in the tubes. The correlation is calculated as the sum of effects due to the arithmetic mean temperature driving force, the liquid flow rate and the vapour flow rate. For example, using the variables of the preheater

$$Ug = a + b\left(T_4 - \frac{(T_1 + T_2)}{2}\right) + c\,M_1 + d\,V_3 \qquad 6.5.1$$

where a, b, c and d are constants. The correlations are incorporated into the derivative section of a simulation program and thus vary continuously as plant conditions change.

Measured disturbances in the evaporator variables are due to step changes in either the steam feed rate or the liquid feed to the preheater. When the derivatives of the dynamic model are set to zero, the differential equations are disturbed by an identical step change so that the results of the dynamic log and simulation can be compared graphically.

6.5.3 Implementation of Comprehensive Model

Prior to simulation, the comprehensive dynamic model (equations 5.3.1 - 5.3.30) is simplified by substituting the vapour density correlation,

$$\log \rho_v(T) = 1.93 \quad \log\ T - 3.1487 \qquad 6.5.2$$

and its derivative

$$\frac{d\rho_v}{dT} = \frac{1.93\rho_v}{T} = \bar{\alpha}(T) \qquad 6.5.3$$

into the vapour phase dynamic equations (5.3.2, 5.3.3, 5.3.7, 5.3.8, 5.3.20, 5.3.21); equation 6.5.3 is the function $\bar{\alpha}(T)$ utilised in the derivation of the model. Further, to define completely the simulation algorithm, the heat transfer coefficient correlations and loss terms referred to above are stated below. The notation detailed in Section 5.3 is adopted.

Preheater

$$L_1 = M_1 C_p (T_2 - T_1) - U_g A_g \left(T_4 - \frac{(T_1 + T_2)}{2} \right) \quad 6.5.4$$

$$L_2 = V_3 C_p (T_4 - T_3) - V_3 \lambda_3 + V_4 \lambda_4 + U_g A_g \left(T_4 - \frac{(T_1 - T_2)}{2} \right) \quad 6.5.5$$

$$U_g = 682 - 27.55 \left(T_4 - \frac{(T_1 + T_2)}{2} \right) + 13.44\ M_1 + 5.27\ V_3 \quad 6.5.6$$

First Effect

$$L_3 = M_1 C_p (T_7 - T_2) + V_7 \lambda_7 - U_e A_e (T_5 - T_7) \quad 6.5.7$$

$$U_e = 623.66 - 11.3405\ (T_5 - T_7) - 1.039\ M_1 + 58.026\ V_5 \quad 6.5.8$$

Second Effect

$$L_4 = M_{14} C_p (T_{14} - T_{15}) - U_f A_f \left(T_{10} - \frac{(T_{14} - T_{15})}{2} \right) \quad 6.5.9$$

$$L_5 = (V_4 + M_4)\ C_p (T_{10} - T_4) - \lambda_{10} (V_4 - V_{10}) + U_f A_f \left(T_{10} - \frac{(T_{14} + T_{15})}{2} \right) \quad 6.5.10$$

$$U_f = 218076 - 161.6 \left(T_{10} - \frac{(T_{14} - T_{15})}{2} \right) - 66.93\ M_{14} + 85.5\ V_{10} \quad 6.5.11$$

Second Effect Separator

$$L_6 = M_{14} C_p (T_{15} - T_{14}) + M_8 C_p (T_{15} - T_8) + V_9 \lambda_{15} \quad 6.5.12$$

Condenser

$$L_7 = M_{12}C_p(T_{13} - T_{12}) - U_c A_c\left(T_{vac} - \frac{(T_{12} + T_{13})}{2}\right) \qquad 6.5.13$$

$$U_c = 1151.92 - 63.01\left(T_{vac} - \frac{(T_{12} + T_{13})}{2}\right) + 6.634\, M_{12} + 61(V_9 + V_{10}) \qquad 6.5.14$$

The heat transfer coefficient correlations are the results of the multivariable linear regression analysis of steady state data described in Section 7.3.

Combination of the comprehensive model of Section 5.3 with the above equations gives the derivative expressions suitable for simulation with the ASP package. The eighteen first order differential equations are as follows:

Preheater

$$\frac{dT_2}{dt} = \frac{M_1C_p(T_1 - T_2) + U_g A_g\left(T_4 - \frac{(T_1 + T_2)}{2}\right) + L_1}{.5\, W_{tg}\rho_L\, C_p} \qquad 6.5.15$$

$$\frac{dT_4}{dt} = \frac{V_3C_p(T_3 - T_4) + (V_3 - V_4)\lambda_4 - U_g A_g\left(T_4 - \frac{(T_1 + T_2)}{2}\right) + L_2}{W_{sg}\left(C_p(1 - Y_g)_L + Y_g\lambda_4\bar{\alpha}(T_4)\right)} \qquad 6.5.16$$

$$\frac{dY_g}{dt} = \frac{V_3 - M_4 - V_4 - W_{sg}Y_g\bar{\alpha}(T_4)\frac{dT_4}{dt}}{W_{sg}\,(\rho_4 - \rho_L)} \qquad 6.5.17$$

$$\frac{dM_4}{dt} = \frac{(A_g U_g + V_3 C_p)}{\lambda_4} \cdot \frac{dT_4}{dt} - \frac{A_g U_g}{2\lambda_4} \cdot \frac{dT_2}{dt} - \frac{V_3 C_p}{\lambda_4} \cdot \frac{dT_7}{dt} \qquad 6.5.18$$

$$\frac{dV_4}{dt} = \frac{dV_3}{dt} - \frac{dM_4}{dt} \qquad 6.5.19$$

First Effect

$$\frac{dT_7}{dt} = \frac{M_1 C_p (T_2 - T_7) - \lambda_7 V_7 + U_e A_e (T_5 - T_7) + L_3}{W_{te}\left(C_p (1 - Y_e)\rho_L + Y_e \lambda_7 \bar{\alpha}(T_7)\right)} \qquad 6.5.20$$

$$\frac{dY_e}{dt} = \frac{M_2 - M_7 - V_7 - W_{te} Y_e \bar{\alpha}(T_7) \frac{dT_7}{dt}}{W_{te}(\rho_7 - \rho_L)} \qquad 6.5.21$$

$$\frac{dV_7}{dt} = -\frac{(A_e U_e + M_2 C_p)}{\lambda_7} \frac{dT_7}{dt} + \frac{M_2 C_p}{\lambda_7} \frac{dT_2}{dt} \qquad 6.5.22$$

$$\frac{dM_7}{dt} = -\frac{dV_7}{dt} \qquad 6.5.23$$

Second Effect

$$\frac{dT_{14}}{dt} = \frac{M_{14} C_p (T_{15} - T_{14}) + U_f A_f \left(T_{10} - \frac{(T_{14} + T_{15})}{2}\right) - W_{tf} C_p \rho_L \cdot \frac{dT_{15}}{dt} + L_4}{.5\, W_{tf}\, C_p \rho_L} \qquad 6.5.24$$

$$\frac{dT_{10}}{dt} = \frac{(V_4 + M_4) C_p (T_4 - T_{10}) + \lambda_{10}(V_4 - V_{10}) - U_f A_f \left(T_{10} - \frac{(T_{14} + T_{15})}{2}\right) + L_5}{W_{sf}\left(C_p (1 - Y_f)\rho_L + Y_f \lambda_{10} \bar{\alpha}(T_{10})\right)} \qquad 6.5.25$$

$$\frac{dY_f}{dt} = \frac{V_4 + M_4 - M_{10} - V_{10} - W_{sf} Y_f \bar{\alpha}(T_{10}) \frac{dT_{10}}{dt}}{W_{sf}(\rho_{10} - \rho_L)} \qquad 6.5.26$$

$$\frac{dM_{10}}{dt} = \frac{A_f U_f + (M_4 + V_4) C_p}{\lambda_{10}} \cdot \frac{dT_{10}}{dt} - \frac{A_f U_f}{2\lambda_{10}} \cdot \left(\frac{dT_{14}}{dt} + \frac{dT_{15}}{dt}\right) - \frac{(M_4 + V_4)}{\lambda_{10}} \cdot \frac{dT_4}{dt} \qquad 6.5.27$$

$$\frac{dV_{10}}{dt} = \frac{dV_4}{dt} + \frac{dM_4}{dt} - \frac{dM_{10}}{dt} \qquad 6.5.28$$

Second Effect Separator

$$\frac{dT_{15}}{dt} = \frac{M_{14} C_p (T_{14} - T_{15}) + M_8 C_p (T_8 - T_{15}) - V_g \lambda_{15} + L_6}{A_s \rho_L C_p H_s} \qquad 6.5.29$$

$$\frac{dH_s}{dt} = \frac{M_8 - V_9}{A_s \rho_L} \qquad 6.5.30$$

$$\frac{dV_9}{dt} = \frac{1}{\lambda_{15}} \left((T_8 - T_{15}) C_p \frac{dM_8}{dt} + M_8 C_p \frac{dT_8}{dt} - (M_{14} + M_8) C_p \frac{dT_{15}}{dt} + M_{14} C_p \frac{dT_{14}}{dt} \right) \qquad 6.5.31$$

Condenser

$$\frac{dT_{13}}{dt} = \frac{M_{12} C_p (T_{12} - T_{13}) + U_c A_c \left(T_{vac} - \frac{(T_{12} + T_{13})}{2} \right) + L_7}{.5 W_{tc} \rho_L C_p} \qquad 6.5.32$$

The controlled variables are T_1, M_1, M_{14}, M_{12}, T_{12}, T_{vac} and V_5.

In translating the above equations into BASIC, it is necessary to modify the order so that the right hand-side of assignment statements contain all known variables. Thus equation 6.5.20 precedes equation 6.5.18 and equation 6.5.30 precedes equation 6.5.23.

6.5.4 Simulation of Comprehensive Model

Figure 6.2 shows a block diagram of the ASP simulation of the comprehensive model (Program 4 of Appendix 6). At the initialisation section the following operations are performed.

1. The physical constants (heat exchanger dimensions, liquid density, etc.) are assigned to variable names.
2. BASIC functions are defined for calculation of $\alpha(T)$, $\overline{\alpha}(T)$ and λ_T
3. Initial conditions, taken from plant steady state data, are input together with integration step length and order, print interval and final value.
4. The heat transfer coefficients are calculated from the correlations stored in a BASIC subroutine.
5. The loss terms are calculated from the input data and output to the teletype.
6. The first ASP subroutine is called.

In the derivative section the differential equations are stated in the correct order and the output is controlled by calling the second subroutine. During each pass through the derivative section, the heat transfer coefficients are recalculated except at the first pass when the values are available from the calculation of the loss terms.

At the output section the flow and temperature of each stream of the evaporator is printed out.

As described in Section 6.2.2, the integration section consists of a call to the third ASP subroutine followed by eighteen calls to the fourth subroutine to integrate each derivative expression.

6.5.5 Implementation of Reduced Model

The reduced dynamic model, equations 5.4.1 to 5.4.17, is derived from the comprehensive model by assuming the vapour side temperatures are controlled by the vacuum pump. In order to assess the 'goodness of fit' of the reduced model it is necessary to regard the vapour temperatures as measured variables. A record of the response of the vapour temperatures is available from dynamic logging experiments and can be incorporated into simulation programs by utilising the function generation subroutine of ASP.

The heat transfer coefficient correlations and loss terms are identical to those in the comprehensive model equations, and the four first order differential equations are,

$$\frac{dT_2}{dt} = \frac{M_1 C_p (T_1 - T_2) + U_g A_g \left(T_4 - \frac{(T_1 - T_2)}{2} \right) + L_1}{.5 W_{tg} \rho_L C_p} \qquad 6.5.33$$

$$\frac{dT_{14}}{dt} = \frac{M_{14} C_p (T_{15} - T_{14}) + U_f A_f \left(T_{10} - \frac{(T_{14} + T_{15})}{2} \right) + L4}{.5 W_{tf} \rho_L C_p} \qquad 6.5.34$$

$$\frac{dH_s}{dt} = \frac{M_{14}C_p(T_{15}-T_{14}) + M_8C_p(T_{15}-T_8) + M_8\lambda_{15}}{\rho_L A_s \lambda_{15}} \qquad 6.5.35$$

$$\frac{dT_{13}}{dt} = \frac{M_{12}C_p(T_{12}-T_{13}) + U_cA_c\left(T_{vac} - \left(\frac{T_{12}+T_{13}}{2}\right)\right) + L_7}{.5\,W_{tc}\rho_L C_p} \qquad 6.5.36$$

The controlled temperatures are T_1, T_4, T_8, T_{12}, T_{15}, T_{vac} and all mass flows are controlled, except M_8 of equation 6.5.35. which is derived from a steady state energy balance on the first effect,

$$M_8 = M_1 - \frac{A_eU_e(T_5 - T_7) - M_2C_p(T_2 - T_7)}{\lambda_7} \qquad 6.5.37$$

6.5.6 Simulation of Reduced Model

Program 5 of Appendix 6 shows the ASP simulation of the reduced model. The operation of the program is similar to the simulation of the comprehensive model (Figure 6.2). At the initialisation section, the vapour phase data from a dynamic log are input to a number of arrays and the fifth ASP subroutine carries out interpolation on the data throughout a simulation run. Effectively this provides a continuous 'measurement' of the control variables in the derivative section of the program.

6.6 Kalman Filtering

6.6.1 General

In Chapter 5, the development of the comprehensive dynamic model indicated that an accurate mathematical description of the evaporator is represented by a non-linear, 18th order model. While a model of this order is clearly impractical for on-line algorithms, the development of a reduced model produces a more approximate description of plant performance. Since the ultimate objective of dynamic modelling of process plant is to devise a model suitable for optimal multivariable control, it is necessary to use the most accurate model available or devise a method for continuously updating the simplified model to coincide with plant performance. When the results of dynamic simulation and plant data are combined by an on-line sequential estimation technique such as Kalman filtering (Figure 6.4) the unknown model parameters and state variables can be estimated accurately. This assumes a knowledge of the model and measurement error statistics and sufficient computer time to execute the filter algorithm, take measurements and output results. Thus, when the filter estimation errors converge to their minimum values, the estimate of the states and parameters represents the 'best available' description of the plant based on current and previous measurements. Furthermore, the dynamic model, including the estimated parameters, will be the 'best' mathematical representation of the process at that time.

One important factor in judging the performance of the filter algorithm is the reliability of both initial statistics defining estimation error ($P(0|0)$) and the constant statistics that define measurement and process noise (R and Q). In particular, process noise statistics can be considered to be contributed to from

FIGURE 6.4

THE KALMAN FILTER ALGORITHM

PREDICTION

1. $$x(k+1|k) = x(k|k) + \int_{t_k}^{t_{k+1}} f(x(k|k),u(k))dt \qquad 6A$$

2. $$P(k+1|k) = \bar{\Phi}(k+1,k)P(k|k)\bar{\Phi}^T(k+1,k) + Q(k+1) \qquad 6B$$

ESTIMATION

3. Set i=1.

4. $$K_i(k+i) = P(k+1\,k)M_i^T(k+1)\left[M_i(k+1)P(k+1\,k)M_i^T(k+1) + R_i(k+1)\right]^{-1} \qquad 6C$$

5. $$x(k+1|k+1) = x(k+1|k) + K_i(k+1)\left[y_i(k+1) - M_i(k+1)x(k+1|k)\right] \qquad 6D$$

6. $$P(k+1|k+1) = \left[I - K_i(k+1)M_i(k+1)\right]P(k+1|k) \qquad 6E$$
$$\left[I - K_i(k+1)M_i(k+1)\right]^T + K_i(k+1)R_i(k+1)K_i^T(k+1)$$

7. If i<m put i=i+1 and return to step 4

8. Set k=k+1 and return to step 1.

m = no. of measurements.

three sources,

1. Errors in the model due to all types of assumption and simplification

2. Numerical errors in the calculation of the transition matrix

3. Random disturbances to system inputs (measured or unmeasured) and controls.

Since, as yet, there is no method of computing Q during a filter cycle for non-linear problems (Section 2.5), the numerical value of Q is determined by trial and error and an intuitive feel for the accuracy of estimation. While it seems that the correct selection of Q will account for modelling errors, the effect of the higher uncertainity on estimation of parameters is unsure. Further, one criticism of the filter performance (13), is that once converged it 'learns' the process too well so that when plant conditions change, the estimated state variables are considerably slower in response. Again, this must be accounted for in the selection of Q since it is only at equation 6B of Figure 6.4 that the predicted estimation error covariance matrix can be 'loosened' to take account of changes of this type.

The objectives of the on-line Kalman filtering experiments are as follows:

1. To develop and test a FORTRAN subroutine to execute the Kalman filter algorithm in real time. From both hardware and software considerations, the timing of filter cycle and data logging is critical so that a knowledge of computation time is necessary before going on-line to the evaporator.

2. To provide a comparison between the performance of the reduced model and the plant in real time, thus confirming the filtering technique as a possible basis for a multivariable control scheme.

3. To investigate the performance of the filter algorithm in estimating plant parameters (heat transfer coefficients) over a wide range of dynamic operations.

4. To determine the effects of uncertainty in the process noise error statistics upon the filter convergence at steady state and the loosening of the filter during transient operations.

In the reduced model, the parameters are the overall heat transfer coefficients for which correlations are available. The correlations are themselves approximate due to inherent errors in the on-line calculation of the steady state model. This provides an opportunity for testing the convergence of the parameter estimates when they are predicted at equation 6A by the correlations, and when they are driven to steady state by assuming a zero derivative state equation.

The examination of the filter performance in 3. and 4. above is carried out off-line using previously stored plant measurements. This removes the time consuming plant operations from experiments and permits repetitive processing of identical sets of data to examine the effect of process noise statistics on convergence and loosening of the filter.

6.6.2 Kalman Filter Software

During on-line experiments, the extended Kalman filter, Figure 6.4, is used. The first order approximation to the transition matrix has the disadvantage that the numerical error increases as the sampling interval between measurements increases. In order to minimise computation time and to avoid the matrix inversion involved in the classical form of the algorithm, the sequential processing algorithm described in Section 2.5, is utilised. It is reasonable to assume that measurements are uncorrelated, in which case the sequential algorithm represents a substantial saving in filter execution time. It is also advantageous to separate the computational

features of the algorithm into two parts.

1. Equations 6A and 6B of Figure 6.4 represent the part of the algorithm contributed to direct by the mathematical model. For non-linear problems computation of the transition matrix, $\Phi(k+1,k)$, is required at each filter cycle. These operations differ according to the mathematical model and the method of integration selected.

2. Once the integration step is performed and the transition matrix is computed, the calculation of the remainder of the filter algorithm is common to all filtering applications. Provided the measurements are available at the appropriate time, the necessary matrix operations should be executed as quickly as possible and with minimum programming effort.

These two features of the filter algorithm require different methods of programming. Integration and calculation of transition matrix are problem orientated and are written in BASIC where interactive execution and editing is a great advantage. The calculation of the filter cycle is a fixed operation and is programmed once only in FORTRAN as a subroutine. The compiled subroutine is then loaded into memory with other BASELINE subroutines and is thus permanently available in on-line applications.

Subroutine KALMAN executes the problem independent Section of the algorithm, Section A3.7. Due to difficulties in loading the subroutine into the BASELINE package, described in Appendix 3, all matrices that are transferred as subroutine arguments are singly subscripted arrays. This is a requirement of the FORTRAN translator package which permits the mixing of assembler and FORTRAN instructions that is necessary to effect loading of the subroutine. The disadvantages of this

complex operation are compensated for by the benefit of processing speed at the FORTRAN level. Since the filter algorithm is most conveniently programmed in two dimensional form, a non-standard FORTRAN function is used to translate a doubly subscripted expression into a single subscript. This requires the maximum dimension of the matrices to be stated and it is set to 10. In practice this represents a maximum of 10 state variables and 10 measurements. The subscript function is,

$$L1(I, J) = I + (J - 1) * 10$$

and thus a two dimensional filter algorithm is executed in one dimensional form. From the BASIC level, the subroutine is accessed by the instruction

```
CALL (8, P(0,0), Q(0,0), R(0,0), M(0,0), F(0,0), X(0), Y(0), E2,
      S(0,0), K(0,0), N, M)
```

where P, Q, R, M, F, S and K are the matrices $\bar{\Phi}$, Q, R, M, P, S and K of Figure 6.9, X is the state vector of N elements and Y is the M- measurement vector. E2 is the filter memory weighting factor (c).

In order to minimise redundant computation time during on-line Kalman filtering, it is necessary to determine the program execution time a priori. The total time to perform a filter cycle is the sum of the time for measurement, subroutine execution, integration and calculation of $\bar{\Phi}$. The error of approximation involved in the calculation of the transition matrix is thus reduced by selecting the minimum sampling interval. Program 6 shows a simple BASIC program that determines the execution time of the Kalman filter cycle for various numbers of state variables and measurements. Before and after each call to the subroutine the MDP200 clock is read and the numerical difference in seconds

is printed at the teletype. Program 7 includes a listing of the results.

The filter subroutine is incorporated into on-line programs as shown in Figure 6.1 . Following the input of initial conditions for the state variables and the filter error statistics, the transition matrix is calculated and the numerical integration (state variable prediction) is performed over the sampling interval. Channel scanning is then initiated by a call to the seventh BASELINE subroutine after which the scanning sequence is repeated at the required sampling interval. When fresh measurements are available to the program, they are converted by the calibration constants, the filter cycle is executed and the state variable estimates are output to the teletype. The quantity of output is dependent upon the available time during the computations but in real-time operations it is restricted to the estimates and their error statistics. When the filter cycle and output is complete, the integration is performed up to the next sampling interval and the new transition matrix is prepared. The program then waits for the real time clock to interrupt program execution. Each time the measurements become available, the complete cycle of data conversion, filtering, output, integration and calculation of $\bar{\bar{\Phi}}$ is repeated.

The general program structure, shown in Figure 6.1 can be adapted for off-line use by reading in data from paper tape at each sampling interval rather than taking actual measurements on interrupt. This removes both the on-line plant operation and the timing co-ordination from experiments.

6.6.3 Filter Representation of Reduced Model

State Equations

For filtering experiments the state vector of the reduced model, (equations 6.5.33 to 6.5.37,) contains 8 state variables. Thus the state vector X of Figure 6.4 is

$$X = \begin{bmatrix} T_2 \\ T_{14} \\ T_{13} \\ H_5 \\ U_g \\ U_f \\ U_c \\ U_e \end{bmatrix} \qquad 6.6.1$$

where the heat transfer coefficients are unknown system parameters.

The dimension of the measurement vector is reduced by assuming the input disturbances and controlled variables are noise free measurements and are used in the calculation of the elements of the transition matrix at each filter cycle. In particular, this includes the measurements of vapour pressure (temperature) which, from plant observations, are known to vary when the plant is at unsteady state. This method of utilising reliable measurements, not in the state vector, directly is used by Schmidt et al (41). The measurement vector is thus,

$$y = \begin{bmatrix} T_2 \\ T_{14} \\ H_s \\ T_{13} \end{bmatrix} \qquad 6.6.2$$

and since calibration constants are used for conversion from raw measurements, the measurement state equation is,

$$y = \begin{bmatrix} 1 & 0 & 0 & 0 & 0 & 0 & 0 & 0 \\ 0 & 1 & 0 & 0 & 0 & 0 & 0 & 0 \\ 0 & 0 & 1 & 0 & 0 & 0 & 0 & 0 \\ 0 & 0 & 0 & 1 & 0 & 0 & 0 & 0 \end{bmatrix} \times \qquad 6.6.3$$

The plant state equations are given in equations 6.5.33 to 6.5.37. Classically, the parameter state equations can be represented by zero derivative expressions. However, further information is available in the form of the steady state correlations (equations 6.5.6, 6.5.8, 6.5.11, 6.5.14) which relate the overall heat transfer coefficients to the operating conditions of the plant. Although the correlations are not dynamic equations, and hence their diagonal elements on the transition matrix will be unity, it is clearly beneficial to use all state variable information at the prediction stage. This provides an opportunity for comparing both methods of predicting parameters.

Prediction Stage

At the prediction step (equation 6A) the filter algorithm is influenced by the process model. At the state variable prediction,

$$x(k+1|k) = x(k|k) + \int_{k}^{k+1} f(x)\,dt \qquad 6.6.4$$

the state equations are integrated over the sampling interval. Since the ASP and BASELINE subroutines cannot be combined, the integration step is programmed in BASIC. One important consideration in selecting a numerical integration method is the time required to carry out an integration step. It is necessary to minimise the number of derivative function evaluations whilst maintaining numerical precision. In terms of BASIC programming, the most efficient method (i.e. requiring the least number of statements to be interpreted) is the Euler method, where the four derivative equations can be stated briefly and repetitively integrated over a small step length.

The influence of the process model at the prediction of the estimation error covariance matrix,

$$P(k+1|k) = \bar{\bar{\Phi}}(k+1,k)\ P(k|k)\ \bar{\bar{\Phi}}^{T}(k+1,k) + Q(k) \qquad 6.6.5$$

is accounted for by the transition matrix. Since the state equations are non-linear, the transition matrix is a function of the state. If the dynamic model is expanded in a Taylor series expansion and truncated after the first derivative terms the transition matrix elements are,

$$\bar{\bar{\Phi}}(1,1) = 1 - \frac{\left(M_l C_p + \frac{U_g A_g}{2}\right)\Delta t}{.5\, W_{tg} \rho_L C_p} \qquad 6.6.6$$

$$\bar{\bar{\Phi}}(1,5) = \frac{A_g\left(T_4 - \frac{(T_1 + T_2)}{2}\right)\Delta t}{.5\, W_{tg} \rho_L C_p} \qquad 6.6.7$$

$$\bar{\bar{\Phi}}(2,2) = 1 - \frac{\left(M_{14} C_p + \frac{U_f A_f}{2}\right)\Delta t}{.5\, W_{tf} \rho_L C_p} \qquad 6.6.8$$

$$\bar{\bar{\Phi}}(2,6) = \frac{A_f\left(T_{10} - \frac{(T_{14} + T_{15})}{2}\right)\Delta t}{.5\, W_{tf} \rho_L C_p} \qquad 6.6.9$$

$$\bar{\bar{\Phi}}(3,3) = 1 - \frac{\left(M_{12} C_p + \frac{U_c A_c}{2}\right)\Delta t}{.5\, W_{tc} \rho_L C_p} \qquad 6.6.10$$

$$\bar{\bar{\Phi}}(3,7) = \frac{A_c\left(T_{vac} - \frac{(T_{12} + T_{13})}{2}\right)\Delta t}{.5\, W_{tc} \rho_L C_p} \qquad 6.6.11$$

$$\bar{\bar{\Phi}}(4,1) = \frac{-M_2 C_p\, (C_p(T_{15} - T_8) + \lambda_{15})\, \Delta t}{\lambda_7 \rho_L A_s \lambda_{15}} \qquad 6.6.12$$

$$\bar{\bar{\Phi}}(4,2) = \frac{M_{14} C_p \Delta t}{\rho_L A_s \lambda_{15}} \qquad 6.6.13$$

$$\bar{\bar{\Phi}}(4,4) = 1 \qquad 6.6.14$$

$$\bar{\bar{\Phi}}(4,8) = \frac{(C_p(T_{15} - T_8) + \lambda_{15})(T_5 - T_7)\, A_e\, \Delta t}{\lambda_7 \rho_L A_s \lambda_{15}} \qquad 6.6.15$$

$$\bar{\bar{\Phi}}(5,5) = \bar{\bar{\Phi}}(6,6) = \bar{\bar{\Phi}}(7,7) = \bar{\bar{\Phi}}(8,8) = 1 \qquad 6.6.16\text{-}19$$

and all other elements of $\bar{\bar{\Phi}}$ are zero. The above expressions contain the measured control variables and input disturbances - M_1, T_4, T_1, M_{14}, T_{10}, T_{15}, T_{vac}, T_{12}, T_8, T_7.

Filter Statistics

In the real-time application of the Kalman filter, it is necessary to state initial values of the state variables, their estimation error covariances and the error covariance matrices of the measurement and process noise (R and Q). The most accurate initial estimates of state variables are obtained by making an initial measurement, prior to filtering, and utilizing these measurements and a prediction of the parameters (based on either an approximate guess or the steady state correlations) in the vector $x(0 \mid 0)$. The effects of the magnitude of $P(0 \mid 0)$ has been extensively reported (20). Off-line experimentation indicates that the magnitude of the diagonal elements should be sufficient to guarantee convergence of the algorithm within a few filter cycles.

The numerical values of the diagonal elements of the measurement noise covariance matrix, R, are determined by examining the standard deviations in the analogue output section of the steady state logging program. Although the plant is never at true steady state this represents the most accurate available estimate of R. Selection of the diagonal elements of Q is not so straightforward. The process noise matrix can be regarded as the compounded result of errors from different sources and the selection of the numerical values depends upon the accuracy of the model and the dynamic state of the plant. The influence of variations in Q on the performance

of the filter algorithm is a principal study in this research.

6.6.4 On-line Real-Time Filter Program

One important objective in writing the real-time Kalman filter program is the provision of a general programming facility, so that the experimental variables such as sampling interval, integration step length, error covariance matrices, etc., can be changed without major programming effort. A listing of the on-line real-time program is shown in Program 7 of Appendix 6 . The program is written with a number of BASIC subroutines which are called from a central program based on the dynamic logging program which performs the essential task of plant measurement. The subroutines and the statement numbers of Program 8 at which they commence are as follows:

1. Initialisation Subroutine - 300

Prior to measurement on interrupt, each channel is scanned once to provide initial conditions. The raw analogue data are converted into SI units and the steady state loss terms are calculated. This implies that the filtering operations are initialised when the evaporator is at steady state which is necessary when the heat loss terms are unknown. The initial transition matrix, based on the initial measurements, is then computed.

2. Transition Matrix Subroutine - 1000

Here, each non-zero element of the transition matrix (equations 6.6.6 to 6.6.19) is calculated and assigned to the appropriate doubly subscripted BASIC variable.

3. Kalman Filter Subroutine - 1110

When a measurement set is available the FORTRAN subroutine (KALMAN) is called from BASIC and a filter cycle is executed.

4. Output Subroutine - 2000

Following the execution of a filter cycle, an optional printout of all output variables from the filter subroutine is available. By simple programming in BASIC, this subroutine can be by-passed or reduced according to the available output time.

5. Heat Transfer Coefficient Subroutine - 4000

The steady state correlations are evaluated based on the current estimates of state variables and measurements of control variables.

6. Conversion Subroutine - 5000

Analogue measurements are converted to SI units by the appropriate calibration constants. The steam flow rate to the first effect is calculated from a polynomial.

7. Enter Integration Subroutine - 6000

The dynamic state equations are integrated over the sampling interval using a small step length. The total computation time, and hence integration step length, is determined by trial and error and is arranged to occupy all available processor time during a measurement cycle.

Execution follows the form shown in Figure 6.1. After the program is initiated the necessary arrays are dimensioned and the calibration data is stored. The program then prints out the start time by reading the MDP200 clock, the elements of the covariance matrices are assigned, and the sampling interval and ensemble are

input. The initialisation subroutine is then called and the explicit call to BASELINE subroutine 7 is made after which the measurements are taken automatically at the required sampling interval. After each measurement the raw data is converted, a filter cycle is executed, the results are printed out and the integration step is performed. In the remaining time, the program waits for the next sampling time to be reached. The program can be terminated by manual intervention at the BASIC level by pressing sense switch 1 and creating a program break.

For off-line processing of measurements stored on paper tape, the program is essentially the same. Whereas in real-time execution BASELINE subroutine 7 is executed automatically to perform measurements, in off-line execution the sampling interval is fixed when the measurements are stored on paper tape and thus data are input from the tape reader when required.

6.6.5 Filtering Experiments

The following on-line, real-time experiments are performed

1. Testing of the subroutines and the feasibility of filtering the evaporator system in real time.

2. Estimation of the optimum integration step length to maintain numerical precision during state variable prediction.

3. Determination of suitable initial statistics for real-time state variable and parameter estimation.

4. Real-time parameter estimation based on both the steady state correlations and the zero derivative expressions at the state variable prediction step.

5. By means of the modification to the BASIC program, permitting paper

tape input/output, the measurements of a steady-state and dynamic run are dumped onto paper tape for off-line processing.

Paper-tape measurements provide a permanent record of plant operating conditions so that repetitive off-line filtering experiments can be performed as follows:

1. Examination of the filter matrices not available during real-time processing. In particular, filter convergence and loosening during both steady state and dynamic operations.

2. Investigation of the effect of the numerical value of the process noise statistics upon convergence and loosening of the filter.

6.7 Chapter Review

Chapter 6 describes the on-line implementation of steady state and dynamic models with the interactive program packages, ASP and BASELINE. The on-line experimental method and computer programs are described for calibrations, steady-state runs, dynamic logging and Kalman filtering. Off-line simulation of the comprehensive and reduced models of Chapter 5 is performed prior to filtering in order to compare theoretical and measured dynamic responses. The fourth order reduced model is adopted for use in eighth order Kalman filtering experiments where the four plant overall heat transfer coefficients are unknown parameters to be estimated.

CHAPTER 7

RESULTS, ANALYSIS AND DISCUSSION

7.1 Introduction

In Chapter 6, the experimental method and on-line programs are described. The objective of this chapter is to report and discuss the experimental results and their analyses in the following order.

1. Preparatory experiments - namely on-line instrument calibrations and computation of thermodynamic correlations.

2. On-line steady-state runs over the whole range of operation of the evaporator.

3. Analysis of the teletype output resulting from steady-state experiments to determine heat transfer coefficients for each heat exchange unit. Comparison of calculated heat transfer coefficients with theoretical values derived from well-known published relationships and computation of correlations based on plant operating conditions.

4. On-line recording of the dynamic response of the evaporator (dynamic logs).

5. Simulation of comprehensive and reduced models and comparison of simulated response with the results of dynamic logs.

6. On-line real-time Kalman filtering experiments to perform estimation of plant parameters (heat transfer coefficients). Off-line filter timing experiments are performed before operating on-line.

7. Off-line filtering experiments based on real plant measurements permanently stored on paper tape. Repetitive processing of data permits the analysis of the influence of the filter statistics on the performance of the algorithm

and the accuracy of the estimation.

The fixed order of experimentation described above is necessary to achieve the objectives of implementing the Kalman filter on-line to the double effect evaporator and investigating the effect of variations in the filter noise statistics. The flow of information between each experimental stage is shown in Figure 7.1. Clearly, any on-line operations cannot proceed without instrument calibrations and evaluation of thermodynamic relationships while for simulation and filtering, the dynamic model and heat transfer coefficient correlations are prerequisite. Comparison of the results of dynamic simulation with recorded measurements provides both a qualitative estimate of the accuracy of the mathematical model and an indication of the suitability of the reduced model at the state variable prediction stage of the filter algorithm.

Graphs and tables of data are presented in Appendix 7. Where results are analysed by computer, the relevant programs are presented in Appendix 6.

7.2 Preparatory Experiments

7.2.1 Instrument Calibration

When the evaporator is operating continuously on-line to the computer system, the cumulative effects of mechanical vibrations and temperature variations cause drift in the performance of the d.c. transducers. In order to maintain maximum accuracy, it is necessary to recalibrate some instruments periodically. The calibration procedure described in Section 6.2.4 and Program 2 of Appendix 6 can be executed at any time to produce analogue values for corresponding transducer positions.

FIGURE 7.1

FLOW OF RESULTS INFORMATION

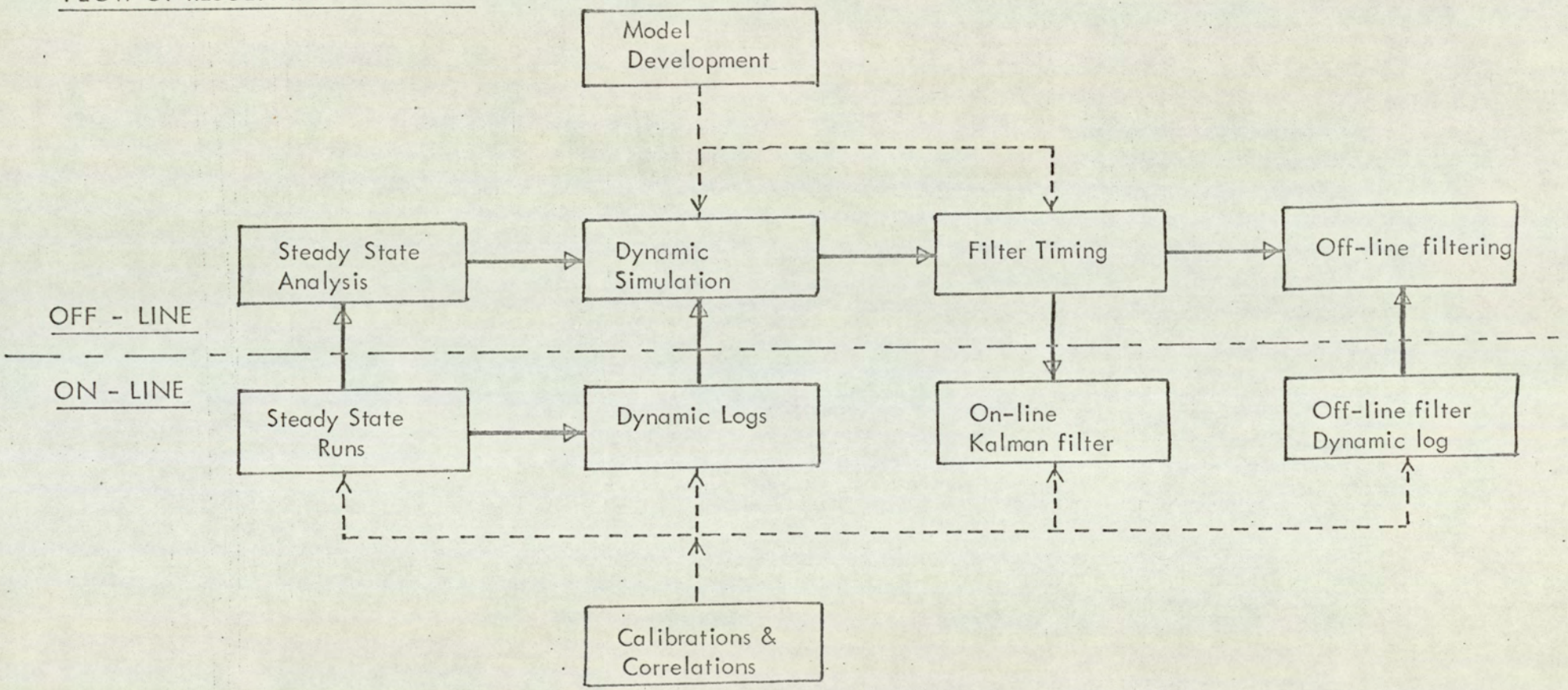

There are two distinct classes of instrument calibration. Firstly, calibration of flowmeters, pressure transducers and differential pressure gauges where the relationship between the electrical transducer output and the flow or pressure input is not known a priori. Thus the analogue results and regression equations cannot be compared with standard equations or manufacturers data. Furthermore, it is this class of instrument that requires periodic recalibration. The second class is the calibration of thermocuples where the instrument itself produces a d.c. voltage which is more accurate than the available devices against which to calibrate. In this case, once only calibration experiments serve as a check against faulty thermocouple connections and provide a qualitative estimate of the reliability of manufacturers calibration data. When thermocouple extension or compensation cabling is used to carry the analogue signal to the remote cabinet of the MDP200, it is possible for secondary couples to be set up where poor or reverse connections are made.

For both classes of calibration it is essential to calibrate on-line to the computer system to include noise and/or bias effects produced by the MDP200 and the logger/computer interface. All analogue inputs to the MDP200 remote cabinet are connected so that the digitised signals are negative when the evaporator is operating under normal vacuum conditions. This provides an instant check of instrument failure during on-line operations by observing the sign of the ADC output signal at either the remote cabinet VDU or in the analogue output section of the teletype output as shown in Figure 6.5. To obtain maximum numerical precision the four digit BCD integer output from the ADC is converted to a corresponding four digit real decimal number by the BASELINE subroutines, i.e. the maximum absolute value stored at the BASIC

level is 9999.0 and the minimum is 0.0.

A detailed discussion of the calibration of each analogue channel is unnecessary and the following results are taken as typical of each type of instrument.

1. Channel 17-Flowmeter to 2nd Effect Separator

Figure A7.1 shows the calibration of the second effect flow meter. The data pairs are flow rates, recorded by measuring cylinder and stop watch, and corresponding analogue signals produced by Program 2. The data are input to the Honeywell SLS program from which the graph and statistical output shown in the Figure are extracted. Operating experience has shown that with the exception of the steam orifice plate differential pressure gauge, the Fischer-Porter magnetic variable-area flow meters are the least reliable instruments and require frequent recalibration. Principally, this is due to friction effects on the potentiometer arm of the linear displacement transducers. Also, as can be observed in Figure A7.1, a small amount of hysteresis is present in the movement of the flowmeter magnetic plug.

2. Channel 15-Second Effect Shell Pressure Transducer

Calibration of the vacuum pressure in the shellside of the second effect is shown in Figure A7.2 All pressure transducers are calibrated by removing the instrument from the evaporator to a simple mercury manometer circuit. In all cases the linear correlation coefficient between the pressure (kNm^{-2}) and analogue output is very nearly unity. Since the pressure transducers contain few mechanical parts and each unit is protected from external disturbance, recalibration is seldom required.

3. Channel 18 Liquid Level in Second Effect Separator

Like the pressure transducers, the differential pressure meters cannot be disturbed externally and a strong linear correlation is evident, as shown in Figure A7.3. During normal operation of the evaporator, the liquid head in the second effect is fluctuating rapidly due to boiling. Instantaneous measurement of fluctuations is avoided by increasing the mechanical damping applied to the differential pressure diaphragm, thus smoothing the resulting analogue signal. The response of the average liquid level in the separator is never fast enough to be smoothed itself by adjustment of the mechanical damping.

4. Channel 19 Steam Flow Rate

Although the pressure in the steam supply is regulated to 240 kNm^{-2} (20 psig) pressure fluctuation occurs due to condensate in the delivery lines and the requirements of other users in the laboratory. Thus the acquisition of a single undisturbed steady-state reading requires the collection of condensate over a long period. Since the steady-state mathematical model contains redundancy, the steam flow rate is computed during steady-state runs and at the same time the condensate flow rate is measured. When the standard deviations on the analogue measurement of channel 19 is small, the data is included in the steam flow calibration. From the results of 100 steady state runs, the steam rate is related to the analogue value by carrying out a polynomial regression as shown in Figure A7.4 The resulting polynomial is required for simulation of the reduced model and on-line Kalman filtering.

5. Channels 20-27 Thermocouple Calibrations

The once only calibration of thermocouples is shown in Figure A7.5. The line shows the manufacturers data relating millivolt signal to temperature,

and the points are measurements recorded by Beckman thermometer and plotted against the logged analogue value for all thermocouples. The results satisfactorily confirm the manufacturers recommended correlation within the limits of experimental accuracy.

A summary of the results of all calibrations is shown in Table A7.1. The linear correlation coefficients are included to indicate the reliability of the linear equations. In all cases the conversion is effected by multiplying the slope by the negative, four digit, analogue voltage and adding to the intercept. Instrument type is denoted by PT - pressure transducer, DP - differential pressure gauge, FM - magnetic flow meter and TC - thermocouple.

TABLE 7.1 - Results of Calibrations

Channel No.	Instrument Type	Units	Slope	Intercept	Correlation Coefficient
12	PT	kNm^{-2}	0.0264	103.993	0.9999
13	PT	kNm^{-2}	0.0518	100.221	0.9997
14	PT	kNm^{-2}	0.0235	97.36	0.9997
15	PT	$kNm^{-}2$	0.0863	99.08	0.9999
16	FM	gs^{-1}	-0.836×10^{-2}	-26.43	0.9962
17	FM	gs^{-1}	-0.521×110^{-2}	-15.04	0.9978
18	DP	$m(H_20)$	-0.43×10^{-3}	0.031	0.9998
20-27	TC	^{o}C	-0.025	0	0.99999

The polynomial for the steam flow rate (gs^{-1}) to the first effect is,

$$V_6 = -11.381 - 0.3255 \times 10^{-2} Av - 0.234755 \times 10^{-6} Av^2$$

where Av is the voltage reading. The correlation coefficient is 0.995661.

7.2.2 Thermodynamic Correlations

The statement and solution of the mathematical models of the evaporator require a knowledge of the relationship between physical and thermodynamic properties and the state variables. When the model is to be solved on-line in real-time, it is most convenient to correlate the available data into algebraic equations, thus avoiding storage and interpolation of large arrays of physical property data. For the liquid phase the physical properties are assumed constant but for the vapour phase, the variation of pressure, density, latent heat and enthalpy with temperature is greater and must be considered.

1. Pressure-temperature

A computer algorithm for the calculation of vapour temperature from pressure is described in Section 6.2.3. A BASIC subroutine derived from the algorithm is included in all on-line programs where pressure measurement is recorded. Within the range of vacuum operation of the evaporator, the algorithm is accurate to within the approximations of the state equation from which it is derived (0.1%)

2. Density-temperature

Figure A7.6 shows the results of a linear regression analysis on density-temperature data derived from steam tables (105). The best fit is found by correlating the natural logarithms of the data. The resulting equation is

$$\log \rho_v (T) = 1.93 \log T - 3.1487 \qquad 7.2.1$$

with a correlation coefficient of 0.9935 where Pv is in g m^{-3}. For the implementation of the comprehensive dynamic model the derivative of density with respect to temperature is required,

$$\frac{d\rho_v}{dT} = \frac{1.93\rho_v}{T} \qquad 7.2.2$$

3. Latent heat-temperature

Figure A7.7 shows the results of a linear regression analysis on latent heat-temperature data. The resulting equation is

$$\lambda(T) = 2501\text{-}64 - 2.407T \quad (J\,g^{-1}) \qquad 7.2.3$$

with a correlation coefficient of 0.9996.

4. Enthalpy - temperature

The relationship between vapour enthalpy is given by

$$H(T) = Cp\,T + \lambda(T) \quad (J\,g^{-1}) \qquad 7.2.4$$

where the specific heat Cp is 4.1868 $J\,g^{-1}K^{-1}$.

7.3 Steady State Experiments

7.3.1 Introduction

On-line operation of the evaporator at steady state is beneficial in two ways. Firstly, a qualitative feel for the operation of the evaporator is acquired at the same time as obtaining numerical results to the solution of the steady state model. With such interaction between visual observation and computer program, new modelling ideas can be incorporated into the program and tested immediately. The second benefit, once the steady state model is established, is the collection of on-line data across the whole range of operation of the evaporator. As described in Section 6.3, the acquisition of such data is aided by an informative teletype output and the ability to reject unsatisfactory data prior to the solution of the mathematical model.

When a representative sample of results is available, the data are processed off-line to determine experimental heat transfer coefficients and at the same time compare the results with coefficients calculated from established correlations. From the on-line records and experimental heat transfer coefficients, steady state correlations are computed by multivariable linear regression analysis.

7.3.2 On-line Experiments

Formerly the steady state mathematical model was derived with only vapour assumed to be present in the shell sides of the heat exchangers. Consequently, initial steady state runs produced inconsistency in the numerical solution of the model. One example is the shellside of the preheater where the heat gained by the liquid in the tubes cannot be accounted for by the enthalpy loss due to a small drop in vapour temperature. A similar effect was observed in the shellside of the second effect. The only conclusion from these observations is that vapour is condensing in the exchanger shells, the enthalpy being provided by latent heat of condensation. These numerical observations were confirmed visually by inserting a glass section in the pipe from the second effect shell to the condenser when large quantities of condensate were seen to be present. Prior to visual observation, the mathematical model was modified while on-line to the evaporator to determine condensate rates; the vapour only steady state model contains sufficient redundancy to permit this. Satisfactory experimental results with reproducibility were obtained. This clearly demonstrates the benefit of the interactive facility of BASELINE, where BASIC instructions can be quickly edited while the evaporator is running so that alternative models can be tested. As a result of the modifications described above, the two-phase model was concluded to be the best representation of the process and steady state runs were collected across the whole range of operation of the evaporator.

Output produced by an on-line steady state run is shown in Figures 6.3 & A7.8 including the preliminary input data and the analogue and converted output sections. In all, a total of 96 steady state runs based on the steady state model of Chapter 5 were collected. Presentation of the output resulting from all on-line experiments is voluminous and thus a representative sample of 8 converted outputs, representing results over the whole range of operating conditions, are presented in Figures A7.8 to A7.15. The figures are copies of results obtained during actual experimental runs.

The converted output section of each steady state run presents an informative analysis of each unit of the evaporator. For example, in Figure A7.8 the temperature, mass flow and enthalpy flow of each stream is shown. The symbols L and V refer to the liquid and vapour streams respectively. At the preheater shell, the exit stream is a mixture of both liquid and vapour which is input to the shellside of the second effect where further condensation occurs. At the climbing film first effect, the liquid entering the tubes is partially vaporised by steam (symbol S) which is assumed to lose heat by condensation only - the steam condensate is denoted by SC. The partially vaporised tubeside stream is separated at the cyclone where the liquid stream is fed to the second effect separator (L IN FROM CS) and the vapour passes to the preheater shell. Liquid circulates from the second effect to the second effect separator (L IN FROM E2) where boiling occurs and the liquid level is continuously changing (ACCUMULATION). At the condenser, vapour from the second effect separator (V IN (E2S)) and liquid and uncondensed vapour from the shellside of the second effect (V IN (E2), L IN), are fed to the shellside. Following the output of flow, temperature and enthalpy of each stream of each unit, additional information on pump circulation rate, condenser cooling

water rate (calculated and input), accumulation, steam rate and steam valve position are printed.

Each figure represents data collected over a 30 minute period with a sampling interval of 30 seconds and an ensemble of 12 samples at each sampling time. This represents continuous channel scanning for virtually the complete sampling interval with a small period allotted for data conversion and summation. Notable features of the eight representative listings are summarised in Table 7.2.

The symbols H and L in Table 7.2 indicate high and low settings of the controlled variables. For comparative purposes, the sample listings are arranged factionally. The rate of circulation through the second effect is computed from a heat balance on the second effect separator and is consistently of the order of 3200 gs^{-1}. The accumulation in the second effect separator varies according to the total thermal load and liquid feed rate. When the steam rate is high, the accumulation is small and in particular, when the liquid feed rate is low, there exists a negative accumulation (Figures A7.10, A7.11 and A7.14). The accumulation is independent of the condenser cooling water rate where the available thermal capacitance for condensation is far in excess of the evaporator requirements.

Although the steady state flows and temperatures for the liquid streams are self-evident, the vapour phase temperatures require further discussion. Since the system is operating under vacuum it would be expected that the vapour temperature throughout the evaporator is uniform. From the condenser shell, the vacuum is drawn on both the second effect separator and the second effect shell and hence the preheater shell and cyclone. As Table 7.2 clearly indicates, there is an obvious

TABLE 7.2 Summary of Steady State Results Figures A7.7 to A7.14

	Units	Figure A7.8	Figure A7.9	Figure A7.10	Figure A7.11	Figure A7.12	Figure A7.13	Figure A7.14	Figure A7.15
Steam Rate	gs^{-1}	17.5 H	12.4 L	12.52 H	11.71 L	18.32 H	16.92 L	16.74 H	13.25 L
Liquid feed rate	gs^{-1}	31.3 H	32.25 H	16.2 L	16.2 L	46.09 H	39.48 H	23.69 L	28.09 L
Condenser water rate	gs^{-1}	800 H	800 H	633 H	633 H	483 L	479 L	504 L	504 L
2nd effect circulation rate	gs^{-1}	3509	3023	3246	3487	3833	2937	3175	3505
Condensate rate	gs^{-1}	27.7	17.2	17.5	17.1	28.5	23.7	24.8	22.79
Accumulation	gs^{-1}	3.59	15.03	-1.28	-0.97	17.62	15.78	-1.15	5.3
Vacuum temperature	°C	34.16	31.23	35.11	34.68	41.18	40.47	43.7	43.77
2nd effect shell temperature	°C	47.07	34.5	37.22	37.45	49.31	47.8	52.4	51.53
Preheater shell temperature	°C	48.58	34.4	35.68	35.42	40.96	46.05	46.05	46.36
Cyclone temperature	°C	51.3	39.5	39.96	40.21	41.82	48.58	48.94	48.64
Coolant inlet temperature	°C	13.83	13.07	11.48	11.58	4.61	14.07	13.63	13.76
Coolant outlet temperature	°C	22.5	18.28	17.97	17.74	17.85	26.24	25.28	24.75

temperature variation between successive exchanger shells. This is due to the pressure drop produced by the formation of condensate in the vapour pipe lines between the heat exchangers.

One further observation from Table 7.2 is the variation in vacuum temperature throughout all steady state runs. This is true of all on-line operations. Although the operating characteristics of the vacuum pump are unknown it is always set to operate at the maximum obtainable suction of 6 kNm^{-2} (28" Hg). There is some apparent correlation between the vacuum temperature and the condenser cooling liquid rate. As Table A7.4 shows, this is by no means reproducible. Once the condenser cooling water rate is set and the plant is settled, reproducibility of steady state results is possible, with small variations in operating vacuum temperature, as long as the cooling water rate is maintained constant. These small variations are due to condensate leaving the condenser at approximately the same level as that at which the vacuum is drawn.

As a result of the above discussion, the condenser cooling water rate is maintained constant during dynamic logs and real-time Kalman filtering. This means that the vacuum temperature is maintained approximately constant thus avoiding the complex interaction between vapour rate, cooling liquid rate and vacuum temperature.

In the case of comparison of simulated results with dynamic state logs the small variations in vacuum temperature are regarded as inputs to the dynamic model. Thus while variations in vacuum temperature are considered in this way, no attempt is made to describe their dynamic behaviour mathematically. An investigation into the vacuum dynamics of the condenser is suggested for future

work in Section 8.3 .

7.3.3 Off-line Analysis

For economy of processing and on-line program execution, it is convenient to terminate steady state calculations at the converted output section. Further useful information that can be obtained from an individual steady state run is the calculation of experimental heat transfer coefficients for each exchanger and the overall system heat losses. At the same time it is beneficial to compare the calculated heat transfer coefficients with those derived from published correlations. These additional calculations are performed off-line and relevant data from the on-line records are input from the paper tape reader.

When the results of off-line processing for all steady state runs are available, the heat transfer coefficient correlations are computed by multivariable linear regression analysis. The analysis is programmed in FORTRAN and performed by an ICL 1905E computer.

For each heat exchanger unit, the results of all steady state runs are summarised in Tables A7.1 - A7.4. The table contains the shellside vapour and tubeside liquid flow rates, the vapour temperature and the liquid inlet and outlet temperatures. For the description of the theory of the results analysis, the stream notation of Section 3.2.3 is adopted.

7.3.3.1 Theory

1. System Heat Losses

For a given steady state run the total heat input rate to the evaporator is given by,

$$H_{TOT}\,(in) = H_1 + H_5 + H_{12} \qquad 7.3.1$$

and the total heat output by,

$$H_{TOT}(out) = H_{11} + H_{13} + H_6 \qquad 7.3.2$$

Thus the total system heat loss is given by,

$$H_{TOT}(loss) = H_{TOT}(in) - H_{TOT}(out) - H_{ACC} \qquad 7.3.3$$

where H_{ACC} is the enthalpy accumulation in the second effect. All enthalpy rates in Equation 7.3.1 to 7.3.3 are calculated directly from measurements. An alternative estimate of the heat loss is derived from the difference between the measured and calculated condenser cooling liquid rate. The redundancy in the steady state mathematical model permits the independent computation of this flow rate at the final stage of solution and this represents a measure of the theoretical heat load on the condenser when heat losses are assumed to be zero. The computed heat loss is given by,

$$H^*_{TOT}(loss) = (M_{12}(calc) - M_{12}(meas))Cp\,(T_{12} - T_{13}) \qquad 7.3.4$$

and the experimental and computed heat losses as a percentage of the total heat input are given by,

$$\eta = \frac{H_{TOT}(loss)}{H_{TOT}(in)} \cdot 100 \qquad 7.3.5$$

$$\eta^* = \frac{H^*_{TOT}(loss)}{H_{TOT}(in)} \cdot 100 \qquad 7.3.6$$

2. Heat Transfer Coefficients

For the general heat exchanger with an isothermal condensing vapour in the shell, the experimental overall heat transfer coefficient is given by

$$U = \frac{Q}{A\,\overline{\Delta T}_{lm}} \qquad 7.3.7$$

where Q is the heat transferred per second, A is the total surface area of the outside of the tubes and ΔT_{lm} is the ideal log mean temperature difference (LMTD). For off-line processing, the surface area of the tubes is calculated from engineering drawings (Appendix 1) and the heat transferred and LMTD are derived from the steady state converted output. For example, for the preheater,

$$\Delta T_{lm} = \frac{T_2 - T_1}{\log\left(\frac{T_4 - T_1}{T_4 - T_2}\right)} \qquad 7.3.8$$

and the heat transferred is given by,

$$Q = M_1 Cp(T_2 - T_1) \qquad 7.3.9$$

The climbing film first effect is an exception to this calculation procedure since both the shell and tubes are assumed to be isothermal and tubeside vaporisation takes place. The total heat transferred is calculated from the measured steam rate. The steam is assumed to condense at the operating pressure and there is no liquid subcooling.

$$Q = V_5(Cp\,(T_5 - T_6) + \lambda_5) \qquad 7.3.10$$

and the temperature driving force is given by the difference in shellside and tubeside temperatures.

$$\Delta T = T_6 - T_7 \qquad 7.3.11$$

Theoretical heat transfer coefficients are calculated by the method of Kern (106). For heat exchangers with an isothermal condensing vapour in the shell, the tubeside heat transfer coefficient is given by the Seider and Tate equations,

$$\frac{h_t d}{k} = 1.86 \left(\frac{4}{\pi} \frac{M C_p}{k L} \right)^{0.33} \left(\frac{\mu}{\mu_w} \right)^{0.14} \qquad 7.3.12$$

for Re < 2100, and

$$\frac{h_t d}{k} = 0.027 \left(\frac{d G}{\mu} \right)^{0.8} \left(\frac{C_p \mu}{k} \right)^{0.83} \left(\frac{\mu}{\mu_w} \right)^{0.14} \qquad 7.3.13$$

for Re $\geqslant$ 2100, where for both correlations,

$$Re = \frac{dG}{\mu}$$

and

h_t is the tubeside heat transfer coefficient ($Wm^{-2}\ C^{-1}$)

d is the tube inside diameter (m)

L is the length of a single tube pass (m)

M is the mass flow of liquid (gs^{-1})

Cp is the liquid specific heat ($Jg^{-1}\ C^{-1}$)

k is the liquid thermal conductivity ($Wm^{-1}\ C^{-1}$)

μ is the liquid viscosity (Nsm^{-2})

μ_w is the liquid viscosity of the temperature of the tube wall (Nsm^{-2})

G is the liquid mass velocity ($gs^{-1}m^{-2}$)

Shellside heat transfer coefficients are given by the Nusselt equation for condensate films,

$$\frac{h_s L}{k} = 0.925 \left(\frac{k^3 \rho^2 g}{\mu G^1} \right)^{0.38} \qquad 7.3.14$$

where $G^1 = \frac{V}{N_t P}$ 7.3.15

and all physical properties are taken at the temperature of the condensed liquid. G^1 is the condensate loading per unit length of tube and the modified symbols are as follows.

h_s is the shellside heat transfer coefficient ($Wm^{-2}\ C^{-1}$)

V is the mass flow of condensing vapour (gs^{-1})

P is the wetted perimeter of the tubes (m)

N_t is the total number of tubes

g is the gravitational acceleration ($9.807\ ms^2$)

The clean overall heat transfer coefficient is given by

$$U = \frac{h_s h_t}{h_s + h_t} \qquad 7.3.16$$

3. Physical Properties

Calculation of the theoretical heat transfer coefficients requires a knowledge of the variation of viscosity and thermal conductivity with temperature. The temperature dependance of the physical properties of water is reported by Singh and Dass (107). The following correlations are proposed,

$$\log \mu = -3.438 + \frac{475.45}{T + 118} \qquad 7.3.17$$

$$\log k = 2.241 - \frac{62.58}{T + 118} \qquad 7.3.18$$

where T is $^{\circ}C$. The units of equations 7.3.16 and 7.3.17 are consistent with equations 7.3.12 to 7.3.15 and the reported maximum errors are 1.5% and 2.2% respectively in the range 0-100$^{\circ}C$.

The dimensions and geometry of each exchanger are given in Table A1. of Appendix 1. For the preheater and condenser, the tube length is given by the product of the length of a single tube and the number of tubes. The first and second effect evaporators are single-pass multitube exchangers and for calculation of heat transfer coefficients the tube length is given by the height of a single tube.

4. Heat Transfer Coefficient Correlation

The results of all steady state runs are correlated into the linear equation of the type implemented by Heidemann et al (79). The heat transfer coefficient is assumed to be a function of the arithmetic mean temperature driving force, the shellside vapour flow rate and tubeside liquid flow rate. For example, for the preheater the function is of the form

$$Ug = a + b\left(T_4 - \frac{(T_1 + T_2)}{2}\right) + cM_1 + dV_3 \qquad 7.3.19$$

where a, b, c and d are constants. The theory of multivariable regression analysis is taken from Gore (108) and is not reported.

7.3.3.2 Computer Programs

1. Steady State Analysis Program

A BASIC listing of the steady state analysis program is given in Program 8 of Appendix 6. The principal operation of calculating experimental and theoretical heat transfer coefficients is performed by a BASIC subroutine which is accessed four times, (i.e. once for each heat exchanger) during the processing of data from a steady state run. Program data, derived from steady state listings, are punched onto paper tape in the following order.

a) Data required in the calculation of overall system heat losses as described in Section 7.3.3.1. This consists of the enthalpies of the inlet and outlet streams, the computed condenser cooling water rate and the cooling water inlet and outlet temperatures.

b) For each exchanger, data required in the calculation of the heat transfer coefficients - the vapour and liquid flow rates and temperatures, and the physical dimensions of the exchanger.

Once the program is initialised, the overall run data are input from the tape reader and the actual and computed heat losses are output to the teletype as shown in Figure A7.16. The program then outputs the title of the first heat exchanger (preheater) and enters the subroutine where the exchanger data are input. The heat transferred, heat flux, log mean temperature difference and heat transfer coefficient, based on the experimental record, are then calculated and output. From the experimental data, the theoretical heat transfer coefficient is calculated as follows.

a) Tubeside - the average liquid temperature is determined from the arithmetic mean of the inlet and outlet temperatures, the Reynolds number is computed and the appropriate Seider and Tate equation (7.3.12 or 7.3.13) is solved to determine the tubeside heat transfer coefficient.

b) Shellside - Since the mean film temperature is not available it is approximated by (for example, in the preheater shell)

$$T_m = T_4 + \frac{h_s h_t}{h_s + h_t}(T_1 - T_4) \qquad 7.3.20$$

where h_s is an estimate of the shellside coefficient and h_t is the tubeside coefficient calculated as described above. The Nusselt equation (7.3.14) is

is then solved iteratively until the numerical value of h_s converges.

c) Overall - From the tubeside and shellside coefficients, the theoretical overall heat transfer coefficient is calculated (equation 7.3.16) and output to the teletype.

When the analysis of one exchanger is complete, the subroutine is re-entered until all four heat transfer coefficients are calculated and the processing of a single run is complete. Program execution order then returns to process data for the next run. Processing of data for the first effect does not follow the same procedure as the other exchangers. Since vaporisation takes place in the evaporator tubes, the total heat load is determined from the measured steam rate rather than from the liquid temperature change. Thus the analysis subroutine is called after the first effect data are input and the heat load is calculated. This is executed simply by programming a jump to the appropriate BASIC instruction in the subroutine, the subroutine exit is the same. This facility is specific to the BASIC language where subroutines are not compiled independently and hence there are no dummy variable names. One advantage of this subroutine processing procedure is the ability to inhibit or add to the teletype output interactively. Once the data from all steady state runs is available on paper tape the processing can be repeated and any output extracted from the subroutine each time it is accessed.

2. Regression Analysis Program

The regression analysis program is run on an ICL 1905E computer and accepts data for each steady state run from punched cards. A single data set consists of experimental heat transfer coefficient, arithmetic mean temperature difference,

tubeside liquid flow rate and shellside vapour flow rate. The program computes the value of the constants a,b,c and d in equation 7.3.19 and the multiple correlation coefficient from the 96 sets of data for each heat exchanger.

7.3.3.3 Results and Discussion

Figure A7.16 shows the teletype output from the steady state analysis program for a single steady state run. For all 96 runs the output is voluminous and thus the relevant results are summarised in Tables A7.5 to A7.9.

Table A7.5 shows the system heat losses, as a percentage of the total heat entering the system, calculated from measured enthalpies and from the solution of the mathematical model. For each steady state run the loss is approximately 10% when computed by either method. The numerical difference between the results of each method is due to errors in the steam flow rate. For the experimental heat loss the measured steam rate is utilised but for the calculated loss the rate is computed from the steady state model of the first effect which is subject to measurement errors and heat losses. It is not possible to divide the overall heat loss into the individual losses for each heat exchanger as there are insufficient measurements to compute both theoretical and experimental heat transfer rates. For dynamic simulation and on-line Kalman filtering the system heat losses are assumed to be negligible, although as Table A7.5 indicates, this assumption is not always valid. Investigation and correlation of losses for each unit is suggested for further work in Chapter 8.

Tables A7.6 to A7.9 show the experimental and theoretical heat transfer coefficients for each heat exchanger. For the preheater, second effect

and condenser (Tables A7.6, A7.8 and A7.9) the experimental results are close to the theoretical values with varying degrees of scatter due to deviation from steady state operating conditions, measurement noise and the use of unmeasured variables calculated from the steady state model. At the first effect (Table A7.7) the experimental results are consistently three to four times higher than theoretical values. Since the effect is a two-phase climbing film type evaporator and the algorithm for the theoretical heat transfer coefficient is for a general exchanger with a single liquid phase in the tubes, the experimental results are as expected. Improvement in exchanger performance of this magnitude for two-phase flow conditions is within the claim of Kestner's Patent (93) for the climbing film evaporator.

Results of multivariable regression analysis for each heat exchanger unit are summarised in Table 7.3. The table includes values for the constants a, b, c and d of equation 7.3.19 and the multiple correlation coefficient. The form of the correlation equations is shown in Section 6.5.3. The zero coefficient for c in the second effect correlation arises because a constant pump circulation rate ($3200\ gs^{-1}$) is assumed and thus the contribution due to tubeside liquid flow is lumped into the constant a.

TABLE 7.3 Results of Multivariable Regression Analysis for Overall Heat Transfer Coefficient Correlations

	a	b	c	d	Correlation Coefficient
Preheater	682.62	-27.55	13.44	5.27	0.9275
1st Effect	623.66	-11.34	-1.04	58.03	0.9957
2nd Effect	3900.00	-161.6	0.0	85.5	0.8629
Condenser	1151.92	-63.01	0.663	61.00	0.9989

Although the correlation coefficients for the first effect and condenser are near unity, at the preheater and second effect the influence of unmeasured variables is evident. The poor correlation coefficient for those exchangers is due to the errors involved in the calculation of the quantity of liquid and vapour present in the exchanger shells. The heat transfer coefficient is strongly influenced by the shellside vapour rate (coefficient d) and where the vapour rate is calculated by the steady state model, i.e., at the preheater and second effect, errors due to the dynamic state of the plant are evident. However, the above correlations represent the best available relationships between overall heat transfer coefficients and operating conditions and are utilised for dynamic simulation and Kalman filtering.

7.4 Dynamic Logs

7.4.1 General

Between successive on-line steady state runs, the state of the plant in response to disturbance is recorded in the form of dynamic logs. Program 3 of Appendix 6 is used to average measurements over each minute of plant operation and the resulting data are stored in a BASIC array. When the plant is again at steady state, usually after 30 minutes, the results are listed at the teletype. The purpose of this data acquisition is to provide real plant reponses for comparison with the results of simulation of the reduced dynamic model.

There are four controlled variables by which manual plant disturbances can be introduced.

1. Feed rate to the preheater
2. Steam rate to the first effect

3. Operating vacuum

4. Condenser cooling water rate

As discussed in Section 7.3.2, the dynamic effects of disturbances in operating vacuum and condenser cooling water rate are uncertain and so for dynamic logging experiments, the plant response to changes in preheater feed rate and steam rate are considered. Two step changes have been selected to describe qualitatively the dynamic characteristics of the evaporator - an increase in preheater feed rate and an increase in steam rate to the first effect. In both cases, the plant is assumed to be operating at steady state prior to the disturbance and the dynamic logging program is initiated at the same time as the manual step change is introduced.

7.4.2 Step Change in Prehater Feed

In an ideal system, where the vacuum pressure is maintained constant, the effect of an increase in the liquid feed to the system is to decrease the proportion of feed vaporised by the constant steam supply. Thus the flow rate of liquid from the cyclone to the second effect separator increases and the vapour flow from the cyclone remains constant. Since the vapour leaving the cyclone is used in the shellside of the preheater, the increased liquid flow causes a drop in the tubeside exit temperature. The only other apparent change is an increase in the rate at which the liquid level in the second effect separator is changing due to the increased flow from the cyclone.

The response of the real system to an increase in preheater feed rate is shown in Figures A7.17 to A7.22, taken from the output of the dynamic logging program.

The step change in flow rate is immediately transmitted through the first effect to the cyclone separator and is recorded by the flow meter measuring the liquid rate to the second effect (Figure A7.17). The increased flow to the second effect separator causes an immediate increase in the rate of accumulation which then remains approximately constant for the remaining measurement time (Figure A7.18).

An increase in flow to the first effect produces less boiling since a greater proportion of the heat transferred is required for sensible heating. The decrease in the vapour within the system causes the vacuum pump to reduce slightly the operating pressure (and thus the boiling point) so that the vapour rate increases to satisfy the combined capacity of the vacuum pump and condenser. This reduction in vapour temperature occurs throughout the whole system and is conveniently observed at the cyclone separator (Figure A7.19). The decrease in vapour temperature at the cyclone is also apparent at the shellside of the preheater (Figure A7.20). The temperature of the liquid leaving the tubes of the preheater is reduced by two mechanisms. Firstly, by the increased liquid throughput and secondly by the reduction in the temperature driving force due to the small change in shellside vapour temperature (Figure A7.20).

At the second effect separator, the reduction in vapour pressure causes an increase in boiling and a decrease in the temperature of the circulating liquid pumped to the second effect (Figure A7.21) and a corresponding decrease in the temperature of the cooling liquid leaving the condenser (Figure A7.22).

The overall system response to the increase in feed liquid rate follows the response of the ideal system described above. There is, however, the underlying dynamic response of the vacuum pump to changes in the total vapour in the system which affects all heat exchangers to a minor extent.

7.4.3 Step Change in Steam Rate to 1st Effect

In an ideal system, where the vacuum pressure is maintained constant, the effect of an increase in the steam rate to the first effect is to increase the proportion of feed vaporised in the first effect, thus making more vapour available for heat transfer in the shells of the preheater and second effect. Consequently, the temperature of the liquid leaving the preheater increases and the heat transferred to the circulating liquid in the second effect produces more boiling in the second effect separator. The combined effect of a reduction in the liquid rate from the cyclone separator and the increased heat transfer in the second effect causes the rate of change of liquid level in the second effect separator to decrease. The temperature of the cooling liquid leaving the condenser increases as the additional vapour is condensed.

The response of the real system to an increase in steam feed rate is shown in Figures A7.23 to A7.28. At the first effect, there is an immediate increase in the proportion of vapour in the tubes and thus the liquid flow from the cyclone to the second effect separator decreases (Figure A7.23). The rapid increase in vapour within the system causes the vacuum pump to increase the operating pressure (and thus the boiling point) so that the overall vapour rate to the condenser reduces to satisfy the combined capacity of the vacuum pump and condenser. This increase in vapour temperature occurs throughout the whole system and is conveniently observed at the cyclone separator (Figure A7.24). The temperature of the liquid leaving the tubes of the preheater is increased by virtue of the greater temperature driving force created by the increase in shellside vapour temperature (Figure A7.25). The small increase in system operating pressure causes the preheater feed rate to drop due to the resulting reduction in liquid

delivery head (Figure A7.73).

At the second effect separator, the increase in vapour pressure occurs at such a rate that boiling is not increased and the temperature of the circulating liquid pumped to the second effect (Figure A7.26) increases. As the shellside of the second effect contains more vapour available for heat transfer, the temperature rise of the circulating liquid also increases (Figure A7.26). With more vapour being drawn into the condenser from the second effect separator and, as uncondensed vapour, from the second effect shell, the coolant exit temperature rises (Figure A7.27). The rate of change of the head in the second effect (Figure A7.28) decreases as less liquid is fed from the cyclone separator.

The overall system response to the increase in the feed rate to the first effect follows the response of the ideal system. When the step change is large, the response of the vacuum pump performance to changes in the total vapour in the system significantly affects the plant performance.

7.5 Dynamic Simulation

7.5.1 General

Appendix 5 describes the development of an eighteenth order dynamic model of the evaporator. The derivation of the dynamic equations for the shellsides of heat exchangers, where liquid and vapour exist together, cannot be derived by the classical method of setting the accumulation terms equal to the difference between the inlet and outlet flows. In this case, the steady state operating equations are perturbed to give a dynamic equation representing the plant response to small deviations from steady state.

For Kalman filter experiments, the eighteenth order model is impractical and the simplifications described in Section 5.4 are used to reduce the model to a fourth order system. The simplifications are possible because the time constants of the vapour phase dynamic equations are considerably smaller than those of the liquid phase. Thus the vapour phase dynamic equations are replaced by their steady state counterparts. One further justification for the model simplification is that the influence of the vacuum pump on the system dynamics is unknown and not accounted for in the comprehensive model. For the reduced model, the vacuum pressure is assumed to be constant throughout the evaporator system. For simulation of the reduced model, this simple mathematical description of the vapour phase is extended by treating a measured vapour temperature profile as an input to the dynamic model. The simulated response of the liquid phase dynamics is then compared with the measured response. Real plant data are available in the form of dynamic logs.

For simulation, both models are disturbed by the same system changes described under dynamic logging, Section 7.4 - the response to step changes in preheater liquid feed rate and steam rate to the first effect.

7.5.2 Simulation of Comprehensive Model

Program 4 of Appendix 6 shows the ASP simulation of the eighteenth order comprehensive model, equations 6.5.15 to 6.5.32. Initial conditions are taken from a steady state run prior to the introduction of a plant disturbance and subsequent dynamic logging. A step change, equivalent to the disturbance created for the dynamic logging, is programmed at the start of a simulation after solving the steady state equations for the loss terms (Section 6.5.3). The objective of calculating the loss terms is to force the dynamic equations to have zero

derivatives based on the initial condition data.

The program output is shown in Figure A7.29. At each print out interval a teletype listing is produced of the state of each unit of the evaporator. This includes temperatures (^{o}C), flows (gs^{-1}), vapour fraction (where liquid and vapour are together in the shellsides of the exchangers) and the overall heat transfer coefficient ($Wm^{-2}K^{-1}$). The symbols are L - liquid, V - vapour and LV for liquid/vapour mixtures. At the right hand side of each variable is listed the corresponding derivative.

All comprehensive model simulations are initialised with the same steady state conditions. Integration is carried out by the fourth order Runge-Kutta method with a step length of 0.01 seconds. The teletype listing is produced every 0.1 seconds of simulation time.

7.5.2.1 Step Change in steam rate to 1st Effect

The response of the model to a step change in steam flow rate is shown in Figures A7.29 to A7.31. The magnitude of the step is from 15.4 gs^{-1} to 24 gs^{-1} introduced into the system at time zero. Figure A7.29 shows the dynamic state of the model at time zero. The immediate effect of the large step change in steam rate is evident at the first effect. The derivative of the temperature of the liquid/vapour mixture within the tubes is initially large and positive as the dynamic equations responde to the increase in heat input. Similarly, the dynamic equations for the tubeside liquid and vapour flow rates have large derivatives as the increase in heat input immediately affects the boiling rate. The increase in the derivatives of vapour rate and temperature from the first effect is also evident at the shellside of the preheater and hence the shellside of the second effect. This is due to the incorporation of temperature derivative

terms in the dynamic equations of the shellsides (equations 6.5.18, 6.5.19, 6.5.28) as result of the steady state equation perturbation described in Appendix 5.

Since the dynamics of the connecting pipework is not included in the model, the large initial derivative of the temperature of the liquid leaving the first effect tubes (and hence the cyclone) produces a large initial derivative of the boiling rate in the second effect separator (equation 6.5.31).

After 0.1 seconds, Figure A7.30, the variables of the preheater and first effect dynamic equations respond in the same way as the variables measured in the dynamic log response to increase in steam rate (Section 7.4.3). The temperature of the liquid/vapour mixture within the first effect tubes increases by 14°C and at the same time, all shellside derivatives remain considerably larger than those of the tubeside liquid variables. The temperature of the liquid leaving the preheater, second effect and condenser tubes increases; the same trend is observed in the dynamic log. This also applies to the decrease in the liquid head in the second effect separator.

The simulated response of the shellside variables requires further discussion. The effect of the large magnitude of the step change and hence the large derivative for the first effect variables causes the shellside derivatives to be correspondingly large. This is a direct result of the approximation of the dynamic equations as perturbed steady state operating equations. For example, the fact that a step change in steam feed rate causes the initial derivative of the vapour rate in the shellside of the second effect to be large is not a true physical representation of the system. However, equation 6.5.28 is an approximation to the variation around steady state which is dependent upon other approximate derivative

expressions for the vapour and liquid rates leaving the preheater shell (equations 6.5.18 and 6.5.19). In particular, equation 6.5.18 is dependent upon the derivative of the temperature within the tubes of the climbing-film first effect (equation 6.5.20) which is numerically large due to the magnitude of the step change. In the real situation, this derivative would not be large due to the influence of the vacuum pump on the vapour phase of the system. An increase in steam rate causes an increase in boiling rate rather than boiling temperature.

The approximate derivative equation for the boiling rate in the second effect separator (equation 6.5.32) is also dependent upon the derivative of the boiling temperature in the first effect (hence the cyclone separator). The result of this apparent rapid increase in boiling is to reduce the temperature in the separator, equation 6.5.29, thus adding to the error involved in the approximation in equations 6.5.27 and 6.5.28. This produces very large derivatives for the flow of the liquid/vapour mixture in the shellside of the second effect. The rapid increase in shellside vapour rate in the second effect causes the heat transfer coefficient to increase. Furthermore, since the vapour rate derivatives are large and also increase from the first effect to the preheater and second effect, the corresponding temperature derivatives (equations 6.5.16 and 6.5.25) become negative. The negative shellside derivative affects the dynamic equation for the vapour fraction in the exchanger shell (equation 6.5.26) such that there is an apparent drop in the vapour fraction. These effects are apparent at the preheater shell and, to a greater extent, in the shellside of the second effect.

The interaction between the second effect and second effect separator causes the magnitude of the error in the second effect shellside derivatives to increase. Further increase in the shellside vapour rate increases the heat transfer coefficient.

This causes an apparent drop in the shellside temperature which interacts between the shellside liquid rate (equations 6.5.27) and hence the vapour rate (equation 6.5.28). Similarly, the large initial derivative of the vapour leaving the second effect separator (equation 6.5.31) reduces the temperature of the liquid in the separator (equation 6.5.29) which also affects the second effect shellside liquid and vapour rates (equations 6.5.27 and 6.5.28) and the boiling rate itself (equation 6.5.31).

After 0.2 seconds (Figure A7.31), the effect of the large initial derivatives results in an increase in the errors involved in the second effect/separator system such that the variables become unreal e.g., the negative liquid flow rate in the second effect shell and the drop in shellside temperature below the tubeside liquid temperature. However, although the results of the shellside simulations are unsatisfactory, the tubeside liquid temperatures show the same qualitative trend as th dynamic logs.

7.5.2.2 Ramp disturbance in steam rate to 1st effect

In an attempt to simulate the comprehensive model without including the effects of large initial derivatives, the steam rate disturbance is input as a sequence of small steps added to the flow at each output time (0.1 seconds). Figures A7.32 to A7.38 show the response of the comprehensive model to an increase of 0.1 gs^{-1} of steam every 0.1 seconds. Thus an overall increase of 10 gs^{-1} is effected in 10 seconds which compared to an overall simulation time of 30 minutes is representative of a step change.

At time zero seconds (Figure A7.32), the model is at steady steady state and all initial derivatives, with the exception of the head in the second effect separator, are zero. As soon as the output is complete, the steam rate is

incremented by 0.1 gs^{-1} and the simulation continues.

After 0.1 seconds (Figure A7.33), the response of the first effect and preheater follows the same trend as the large step change simulation. At the first effect tubes the temperature of the vapour/liquid mixture increases by 0.3 °C and correspondingly the vapour rate increases and the liquid rate decreases. At the preheater, the tubeside liquid temperature increases but the shellside vapour/liquid temperature decreases. This is due to the magnitude of the initial derivatives of the shellside vapour/liquid mixture when the small step change is introduced. In all cases, the magnitude of the shellside vapour rate derivatives increases throughout the system. For example, in Figure A7.33 the derivative of the vapour rate at the second effect shell is greater than that of the preheater shell which is greater than that of the vapour (boiling) rate at the first effect tubes. This is due to the initialisation of the derivatives of the vapour phase dynamic equations and the effect is to produce a negative derivative for the shellside temperatures (equations 6.5.16 and 6.5.25).

As the simulation continues (Figures A7.34 - A7.37) the instability in the second effect/separator system, described previously, becomes apparent and after 0.6 seconds, negative flows are computed. Examination of the derivatives of the negative flow in the second effect shell at 0.7 seconds (Figure A7.38) shows that the dynamic model compensates for this by increasing the derivative.

Thus the effect of reducing the size of the disturbance and stepping the steam rate at each print interval is to reproduce the same vapour phase trends as for the large step change. The time taken for the simulation to become unrealistic is extended. The qualitative response of tubeside liquid temperatures and the level

in the second effect separator are the same as those recorded by dynamic logging experiments.

7.5.2.3 Step Change in Preheater feed

The response of the comprehensive model to a step change in flow rate of liquid to the preheater is shown in Figures A7.39 to A7.41. A step change from 27 gs^{-1} to 40 gs^{-1} is input to the system at time zero (Figure A7.39). The initial derivative of the preheater outlet temperature is negative, as is expected from the results of dynamic logging experiments for the same step change (Section 7.4.2). As a result of the derivation of the shellside dynamic equations, other derivatives are non-zero. The preheater shellside vapour and liquid rates (equations 6.5.18 and 6.5.19) are dependent upon the preheater tubeside temperature derivative, the first effect tubeside temperature is dependent upon the increased liquid flow rate (equation 6.5.20) and the first effect shellside flows (equations 6.5.22 and 6.5.23) are dependent upon both the increase in flow rate and the derivative of the first effect tubeside temperature. Like the response of the model to a step change in steam rate, the vapour flow derivative at the preheater shell is used in the computation of the boiling rate derivative in the second effect separator (equation 6.5.31).

Examination of the signs of the initial derivatives shows that the qualitative trends for the variables are the same as those of the dynamic log. The increase in liquid feed rate reduces the vaporisation in the first effect tubes and lowers the boilin temperature. At the preheater, the tubeside liquid temperature falls as a result of both the increased flow rate and decreased vapour rate. The increase of the liquid flow from the cyclone to the second effect separator causes the head to increase.

The magnitude of the initial derivatives shows the sensitivity of the vapour phase and shellside dynamic equations to input disturbances. At the first effect tubes the temperature derivative is very large as are the vapour and liquid rate derivatives. The magnitude of the preheater vapour rate derivative is also evident in the computation of the derivative of the second effect shellside vapour rate.

After 0.1 seconds (Figure A7.40) the effect of large initial derivatives in the variables in the exchanger shells is the same as for the response to change in steam feed rate. The interaction between the second effect and second effect separator increases the derivatives so that after 0.2 seconds (Figure A7.41) unrealistic flows are computed for the liquid /vapour mixture in the second effect shell. From steady state and dynamic logging measurements, the highest temperature in the system is observed at the tubes of the climbing film evaporator. The increase in feed to the preheater reduces this boiling temperature (Figure A7.19) and all other vapour phase temperatures. In Figure A7.41, this trend is observed at the first effect and preheater, but at the second effect the reverse situation is observed as the shellside temperature increases. In a practical sense, this situation is impossible since the preheater and second effect shells are connected.

Although the response of the vapour phase dynamic equations shows instability and unrealistic results, the response of the liquid phase variables shows the same qualitative trend as the dynamic log (Figures A7.17 to A7.22). The liquid temperatures in the preheater, second effect and condenser tubes show a reduction in temperature while the head in the second effect separator increases.

7.5.2.4 Ramp Change in Preheater Feed

In order to reduce the effects of large initial derivatives upon the dynamic simulation, the feed disturbance is input as a sequence of small steps added to the flow at each output time (0.1 seconds). Figures A7.42 to A7.47 show the response of the comprehensive model to an increase in feed rate of 0.1 gs^{-1} every 0.1 seconds. Thus a step change of 10 gs^{-1} is input to the system over 10 seconds which when compared to the observed response time of the system is relatively small.

Initially (Figure A7.42), the model is at steady state and all initial derivatives with the exception of the head in the second effect separator, are zero. As soon as the output is complete, the preheater feed is incremented by 0.1 gs^{-1} and the simulation continues.

After 0.1 seconds (Figure A7.43), the response of the first effect and preheater follows the same trend as the large step change simulation. At the first effect tubes and preheater shell, the derivatives are still large by comparison with the liquid side values. While the simulation continues (Figure A7.44 to A7.47), the response of the liquid phase follows the trend of the dynamic logs but the derivatives of the vapour phase increase. Ultimately the simulation will produce unrealistic results. Thus the response of the system to small step changes is the same as the response for the large step change. As expected, the time taken to become unstable is greater.

7.5.2.5 Conclusions

The response of the eighteen order comprehensive model to system disturbances can be divided into two distinct types. Firstly, at the heat exchanger tubes, the response of the liquid temperatures follows the same qualitative trends as the dynamic logs (Figures A7.17 to A7.28). Secondly, in the heat exchanger shells

where the vapour and liquid/vapour mixtures exist, the time constants are much smaller and thus when the simulation begins, the simulated variables become unrealistic. This is due to the fact that the real system is constrained by the operation of the vacuum pump and this is not included in the dynamic model. A step change in steam rate creates an increase in boiling and not in vapour temperature because the vacuum pump attempts to maintain the system vapour pressure constant. The reverse situation applies to a step change in preheater feed rate. Thus the exclusion of the vacuum pump dynamics, however uncertain, produces unsuccessful simulation results. The dynamic model contains simplified equations based on the perturbation of the steady state equations. In particular, at the preheater and second effect shells these approximate equations produce instability in the simulation. Furthermore, the heat transfer coefficient correlations for these two heat exchangers are subject to greater errors than those of the first effect and condenser (Table 7.3).

7.5.3 Simulation of Reduced Model

In the reduced model of the evaporator (equations 6.5.33 to 6.5.36) the dynamics of the vapour and vapour/liquid phases is not considered. This reduction in the order of the model is based upon the assumption that the vacuum operating pressure, and thus the vapour pressure throughout the whole system, is constant. This means that the vapour phase dynamic equations, which have the smaller time constants, are replaced by their steady state equations. Mathematically, the assumption that the vapour pressure is constant is the simplest description. In practice the vapour pressure is observed to change when the system is disturbed by step changes in preheater feed and steam rate to the first effect (Section 7.4). In order to simulate the reduced model with realistic inputs, the measured vapour

temperature response is input to the reduced model throughout the simulation so that the experimental and simulated plant response can be observed. This is carried out by means of the function generation subroutine of the ASP package.

Program 5 of Appendix 6 shows the ASP simulation of the fourth order reduced model. Initial conditions are taken from a steady state run prior to dynamic logging. At the same time, seven BASIC arrays are loaded with the dynamic log output from vapour phase measurements from 30 minutes logging. These are as follows:

Array name	Variable
A	The mean time at which samples are taken
B	The steam flow rate (analogue value)
C	The preheater shellside temperature
E	The cyclone vapour/liquid temperature
F	The vapour temperature at the operating vacuum
G	The second effect shellside temperature
H	The preheater feed temperature

The numerical values input to the arrays depends upon the step change and corresponding dynamic log. For example, the logged response to a step change in preheater feed is shown in Figure A7.48. From this log the appropriate vapour side pressures are converted to temperatures (Section 6.2.3) and loaded from statement 4000 of Program 5 (Figure A7.49). At each integration step a linear interpolation is performed by the fifth ASP subroutine to determine the appropriate vapour temperature at a given time. The preheater feed temperature is included because the temperature of the water supply to the evaporator is known to vary. For each

reduced model simulation, the above data preparation is required. Figures A7.48 and A7.49 are representative of the input data for all simulations.

A step change in preheater feed or first effect steam is programmed at the start of a simulation, after solving the steady state equations for the loss terms (Section 6.5.3). The program output is voluminous and is not included, the simulation and dynamic log data are presented graphically. For comparison purposes, the axes of graphs for the same variable are the same for all simulations. The initial steady state conditions are not the same for each simulation, but are the results of experimental steady state runs prior to dynamic logging.

The dynamic equations of the reduced model are as follows:

Preheater Tubes

$$\frac{dT_2}{dt} = \frac{M_2 C_p (T_1 - T_2) + U_g A_g (T_4 - \frac{(T_1 + T_2)}{2}) + L_1}{0.5 W_{tg} \rho_L C_p} \qquad 7.5.1$$

Second Effect Tubes

$$\frac{dT_{14}}{dt} = \frac{M_{14} C_p (T_{15} - T_{14}) + U_f A_f (T_{10} - \frac{(T_{14} + T_{15})}{2}) + L_4}{0.5 W_{tf} \rho_L C_p} \qquad 7.5.2$$

Condenser Tubes

$$\frac{dT_{13}}{dt} = \frac{M_{12} C_p (T_{12} - T_{13}) + U_c A_c (T_{vac} - \frac{(T_{12} + T_{13})}{2}) + L_7}{0.5 W_{tc} \rho_L C_p} \qquad 7.5.3$$

Second Effect Separator

$$\frac{dH_s}{dt} = \frac{M_{14}C_p(T_{15} - T_{14}) + M_8C_p(T_{15} - T_8) + M_8\lambda_{15}}{\rho_L A_s \lambda_{15}} \qquad 7.5.4$$

where the flow from the cyclone separator to the second effect separator is given by the steady state energy balance on the first effect,

$$M_8 = \frac{M_1 - A_eU_e(T_5 - T_7) - M_2C_p(T_2 - T_7)}{\lambda_7} \qquad 7.5.5$$

Temperatures T_4, T_{10}, T_{15}, T_{vac} and T_7 are available in the form of dynamic log output which is incorporated into the simulation as described above.

When the heat transfer coefficient correlations are included in the above equations the model becomes non-linear. For example, a step change is steam rate changes the heat transfer coefficient in the first effect (equation 7.5.5). This in turn changes the quantity of vapour leaving the first effect (and hence the cyclone A steady state energy balance on the shellsides of the preheater and second effect gives new vapour flow rates which in turn affect the heat transfer coefficients in equations 7.5.1 and 7.5.2. Also, via the steady state energy balance on the condenser shell, the coefficient in equation 7.5.3 changes. The dynamic equation for the head in the second effect separator (equation 7.5.4) is dependent upon equation 7.5.3 and , through equation 7.5.5, upon the heat transfer coefficient in the first effect and equation 7.5.1. This interaction is discussed further in Section 7.6.2.

A step change in preheater feed rate (M_2) influences equations 7.5.1 and 7.5.5 (and hence equation 7.5.4) directly. The change in vapour rate produced

from the first effect, and hence the preheater and second effect, influences the heat transfer coefficients in equations 7.5.1, 7.5.2 and 7.5.3.

7.5.3.1 Step Change in Steam Rate to First Effect

Figures A7.50 to A7.53 show the response of the reduced model to a step increase in steam rate from 15.4 gs^{-1} to 22.3 gs^{-1}. Integration is by the fourth order Runge-Kutta method with a step length of 0.5 seconds. The figures also include the response recorded during dynamic logging experiments when the plant steam rate is changed by an identical step.

At the tubes of the preheater (Figure A7.50) the liquid temperature increases. The rate of increase is initially greater than the experimental response and subsequently, the new steady state temperature is lower than that recorded. A similar effect is observed at the second effect tubes (Figure A7.51) and the condenser tubes (A7.52). In the derivation of the dynamic model, the liquid in the exchanger tubes is assumed to be well mixed. In practice, there is some deviation from this ideal situation. At the preheater and condenser, there is more than one tube pass and thus the difference between simulated and experimental responses is initially large. The second effect is a single pass, forced circulation evaporator with a high circulation rate, thus the well-mixed approximation is near to reality (Figure A7.51). The off-set of the responses is due to the effect of the change in vacuum pressure (observed in dynamic logging Section 7.4.3) and to the change in system heat losses as temperatures increase. This latter effect would diminish the difference between simulated and experimental responses. The prediction of the head in the second effect separator closely follows the measured response. Measurement noise is due to violent boiling that occurs in the separator.

A reverse step change in steam rate from 27.4 gs^{-1} to 16.8 gs^{-1} produces the response shown in Figures A7.54 to A7.57. The response of the liquid temperature in the preheater, second effect and condenser tubes is the reverse of the increase step change. Due to the reduction in the system heat input the accumulation in the second effect separator (Figure A7.57) is considerably greater than the previous simulation (Figure A7.53).

7.5.3.2 Step Change in Preheater Feed Rate

Figures A7.58 to A7.61 show the response of the reduced model to a step increase in preheater feed rate from 30.7 gs^{-1} to 41.2 gs^{-1}. The fourth order Runge-Kutta integration method is used with a step length of 1 second.

At the preheater (Figure A7.58), the simulated temperature response has the same characteristics as the response to steam change - high initial rate of change and deviation from the new steady state value. The magnitude of the temperature change is considerably less than for the steam change responses. At the second effect (Figure A7.59) and condenser (Figure A7.60), the simulated temperature response, like the measured values shows little change. In an ideal system, the increase in preheater feed does not affect these variables since the same proportion of feed would be vaporised by the constant steam rate. In practise, the initial increase in feed rate means that a greater proportion of the steam is required for sensible heating in the first effect. Although this proportion is small, the reduction in boiling in the first effect provides less vapour for the preheater and second effect shells and the temperature of the circulating liquid in the second effect tubes falls (Figure A7.50). The reduction in boiling affects the condenser liquid temperature in the same manner (Figure A7.60). As more feed is entering the system and less boiling takes place the accumulation in the second effect is

large (Figure A7.61).

A reverse step change in preheater feed rate from 41.4 gs^{-1} to 22.1 gs^{-1} produces the response shown in Figures A7.62 to A7.65. The response of the liquid temperature in the preheater, second effect and condenser tubes is the reverse of the increase step change. Since the magnitude of the step change is large, the accumulation in the second effect separator is negative (Figure A7.65).

7.5.3.3 Conclusions

From visual inspection of the graphical results of the reduced model simulation (Figures A7.54 to A7.65), there is close agreement between computed and measured variables. The deviation from the measured response is due to the assumption that the liquid within the heat exchanger tubes is well-mixed. Where the assumption is close to reality, at the second effect, the agreement is best.

As a result of the above investigation the fourth order reduced model is used for Kalman filtering experiments.

7.6 Kalman Filtering

7.6.1 General

In the first place, the objective of the Kalman filtering experiments is to prove that the filter algorithm can be successfully implemented in real-time on-line to to the evaporator system. Secondly, by performing off-line experiments with real plant data, it is hoped to achieve a greater understanding of the influence of the filter statistics in the estimation of states and parameters when the evaporator

is in pseudo steady state and dynamic operation.

Experiments in real time Kalman filtering are constrained by both the system hardware and software. Available computer storage restricts the maximum order of the mathematical model (the number of state variables) and also the number of measurements. Processing speed in numerical integration and execution of the filter algorithm requires consideration in real-time experiments as does the time taken for scanning channels of the data logger. In off-line processing none of these constraints are present. If the available computer core is too small, then programs can be run on a larger machine. Program execution time is also irrelevent since measurements are not required in real time but can be made available as conventional program data.

7.6.2 Preliminary Considerations

Implementation of the reduced dynamic model of the evaporator for Kalman filtering experiments gives a state vector containing four measurable variables and four parameters (the overall heat transfer coefficients).

Prior to performing on-line filter experiments and considering the real-time implementation of the algorithm it is necessary to consider,

a) System controllability

b) System observability

c) As a result of a) and b) to determine the best measurement strategy

d) The measure of filter performance.

The model, equations 7.5.1 to 7.5.4, is non-linear and the truncated Taylor series expansion from which the transition matrix is derived gives the following

incidence relationship (where an element is unity, the corresponding element of the transition matrix is non-zero).

$$x(k+1|k) = \begin{bmatrix} 1 & 0 & 0 & 0 & 1 & 0 & 0 & 0 \\ 0 & 1 & 0 & 0 & 0 & 1 & 0 & 0 \\ 0 & 0 & 1 & 0 & 0 & 0 & 1 & 0 \\ 1 & 1 & 0 & 1 & 0 & 0 & 0 & 1 \\ 0 & 0 & 0 & 0 & 1 & 0 & 0 & 0 \\ 0 & 0 & 0 & 0 & 0 & 1 & 0 & 0 \\ 0 & 0 & 0 & 0 & 0 & 0 & 1 & 0 \\ 0 & 0 & 0 & 0 & 0 & 0 & 0 & 1 \end{bmatrix} x(k|k) \qquad 7.6.1$$

where

$$x = \begin{bmatrix} T_2 \\ T_{14} \\ T_{13} \\ H_s \\ U_g \\ U_f \\ U_c \\ U_e \end{bmatrix}$$

and the symbols are defined in Section 5.2.

Inspection of the incidence matrix shows that one effect of the assumptions used to reduce the order of the comprehensive dynamic model is to remove the links between the state equations. If the equations are completely independent, then the four equation system is not observable and controllable, and thus the filter algorithm is not suitable for state variable and parameter estimation. It is necessary to examine the incidence matrix and the available measurements to determine at which point the system is completely observable and controllable and

hence determine the best measurement strategy.

7.6.2.1 Controllability

A system is controllable if it can be moved from any state $x(t_o)$ at $t = t_o$ to any other desired state $x(t_1)$ in a finite time interval τ ($\tau = t_1 - t_o$) by applying a piecewise continuous input-vector $u(t)$ throughout τ . Thus a system is controllable if every state variable is affected by the control and random inputs. For the evaporator system the control inputs are the preheater feed rate and temperature and the steam flow rate to the first effect. The condenser cooling water rate and the process vacuum pressure are not changed manually. Although the vacuum pressure is set constant initially, it is observed to vary throughout normal plant operations (Section 7.4). Thus in the real system, changes in input variables are observed to affect all the state-variables. In the reduced model, the system is controllable only if the vapour phase temperatures (T_4, T_7, T_{10}, T_{15}, T_{vac}) that appear in the state equations and the transition matrix are also regarded as system inputs. This is confirmed by the results of reduced model simulation where the same vapour phase measurements are regarded as system inputs.

7.6.2.2. Observability

A system is observable if all its states can be derived from the measurement vector of the system, directly or indirectly. Examination of the incidence matrix of equation 7.6.1 shows that the third state variable, T_{13}, must be measured in order to determine U_c. Any combination of this measurement with one other measurable state variable will give an observable system because of the relationship between the fourth state variable H_s and T_2 and T_{14}. From two such measurements all the states can be derived.

7.6.2.3. Measurement Strategy

For filtering experiments, the minimum measurement strategy is to sample the vapour temperatures, the condenser cooling water outlet temperature and one other state variable. In practice, all 16 plant measurements are available within two seconds and so the four state variables are measured in addition to the vapour temperatures. The effect of reducing the number of measured state variables is not considered.

Executing the filter algorithm for an eighth order system with a measurement vector of 16 elements is beyond the storage capacity of the computer. Consequently, the measurement vector is reduced to the four measured state variables. The remaining measurements are input directly to the state equations and the transition matrix. This means that at the state variable and estimation error covariance matrix prediction step, 'noise-free' measurements are included to obtain the best possible prediction and to maintain control ability. At the estimation error covariance prediction step, the effect of random disturbances on the vapour phase 'noise-free' measurements can be accounted for in the selection of the elements of the process noise matrix, Q.

The measurement strategy described above thus

a) reduces the measurement vector, thus minimising filter execution time,

b) maintains observability and controllability by including the 'noise-free' measurements

c) maintains accuracy at the state variable prediction step by including the 'noise-free' measurements

d) Utilises all available state information by including measurements of four state variables.

7.6.2.4 Filter Performance

In a real-time, on-line situation, where the true values of states and parameters are unknown, some measure of filter performance is required. In the linear case, with Gaussian measurement and process noise, the true state is given by the vector of state estimates once the filter has converged. The convergence can be observed by examining the estimation error covariances (or deviations) as each filter cycle is executed. In non-linear system convergence to the true state is not guaranteed and the estimates may diverge or be biased.

The size of non-linearities depends on both the magnitude of the second partial derivatives in the truncated Taylor series expansion defining the transition matrix and on the estimation error covariance. These are termed the real and induced non-linearities respectively, the combination of both sources is termed mixed non-linearity. A non-linearity can always be induced by setting the initial estimation error covariance matrix, P(0,0), sufficiently large.

The published reports of the significance of non-linearities are described in Section 2.4.2. In general, non-linear effects are significant when noise inputs are small while the estimation error variance is relatively large. Intuitively, this is obvious since large noise inputs can effectively mask neglected non-linearities. If Q is sufficiently large in equation 6B of Figure 6.9, then P cannot become very small as a result of information contained in the observations, since noise is continuously added to the system. If Q is small and P is initially large but subsequently becomes small, then even small bias or divergence can be significant.

Thus, in addition to the numerical value of the state variables, the diagonal elements of the error covariance matrix represent a measure of the filter performance when considered together with the real system non-linearities and the numerical value of Q. The equations of the reduced model (equation 7.5.1 to 7.5.4) are linear in the measured state variables if the parameters are assumed to be constant. When the parameters are treated as state variables, the second order derivative terms become small (differentiation of equations 6.6.6 to 6.6.19) and the terms above second order are zero. . In light of the 'small' non-linearities in the state equations the diagonal elements of the error covariance matrix are taken to represent some measure of the filter performance.

7.6.3 On-Line Experiments

7.6.3.1 Program Timing

The on-line filtering program is described in Section 6.6.2. Within a single filter cycle the following five operations require computation time.

1. The execution of the filter cycle for the given number of state variables and measurements.

2. Repetitive channel scanning with ensemble averaging to minimise signal noise.

3. Numerical integration of the state equations and calculation of the variable elements of the transition matrix.

4. Teletype output of relevant results.

5. Other computation at the BASIC level, such as conversion of measurements and waiting for real time clock interrupt.

When the Kalman filter subroutine (Program A3.19) is accessed from BASIC, the processing time for a given number of state variables and measurements is fixed and is independent of the sampling interval. Filter subroutine timing experiments are performed prior to on-line operation. The time taken to execute the program for various numbers of state variables, and measurements is shown in Figure A7.66. A system comprising of 8 state variables and 4 measurements requires approximately 18 seconds of computation time.

The maximum rate of measurement is fixed at 10 channels per second. Higher rates are possible with the MDP200 but the adverse effects of reed relay noise outweigh the benefits of signal averaging. Thus sixteen measurements scanned repetitively with ensemble of 5 requires approximately 8 seconds of computer time.

A number of methods are available for performing numerical integration, e.g., Runge-Kutta, Euler, etc., but it is advantageous to select the method that provides the greatest accuracy with the least processing time. Unlike other comparative studies of methods of numerical integration (46), it is the total number of BASIC statements and not the number of derivative function evaluations that determines the optimum processing speed. For this reason, the Euler method with a step length of 0.5 seconds is selected. By this method, 120 seconds of simulation time can be executed in approximately 75 seconds, providing accurate state variable prediction.

An overall sampling interval of 120 seconds thus requires approximately 101 seconds to complete a filter, measurement, and numerical integration cycle.

The time available for output of results and other BASIC computations is approximately 19 seconds which, at a teletype speed of 10 characters per second, permits only the output of the estimates and the diagonal elements of the transition matrix. Consequently, the output of other relevant matrices is not included in real-time filtering experiments, but is output during off-line processing where computation time is not at a premium.

7.6.3.2 Parameter Prediction

The state equations for the parameters are given by equating the derivatives to zero, thus giving unity on the corresponding diagonal elements of the transition matrix. This technique is suitable for updating the estimation error covariance matrix (equation 6B of Figure 6.9) but at the state variable prediction (equation 6A), an alternative strategy is available. This is to utilize the heat transfer coefficient correlations, based on the current estimates (and the current non-state variable measurements) to calculate the parameters at each filter cycle. It is beneficial to use all available information to provide the best predicted values of state variables. A comparison of these two methods of parameter prediction is included in the off-line filter experiments.

7.6.3.3 Program Output

The teletype output from an on-line filtering experiment is shown in Figures A7.67 to A7.69. At each filter cycle the predicted (P), estimated (E), and measured (M) variables are printed together with a list of the square roots of the diagonal elements of the estimation error covariance matrix. The state variables are printed in the order,

T_2	T_{14}	T_{13}	H_s
U_g	U_f	U_c	U_e

and the measured variables in the order

$$T_2 \qquad T_{14} \qquad T_{13} \qquad H_s$$

The order of the estimation error deviations is the same as for the state variable output. The single integer above the output for each cycle refers to the number of that cycle.

7.6.3.4 Filter Statistics

In the example shown in Figures A7.67 to A7.69, the strategy of parameter prediction by the correlations is adopted. The filter statistics are

$$P(0,0) = 1000.\,I$$

$$Q = 0.1\,.\,I$$

$$R = \begin{bmatrix} 0.1 & 0 & 0 & 0 \\ 0 & 0.1 & 0 & 0 \\ 0 & 0 & 0.1 & 0 \\ 0 & 0 & 0 & 0.15 \end{bmatrix}$$

The high initial estimation error covariance implies a lack of confidence in the initial state variable estimates. The smaller numerical value of the diagonal elements of Q signifies confidence in the model, the accuracy of the linearisation and also indicates that random input disturbances are small. Since the measurements are not scaled variables, the diagonal elements of the measurement noise matrix R require interpretation. The first three diagonal elements refer to temperature measurements which are known to be accurate. A value of 0.15 at R(4,4) signifies a larger error in the measurement of the head in the second effect separator. This is known to be the noisiest of all process signals (Figure A7.52) and the magnitude of R(4,4) relative to the absolute value

of the head is considerably greater than the other diagonal elements.

7.6.3.5 Experimental Procedure

The on-line filter experiment (Program 7 of Appendix 6) proceeds as follows

0. The evaporator is brought to steady state.

1. Run time data - sampling interval and ensemble size - are input to the program and the diagonal elements of the covariance matrices, described above, are assigned.

2. An initial measurement cycle establishing the interrupt frequency, is executed to provide initial values for the predicted state variables. The heat transfer coefficient correlations are solved to give initial values for the parameters.

3. The steady state mathematical model, including the heat transfer coefficient correlations, is solved to provide the initial loss terms for the numerical integration. This means that prior to on-line filtering the plant is always at pseudo steady state.

4. The problem independent section of the filter algorithm is executed to filter the measurements. The estimated and measured state variables are output to the teletype.

5. The elements of the transition matrix are computed from the estimates and the noise-free measurements.

6. The state equations (including the heat transfer coefficient correlations where applicable) are solved numerically up to the next measurement time. The future predictions of the state variables are output to the teletype.

7. The computer waits for the next measurement time to occur.

8. On interrupt, the analogue channels are scanned and the resulting measurements are converted to SI units.

9. The experiment proceeds recursively from 4. above.

7.6.3.6 On-line Results

Figure A7.67 shows the teletype output for the first 3 filter cycles. At time zero the measurements and initial predictions are the same and so the estimates are equal to the predicted values regardless of the initial statistics. For the measured state variables, the effect of the large initial values of the diagonal elements of P(0,0) combined with the correspondingly small values of Q, is to force the filter gain matrix K to be nearly unity on the diagonal elements. This results in estimates that tend towards the measurements initially and the diagonal elements of the estimation error covariance matrix converge rapidly. This condition is only desirable when the measurements are good, but it has the disadvantage that the algorithm will not 'loosen' when the plant conditions change due to the magnitude of Q.

The relationship between the initial statistics and the estimation of parameters is more complex. When Q is small, i.e. there is confidence in the model, the filter algorithm will adjust the parameters to 'fit' the transition matrix. The rate of convergence also depends upon the magnitude of the off-diagonal elements of the transition matrix which relate measured state variables to the parameters and also the confidence in the predicted state variables. Thus, although the measured variable diagonal elements of the estimation error covariance matrix converge rapidly, the fact that the parameter deviations also converge (Figures A7.68, A7.69) does not imply that the parameter estimates are best. For this reason, it is necessary to perform off-line filter experiments in order to 'tune' the filter to give the best estimates under all operating conditions.

The 8th state variable, the overall heat transfer coefficient in the first effect, does not converge. This is discussed further under off-line processing (Section 7.6.4).

It is worth noting that the prediction of the 1st state variable, T_2, is some way from the measurement but the predictions of the remaining three measured state variables is good.

7.6.4 Off-line Experiments

The off-line filter investigation is concerned with 'tuning' the filter by observing the effect of variation in the elements of the Q matrix to obtain best estimates of states and parameters. Clearly, determination of the best Q matrix for a single set of data does not imply that the matrix is suitable for all plant operating conditions. Consequently, two sets of measurements, collected by the dynamic logging program and stored on paper tape, are selected for off-line filtering experiments. The data sets are as follows.

a) DATA 1 consists of measurements taken over 30 minutes with a sampling interval of 30 seconds. The plant is initially at pseudo steady state, which is maintained, without adjusting controls, for the whole period.

b) DATA 2 consists of measurements taken over 60 minutes with a sampling interval of 30 seconds. The plant is initially at steady state and the following disturbances are introduced.

A. After 7 minutes the steam flow rate to the first effect is increased.

B. After 28 minutes the liquid feed to the preheater is increased.

C. After 40 minutes both the steam and feed rates are decreased.

As described in Section 7.6.3.2, there are two alternative parameter prediction strategies. These are PREDICTION 1, where the predicted heat transfer coefficient is equal to the previous estimate, and PREDICTION 2, where the heat transfer coefficient correlations provide predictions of parameters based on current estimates and 'noise-free' measurements. When filtering is carried out off-line to the evaporator, the constraint of numerical integration in real time is not applicable. Thus the prediction of state variables is carried out with a smaller step length so that any possibility of numerical error is removed.

Measurements are processed by the same program as the on-line experiments except that data are derived from the paper tape reader and not the MDP200. The filter statistics, with the exception of the Q matrix, are identical, i.e. the diagonal elements of P(0,0) are 1000 and those for R are .1, .1, .1 and .15 respectively. For each set of data and prediction strategy, the diagonal elements of the Q matrix are set to 0.1, 1 and 10. As a result of observed parameter estimates, the effect of variation along the diagonal elements of Q is also considered for DATA 2. The experimental results consisting of state estimates and measurements, where applicable, are presented graphically. The square roots of the corresponding diagonal elements of the estimation error covariance matrix, σ_p, are also graphed.

7.6.4.1 DATA 1 PREDICTION 1

One effect of increasing the magnitude of the diagonal elements of the Q matrix is to reduce the confidence in the model thus forcing the state variables to the measurements. Since the parameters are related to these measurements by the model, the parameter estimates will be slow to converge, if at all. This effect is exemplified by Figure A7.70, the estimation of the preheater tubeside liquid temperature. As described in Section 7.5.3, this variable is not predicted accurately by the reduced model and thus the estimates tend to the measurements, that is away from the poor predictions, as q increases ($Q = q.I$). As the measurement tends to steady state, the estimate tends to the measurement. Hence, for this state variable, the choice of q is dependent upon the dynamic state of the process.

The magnitude of the diagonal element of the error covariance matrix is maintained large when Q is large at the error covariance prediction stage of the algorithm. Thus when $q = 0.1$ the error covariance matrix becomes small but at the same time the estimate is forced towards the poor prediction. This is divergence. A filter is said to diverge when the error in the estimates far exceeds the error bounds predicted by the error covariance matrix. Divergence is caused by the failure to properly reflect all sources of uncertainty in the filter statistics, resulting in a covariance matrix which is optimistically small, and a filter which may disregard measurements. It is assumed that the measurements of Figure A7.70 are near to the true value of the variables, thus since the model is poor for prediction, the estimate diverges when $q = 0.1$.

This problem is not apparent for at the next state variable - the second effect tubeside liquid temperature, Figure A7.7.1. Both prediction and measurement are

good so that even when q = 0.1, the estimates do not diverge. The results for q = 1.0 and q = 10.0 lie so close to the measurements that they are not presented.

For the third state variable, the condenser tubeside liquid temperature, Figure A7.72, the estimates for all q are good but there is apparent periodic divergence. This is due to an intermittent error in the measurement of the condenser feed liquid temperature. This is not a measured state variable but it is required in the state variable prediction step and in the computation of the transition matrix. The reduction in the order of the system is justified by including measurements of this kind in the mathematical model. Figure A7.72 shows that estimation is poor when such measurements are not noise-free and in particular when their noise statistics are not included in the filter algorithm. Such divergence is compensated for by increasing q but only at the expense of increasing σ_p.

State variable 4, the liquid level in the second effect separator is a noisy measurement that is well predicted, Figure A7.73. Thus when q is small, the noise is filtered and divergence does not occur.

The effect of variation of q upon the parameters is shown in Figures A7.74 to A7.77. Convergence is slow when there is no confidence in the model (q = 10.0). Intuitively, this would appear correct since the filter could not be expected to solve the model for the parameters when the state estimates tend towards the measurements. In the case of SV5, the preheater overall heat transfer coefficient (Figure A7.74), this implies that accurate parameter estimation is only possible after a large number of filter cycles. When q is small the corresponding state variable, T_2, diverges so that the parameter estimate is

inaccurate. State variable 6, the second effect overall heat transfer coefficient Figure A7.75, is linked to an accurate state variable estimate, T_{14}, and so the parameter estimates are good. This is also true for the condenser overall heat transfer coefficient, Figure A7.76, but the influence of the input measurement errors shown in Figure A7.72, produces some deviation.

State variable 8, the first effect overall heat transfer coefficient (Figure A7.77) requires further explanation. The estimate remains constant at the initial prediction and the estimation error deviations increase throughout the experiments. This effect is observed in all on-line and off-line experiments. Equation 7.6.1 shows the incidence relationship to state variable 4, the second effect separator head. Not only is this measured state variable very noisy but the magnitude of the element on the transition matrix is extremely small ($\simeq 1 \times 10^{-6}$). Thus the first effect overall heat transfer coefficient is only weakly observable from a poor measurement. This combination of weak observability and poor measurement means that the estimation errors increase and the estimate is updated by an insignificant quantity at each filter cycle.

The preceding discussion of DATA 1 PREDICTION 1 experiments highlights the problems of applying the Kalman filter to the estimation of the parameters of a real process. When measurements are poor, estimation is not possible unless the model provides an accurate prediction. When the model is poor or the system is weakly observable parameter estimates may not converge unless measurements are accurate.

7.6.4.2 DATA 2 PREDICTION 1

DATA 2 represents plant measurements over a wide range of operating

conditions. Disturbances A, B and C are substantial and are used to examine the performance of the converged filter.

Estimation of the measured state variables, Figures A7.78 to A7.81 follows the same trend as DATA 1. At the preheater tubeside, Figure A7.78 the prediction is poor and when q ' 0.1 the estimates diverge. For state variable 2, Figure A7.79, where prediction and measurement are good, the estimation is always good. The intermittent measurement error on state variable 3 (Figure A7.80) is also apparent in DATA 2. The filter will overcome measurements of this type when the diagonal elements of Q are decreased thus placing less weight on the measurements. At the second effect separator liquid head, Figure A7.81, a substantial measurement error, in additon to a noisy signal, is present. Clearly, when measurement errors of this magnitude, not adequately described by the diagonal elements of R, are present the filter estimates are biased. In practice, it may be possible to adapt the oscillating and limited memory filters suggested by Jazwinski (13) when such errors occur . Apart from the three major measurement errors in Figure A7.81, the filter performs adequately in smoothing the noisy signal.

Parameter estimates for DATA 2 are shown in Figures A7.82 to A7.87. The eighth state variable, the first effect overall heat transfer coefficient , is not presented since the error, like DATA 1, diverges and the estimate is constant. As the plant operating conditions change so the heat transfer coefficients vary accordingly. The degree of variation, i.e. the response of the parameters, depends upon the accuracy of the estimation of the measured state variables and the magnitude of q. Apart from the initial prediction at time zero, the heat transfer coefficient correlations are not implemented. This means that the

parameters will be adjusted according to the dynamic state of the plant and within the error bounds determined by the estimation error covariance matrix P.

Figure A7.82 shows the estimation of the preheater overall heat transfer coefficient, Up. The diagonal elements of the Q matrix are the same for all state variables so that when q = 10 for Up, q is the same for T_2, which follows the measurements closely. Conversely, when q is 0.1, T_2 is divergent and once the filter is converged the parameter is slow to respond. Figure A7.5 shows that the parameter responds when q is large, i.e. there is uncertainty in the model. The same response is observed at Figures A7.83 (U_f) and A7.84 (U_c). In general, it can be seen that once the filter is converged, it does not loosen when dynamic changes occur at the plant. When q is large, the parameter responds slowly to plant disturbances because confidence in the model is not maintained.

When the elements of the Q matrix are divided into q_1 the first four elements corresponding to the measured state variables and q_2 for the parameters, greater response is observed. In Figure A7.85, U_p, q_1 is small while q_2 is large. The parameter responds to the change in conditions rapidly because the model has greater confidence. Comparing Figure A7.85 to A7.82 shows that when q is divided the parameter tends to steady state between each disturbance. Furthermore, the filter loosens as each change occurs by increasing the diagonal element of the P matrix - shown as σ_p. The same effect is observed at U_f, Figure A7.86 and U_c, Figure A7.87. In all cases, the subsequent improvement in the parameter estimates produces better estimates for the measured state variables.

The DATA 2 PREDICTION 1 experiments show that the filter response to dynamic plant conditions is the same as for the steady state (DATA 1) when the

elements along the Q matrix diagonal are identical. When the elements are separated the estimates of state variables tend toward the accurate measurements and the filter loosens to adapt to changes in parameters.

7.6.4.3 DATA 1 PREDICTION 2

The second method of prediction calculates parameters from the heat transfer coefficient correlations. At each filter prediction step the parameters at the next sampling interval are computed from the predicted state variables and the noise-free measurements. At the preheater tubes, Figure A7.88, the effect of continuously updating the heat transfer coefficient is to force the predicted state variable away from the measurement. This enhances the conclusion of the dynamic simulation that the well mixed assumption is inadequate creating a faster response in the predicted state than the measurement. When $q = 0.1$, the estimate diverges and only when $q = 10$ does the estimate tend towards the measurements. The same effect is observed at all the measured state variables (Figures A7.89 - A7.91) although the prediction and measurement are good at the second effect tubes, Figure A7.89 and the input measurement error is apparent at Figure A7.90.

The parameter estimates are shown in Figures A7.92 to A7.95. One effect of the alternative prediction strategy is to generate steady state estimates of the heat transfer coefficients. The disadvantage of this method is that errors in the input measurements affect the correlations. Thus at state variable 5, Figure A7.92 and state variable 7, Figure A7.94, the estimates diverge when the predictions are erroneous. In the steady state condition, this can be overcome by decreasing q which effectively tightens the filter so that it does not respond to dynamic changes. The estimation of state variable 8, Figure A7.95, follows the prediction only and the effect of weak observability is apparent.

By comparison with Figures A7.70 to A7.77, it can be seen that including the heat transfer coefficient correlations in the state variable prediction causes the parameters to converge to their steady state values. The method is unstable when the noise free measurements, required by the correlations, are erroneous.

7.6.4.4 DATA 2 PREDICTION 2

Estimation of the measured state variables, Figures A7.96 to A7.99, follows the same trend as DATA 1. At the preheater tubeside, Figure A7.96, the prediction is poor and when q = 0.1 the estimates diverge. For state variable 2, Figure A7.97, where prediction and measurement are good, the estimation is always good. The intermittent measurement error on state variable 3, Figure A7.98, is smoothed out by decreasing q, thus tightening the filter by placing less weight on the measurements. At the second effect separator liquid head, a substantial measurement error can be smoothed by the same method.

Parameter estimates are shown in Figures A7.100 to A7.102 and include the case where the elements of the Q matrix are split. As a result of the heat transfer coefficient prediction, the parameters respond immediately to any changes in plant operating conditions and are driven to the steady state values. The effect of dividing Q is to loosen the filter by increasing the diagonal elements of the error covariance matrix (e.g. σ_p, Figure A7.102). Since the parameters are predicted by the correlations, loosening of this nature does not produce the substantial changes observed in Figures A7.85 to A7.87(STRATEGY 1).

7.6.4.5 Conclusions

With the exception of the liquid head in the second effect separator, the system measurements are good and can be used to compare the performance of

of the filter.

Errors in the mathematical model that create divergence can be compensated for by increasing the diagonal elements of Q associated with the parameters.

When the parameters are not predicted by the correlations, the filter tightens when q is small such that any deviation from the predicted states due to random or system disturbances is not accounted for.

Including the parameter correlations at the state variable prediction, improves the parameter estimation for all q. As expected, it is beneficial to include all available mathematical models.

In order to apply the filter algorithm in real time, a reduced model based on liquid phase dynamic equations and including noise-free vapour phase measurements has been used. When errors occur in these input measurements they are not compensated for by the filter algorithm. Errors of this type affect both state variable and parameter estimates.

CHAPTER 8

CONCLUSIONS AND RECOMMENDATIONS FOR FUTURE WORK

8.1 Conclusions

8.1.1 Software and Hardware Developments

As part of the research, two major software packages have been developed. The Aston Simulation Program (101), produced for simulation of the comprehensive and dynamic models, provides an interactive digital simulation tool. The on-line logging package, BASELINE, includes fundamental subroutines to perform data logger control functions. Within BASELINE, the benefits of an interactive language have been retained for real time applications with a computer system of minimum configuration.

The application of these packages is not confined to the double effect evaporator system. They are specifically designed to be available to any user with a knowledge of the interactive language BASIC.

Communication between the plant and computer is achieved by conventional instrumentation and a special-purpose electronic interface to a data logger.

8.1.2 Mathematical Modelling

Analysis of on-line results from steady state modelling of the mass and energy flows in the evaporator has produced accurate heat transfer coefficient correlations. These correlations have provided supporting equations for the simulation of both the 18th order comprehensive dynamic model and the 4th order reduced model. Simulation of the comprehensive model proves that the

system response cannot be determined without a knowledge of the vapour phase dynamics. This problem is seen as being beyond the scope of this project. It has been overcome by including the vapour phase measurements in the simulation of the reduced model which contains simplifying assumptions. The results of the reduced model simulation show that the simulated and experimental response to two types of step change are close enough for the model to be adopted for on-line estimation. In addition to the four measured variables, four overall heat transfer coefficients (parameters), are to be estimated.

8.1.3 On-line Estimation

Applying the Kalman filter to a Chemical Engineering system is very different from its original application. In the Aerospace Industries, the mathematical relationships are well known and the measurements are corrupted by noise whereas in Chemical Engineering systems, the mathematics are uncertain and the available measurements are more reliable. The non-linear reduced model has been incorporated into the Kalman filter algorithm for the estimation of state variables and parameters. The filter is suitable for a real time application when the order of the mathematical model and the number of measurements are small. This means that in order to maintain the filter cycle time in proportion to the model time constants, the number of measurements has been reduced to four. Other available measurements, concerned with the vapour phase, have not been disregarded but are included in the prediction stage of the filter as noise-free measurement inputs. With a cycle time of two minutes and the Euler method of state variable prediction, the filter has been executed in real time.

Due to practical constraints, it has not been possible to investigate the influence of process noise statistics on filter performance on-line to the evaporator.

Consequently, off-line experiments, based upon real process measurements have been carried out with two alternative parameter prediction strategies. The first sets the parameter prediction equal to the previous estimate in the classical way and the influence of the magnitude of the diagonal elements of the process noise matrix, Q, are as follows:

(1) When the elements are small, the filter converges rapidly and fails to predict parameters when the plant is in a dynamic state.

(2) When the elements are large, implying a lack of confidence in the model, the state variable estimates tend towards the measurements and the parameters are slow to respond.

(3) The above difficulties have been overcome by separating the diagonal elements of Q such that confidence in the model is reflected by a small constant on the elements corresponding to the measured state variables and a large constant on the elements corresponding to the parameters. This forces the parameters to respond to changes reflected in both the measured and predicted state variables.

(4) In all cases, estimation of states is improved by the separation of the diagonal elements of Q.

In this type of estimation there is a risk of disregarding the meaning of the parameters. They are heat transfer coefficients and not simply coefficients in a dynamic equation that must fit a measured and predicted response. This is overcome by use of the second method of prediction, where the parameters are calculated by the heat transfer coefficient correlations. The conclusions from this estimation are as follows:

(1) Due to the correlations, the parameter estimates respond rapidly to

dynamic changes in plant operating conditions.

(2) The estimation of measured state variables is influenced by the diagonal elements of the Q matrix as described in (1) and (2) above.

(3) For the parameters, separation of the diagonal elements does not substantially improve estimation. However, as for the first method of prediction, the separation does improve estimation of states.

In off-line processing, the combination of parameter prediction and separated elements of the Q matrix has given best estimates. The method is susceptible to errors in the noise free measurements in the same way as the simulation of the reduced model is influenced by errors in measurements of the vapour phase.

The Kalman filter has been shown to be applicable to on-line real-time estimation for the system under consideration.

8.2 Relationship of Results to Published Work

The application of the Kalman filter to a double effect evaporator is reported by Hamilton et al (91). The fifth order model includes the dynamics of liquid concentrations and all state variables are measured. From a linear model a filter gain matrix is precomputed and used in simulation and on-line filter experiments. Like the results of this thesis, the paper indicates the need for off-line tuning of the filter before attempting on-line estimation. However, the use of simulated measurements in off-line filtering and not real plant data, presupposes that the model is a true representation of the plant performance. The investigation into the effect of an unmeasured disturbance proves that these modelling inaccuracies can be accounted for by increasing the magnitude of q (decreasing

the ratio r/q adopted in the paper). Since there is no parameter estimation and the converged filter gain matrix is precomputed, the on-line experiments are simply measurement filtering to provide smoothed signals for a control algorithm. The fact that zero-mean Guassian noise is added to the on-line measurements for the investigation does not prove that the filter algorithm is suitable for state variable and parameter estimation in non-linear systems.

Kalman filtering and parameter estimation have been reported by Joffe and Sargent (69), in a simulation study of the estimation of catalyst activity and decay in the control of a tubular reactor. The non-linear distributed parameter system is decomposed into a non-linear lumped parameter system which is linearised for filtering. The magnitude of the elements of the process noise matrix do not affect convergence of the parameters although with the filter statistics used, induced modelling error causes one parameter to converge to a spurious value.

Wells (40), estimates reaction rate parameters in a simulated, non-linear well stirred, reactor application. Good estimation is achieved by 'judicious' selection of the Q matrix. This selection includes the separation technique suggested in this thesis where the diagonal elements corresponding to the parameters are greater than those of the measured variables. Approximate parameter prediction equations are included by differentiating the known parameter functions with respect to the measured state variables.

More recently, Fortescue and Kershenbaum (109), have reported an on-line real-time study of estimation on a pilot scale CO_2 absorption-desorption unit. The computer system is a member of the Honeywell series 16 machines. Estimation with a distributed parameter model is carried out at steady state to determine

absorption parameters from plant measurements. The influence of filter statistics on convergence and details of the mathematical model are yet to be published but the problems of implementing the filter algorithm for a non-linear system have been overcome and the published results show good convergence of estimates.

8.3 Recommendations for Future Work

The following areas for further work are apparent.

(1) It would be advantageous to extend the ASP package to include an integration method based upon optimised error-controlled step length. The use of this efficient integration method in simulation would be suitable for Kalman filter applications if the data logger and integration subroutines can be successfully loaded into the memory of the Honeywell 316.

(2) The BASELINE package requires further development so that redundant time spent whilst sampling the MDP200-ADC can be utilised more efficiently in background programming.

(3) There is much work to be done in dynamic modelling of the evaporator. Additional instrumentation and steady state runs are required to determine the heat losses at each heat exchanger. Dynamic analysis of the performance of the vacuum pump and the vapour phase may provide an alternative method to the use of noise-free measurements in the prediction step of the filter. The assumption of perfect mixing in the preheater and condenser tubes is inadequate. A model based on a number of well-mixed regions would be more suitable but this has the disadvantage of increasing the order of the system.

(4) There are many possibilities for future work in on-line Kalman filtering. The estimation of unmeasured inputs, the effect of the initial filter statistics and the reduction in the number of state variable measurements are studies that can be based upon the existing reduced model. This project has served to highlight the need for adaptive estimation of the Q matrix. Adaptive filtering including parameter estimation in non-linear chemical engineering systems is, as yet, an unexplored area.

(5) Adaptive estimation, without parameter estimation, is possible when the parameters are predicted by the heat transfer coefficient correlations and are not included in the filter model. This reduces the number of state variables to four so that the increase in available computer time can be dedicated to the necessary additional matrix operations.

LIST OF SYMBOLS

A	plant matrix
B	driving force matrix
c	filter exponential weighting factor
C_l	liquid specific heat in idealised exchanger
C_p	liquid specific heat
C_w	tube wall specific heat in idealised exchanger
d_l	inside diameter of tube
d_w	outside diameter of tube
d_s	shell diameter
f	state function - linear
f'	state function - non-linear
g	vapour enthalpy function
h	measurement function - linear
h'	measurement function - non-linear
H_j	enthalpy of stream j
H_s	head in second effect separator
I	identity matrix
k	discrete step in time
K	filter gain matrix
m	number of measurements
M_j	mass flow rate of stream j
M	measurement matrix
n	number of state variables
P	estimation error covariance matrix
P	vapour pressure (Section 6.2.3)
q	diagonal element of Q
Q	process noise matrix
R	measurement noise matrix
S	predicted residual covariance matrix
t	time
T_j	temperature of stream j
T_L	Liquid temperature

LIST OF SYMBOLS (cont)

T_w	tube wall temperature
T_s	shellside vapour temperature
T_p	filter time constant
u	vector of system inputs
v	vector of measurement disturbances
V_j	vapour flow rate of stream j
w	vector of input disturbances
x	state vector
x_p	a vector of randomly varying parameters
y	measurement vector
Y	vapour fraction

Greek Symbols

$a(T)$	vapour density - temperature function
a_p	autocorrelation coefficient
β	bias parameter
γ	drift parameter
Γ	Input transition matrix
$\bar{\Gamma}$	linearised input transition matrix
Δ	time difference between samples
λ	latent heat
Φ	state transition matrix
$\bar{\Phi}$	linearised state transition matrix
σ_p	square root of diagonal element of P
ρ_L	liquid density
ρ_j	density of vapour stream j

Subscripts

c	condenser
e	first effect
f	second effect
g	preheater
t	tubeside
s	shellside

REFERENCES

1. Gauss, K.F., "Theory of the Motion of the Heavenly Bodies Moving About the Sun in Conic Sections". Dover Press, New York, 1963.

2. Wiener, N., "The Extrapolation, Interpolation and Smoothing of Stationary Time Series", Wiley & Sons, New York, 1949.

3. Kalman, R.E., J. BASIC Eng., Trans. ASME, 82D, pp 33-45, 1960.

4. Smith, G.L., Schmidt, S.F. and McGee, L.A., "Application of Statistical Filter Theory to the Optimal Estimation of Position and Velocity on Board a Circumlunar Vehicle". NASA-TR, R-135, 1962.

5. Coggan, G.C., and Noton, A.R.M., Trans. Inst. Chem. Engrs., 48, pp T245 - T264, 1970.

6. Åström, K.J., "System Identification, a Survey", IFAC Symposium, Prague, 1970.

7. Nieman, R.E., Fisher, D.G. and Seborg, D.E., Int. J. Control, 18, 2, pp 209-264, 1971.

8. Sienfeld, J.H., Ind. Engng. Chem., 62, pp 132-148, 1970.

9. Cuenod, M. and Sage, A., Automatica, 4, pp 235-269, 1968.

10. Bellman, R.E., Kagiwada, H., and Kalaba, R.E., Int. J. Engng. Sci., 3, pp 327-334, 1965.

11. Briggs, P.A.N., Hammond, P.H., Hughes, M.T.G., and Plumb, G.O., Proc. Inst. Mech. Eng., 179, 3H, pp 37-51, 1965.

12. Price, P.R., Ph.D. Thesis, The University of Aston in Birmingham, 1972.

13. Jazwinski, A.H., "Stochastic Processes and Filtering Theory", Academic Press, New York, 1970.

14. Seinfeld, J.H., Garalas, G.R. and Hwang, M., Ind. Eng. Chem. Fund., 8, pp 257, 1969.

15. Noton, M., Gamma European Systems, Nottingham, Private Communication, November, 1972.

16. Kalman, R.E. and Bucy, R.S., J. Basic Eng., Trans. ASME, 83 pp 95-108, 1961.

17. Ho, Y.C., and Lee, R.C.K., IEEE Trans. Automatic Control, AC-9, pp 333-339, 1964.

18. Cox, H., IEEE Trans. Automatic Control, AC-9, pp 5-12, 1964.

19. Bellman, R.E., Kagiwada, H., Kalaba, R.E. and Sridhar, R., J. Astronaut Sci., 13, pp 110-115, (1966).

20. Goldman, S.F. and Sargent, R.W.H., Chem. Engng. Sci., 26 pp 1535-1542, 1971.

21. Aoki, M., "Optimisation of Stochastic Systems", Academic Press, New York, 1967.

22. Sorenson, H.W., "Advances in Control Systems" (ed. C.T. Leondres), 3, pp 219-292, 1966.

23. Fitzgerald, R.J., IEEE Trans. Automatic Control, AC-16, pp 736-747, 1971.

24. Jazwinski, A.H., IEEE Trans. Automatic Control, AC-13, pp 558-563, 1968.

25. Tarn, T.J. and Zaborsky, J., AIAA J. 8, 6, pp 1127-1133, 1970.

26. Leondres, C.T. and Pearson, J.O., Int. J. Control, 17, 4, pp 785-801, 1973.

27. Huddle, J.R. and Wismer, D.A., IEEE Trans. Automatic Control, AC-13, pp 421-423, 1968.

28. Griffin, R.E. and Sage, A.P., IEEE Trans. Automatic Control, AC-13 pp 320-329, 1968.

29. Mehra, R.K., IEEE Trans. Automatic Control, AC-15, pp 175-184, 1970.

30. Mehra, R.K., IEEE Trans. Automatic Control, AC-16, pp 12-21, 1971.

31. Krause, D.J. and Graupe, D., Int. J. Control, 17, pp 1021-1027, 1973.

32. Jazwinski, A.H., IEEE Trans. Automatic Control, AC-11, 765, 1966.

33. Kushner, H.J., SIAM Control, 2, 106, 1964.

34. Friedland, F. and Bernstein, I., J. Franklin Inst., 281, pp 455-480, 1966.

35. Athans, M., Wishner, R.P. and Bertolini, A. IEEE Trans. Automatic Control, AC-13, pp 504-514, 1968.

36. Schwartz, L. and Stear, E.B., IEEE Trans. Automatic Control, AC-13, pp 83-86, 1968.

37. Denham, W.F. and Pines, S., AIAA J., 4, pp 1071-1076, 1966.

38. Wishner, R.P., Tabaczynski, J.A. and Athans, M., Automatica, 5, pp 487-496, 1969.

39. Friedland, B., IEEE Trans. Automatic Control, AC-14, pp 359-367, 1969.

40. Wells, C.H., AIChE J., 17, 4, pp 961-973, 1971.

41. Schmidt, S.F., Weinburg, J.D., and Lukesh, J.S., "Case Study of Kalman Filtering in the C-5 Aircraft Navigation Systems". Case Studies in Systems Control, Workshop Preprints, University of Michegan, 1968.

42. Buffham, B.A. and Kropholler, H.W., "On-line Computer Methods Relevant to Chemical Engineering", Inst. Chem. Engrs. (London), pp 64-70, Nottingham, England, 1971.

43. Wells, C.H., IEEE Trans. Automatic Control, (Correspondence), AC-13, p 445, 1968.

44. Singer, R.A. and Sea, R.G., IEEE Trans. Automatic Control, AC-16, pp 254-257, 1971.

45. McLean, J.D., Schmidt, S.F. and McGee, L.A., "Optimal Filtering and Linear Prediction Applied to a Midcourse Navigation System for the Circumlunar Mission". NASA-TN, D-1208, 1962.

46. Distefano, G.P., AIChE J., 14, p 190, 1968.

47. Athans, M., Automatica, 8, pp 397-412, 1972.

48. Mehra, R.K., IEEE Trans. Automatic Control, AC-16, pp 307-319, 1971.

49. Mendel, J.M., IEEE Trans. Automatic Control, AC-16, pp 748-758, 1971.

50. Coggan, G.C. and Wilson, J.A., Computer Journal, 14, pp 61-64, 1971.

51. Coggan, G.C. and Wilson, J.A., "On-line Computer Methods Relevant to Chemical Engineering", Inst. Chem. Engrs. (London). pp 136-150, Nottingham, England, 1971.

52. Bryson, A.E. and Ho, Y.C., "Applied Optimal Control", Ginn & Co., Massachusetts, 1969.

53. Woodside, C.M., Carleton University, Canada, Private Communication 1972.

54. Smith, G.L., J. SIAM Control, 2, 1, pp 19-32, 1964.

55. Schmidt, S.F., Advan. Control Systems, 3, pp 292-340, 1966.

56. Åström, K.J., "Introduction to Stochastic Control Theory", Academic Press, 1970.

57. Sage, A.P. and Melsa, J.L., "Estimation Theory", McGraw-Hill, Inc. 1971.

58. Wheelwright, S.C. and Makridakis, S., Oper. Res. Quart, 24, pp 55-64, 1973.

59. Ford-Livene, C., "The Kalman-Bucy Filter and Dynamic Programming in Agricultural Rest Control", Proc. 6th Harvic International Conference on System Sciences, Harvic, 1973.

60. Szeto, M.W., Transportation Science (U.S.A.) 6, 4, 419-439, 1972.

61. Sharma, K.L.S. et al, Proc. IEEE, 61, 3, pp 391-2, 1973.

62. Godbole, S.S., IEEE Trans Nuc. Sci., NU-20, pp 661-667, 1973.

63. Belanger, P.R., IFAC, 5th World Congress, Paris, 1972.

64. Tse, E., Proc. 3rd Symposium on Estimation Theory, San Diego, U.S.A. 1972.

65. Noton, A.R.M. and Choquette, P., Proc. IFAC/IFIP Symposium, Toronto, 1968.

66. Choquette, P., Noton, A.R.M., and Watson, C.A.G. Proc. IEEE, 58, 1, pp 10-16, 1970.

67. Noton, A.R.M., IEEE Trans. Automatic Control, AC-16, pp 128-133, 1971.

68. Klinger, A., IEEE Trans. Automatic Control, AC-13, pp 102-3, 1968.

69. Joffe, B. and Sargent, R.H., Trans. Inst. Chem. Engrs., 50, pp 270-281 1972.

70. Seinfeld, J.H., Chem. Eng. Sci. 24, p 75, 1969.

71. Garalas, G.R., and Seinfeld, J.H., Chem. Eng. Sci., 24, pp 625-636, 1969.

72. Yu, T.K. and Seinfeld, J.H., AIChE Jl., 19, pp 389-392, 1973.

73. Williams, T.J. and Morris, H.J., Chem. Eng. Progr. Symposium Series, 36, 57, p 20, 1961.

74. Williams, T.J., Ind. and Eng. Chem., 59, p 53, 1967.

75. Buckley, P.S. "Techniques of Process Control", John Wiley & Son, New York, 1964.

76. Finlay, I.C., and Smith J., J. Mech. Eng. Sci., 9, 3, pp 211-217, 1967.

77. Stainthorp, F.P., and Axon, A.G., Chem. Eng. Sci., 20, pp 107-119, 1965.

78. Stermole, F.J. and Lawson, M.A., Ind. and Eng. Chem. Fund., 2, pp 62-67, 1963.

79. Heidemann, R.A., et al, Can, J. Chem. Eng., 49, 147-153, 1971.

80. Fricke, R.H. et al, Chem. Eng. Progr. Symp. Series. 31, 56, p 80, 1960.

81. Schmidt, J.R. and Clark, D.R., Simulation, 15, pp 15-21, 1969.

82. Dorri, M.K., Heat Transfer-Soviet Research, 1, 2, pp 186-193, 1969.

83. Johnson, D.E. ISA J, 7, pp 46-52, 1960.

84. Nisenfeld, A.E., Hoyle, D.L., Instrum. Technol, 17, pp 49-51, 1970.

85. Anderson, J.A. et al, Trans. Soc. Inst. Tech. pp 21-35, March, 1971.

86. Andre, H. and Ritter, R.A., Can. J. Chem. Eng., 46, pp 259-264, 1968.

87. Ritter, R.A. and Andre, H., Can. J. Chem.Eng., 48, pp 696-701, 1970.

88. Newell, R.B., Ph.D. Thesis, University of Alberta, 1971.

89. Newell, R.B. and Fisher, D.G., Ind. Eng. Chem., Proc. Res.Develop., 11, 2, pp 213-221, 1972.

90. Burdett, J.W. and Holland, C.D., AIChE J, 17, 5, pp 1080-1090, 1971.

91. Hamilton, J.C., Seborg, D.E.and Fisher, D.G., AIChE J, 19, 5, pp 901-909, 1973.

92. Kestnor Evaporator & Engineering Co. Ltd., "Laboratory Size Double Effect Evaporator", Document R-299.

93. British Patent, 24024, 1899.

94. Honeywell Information Systems Ltd., Honeywell 316 Programmers Reference Manual, Document No. 42400343401 A.

95. Honeywell Information Systems Ltd., DAP-16 Manual, Document 41286103126.

96. American Standards Association, FORTRAN-Proposed Standard, 1969.

97. McCracken, D.D., "A Guide to FORTRAN IV Programming", John Wiley & Sons, New York, 1965.

98. Forsythe, A.I.et al, "Computer Science: BASIC language Programming", John Wiley & Sons, New York, 1970.

99. Payne, S.G. and Gay, B., "Development and Use of a High-Level Language Compiler for Interactive Data Acquisition and Processing", The Institution of Chemical Engineers, 1st Annual Research Meeting, April, 1974.

100. Dean, K.J., The Radio and Electronic Engineer, 34, 1, pp 49-54, 1968.

101. Gay, B. and Payne, S.G., Computer Journal, 16, pp 118-121, 1973.

102. Gay, B. and Payne, S.G., "Teaching Simulation in an Engineering Department", UKSC/IMC Symposium, The Hatfield Polytechnic, December, 1973.

103. Chard, R.A., M.Phil. Thesis, The University of Aston in Birmingham, 1973.

104. Richards, J., J Phys.D. App. Phys. (Letters), 4, pp L15-L18, 1971.

105. Mayhew, Y.R. and Rogers, G.F.C., "Thermodynamics and Transport Properties of Fluids", Oxford Press, 1970.

106. Kern, D.Q., "Process Heat Transfer", McGraw-Hill Book Co., New York, 1960.

107. Singh, O. and Dass, N. Indian Pure App. Phys. 9, pp 92-94, 1971.

108. Gore, W.L., "Statistical Methods for Chemical Experimentation", John Wiley & Sons, New York, 1963.

109. Fortescue, T.R. and Kershenbaum, L.S., "On-line Estimation and Control of a CO_2 Absorption Plant", The Institution of Chemical Engineers, 1st Annual Research Meeting, Imperial College, London, April, 1974.